June 2021

SURFACE ENHANCED RAMAN SPECTROSCOPY (SERS) AS AN APPROACH FOR THE EMERGING LIQUID BIOPSY DIAGNOSTICS

Nariman Banaei
University of Massachusetts Amherst

Surface Enhanced Raman spectroscopy (SERS) as an approach for the emerging liquid biopsy diagnostics

A Dissertation Presented

by

Nariman Banaei

Submitted to the Graduate School of the
University of Massachusetts Amherst in partial fulfillment
of the requirements for the degree of

DOCTOR OF PHILOSOPHY

May 2021

MECHANICAL ENGINEERING

SURFACE ENHANCED RAMAN SPECTROSCOPY (SERS) AS AN APPROACH FOR THE EMERGING LIQUID BIOPSY DIAGNOSTICS

A Dissertation Presented

by

Nariman Banaei

Approved as to style and content by:

DocuSigned by:
Byung Kim
650243308212411...
1/28/2021

Byung Kim, Adviser

DocuSigned by:
Jungwoo Lee
0670CE3974584BE...
1/28/2021

Jungwoo Lee, Member

DocuSigned by:
Wen Chen
8A8BF456454147D...
1/28/2021

Wen Chen, Member

Sundar Krishnamurty

Sundar Krishnamurty, Department Head

DEDICATION

This thesis is lovingly dedicated to my mother, Zari Daroughe, and my father, Taghi Banaei. Without their endless love and encouragement, I would never have been able to complete my graduate studies. I love you both and I appreciate everything that you have done for me.

ABSTRACT

SURFACE ENHANCED RAMAN SPECTROSCOPY (SERS) AS AN APPROACH FOR THE EMERGING LIQUID BIOPSY DIAGNOSTICS.

May 2021

B.E., QAZVIN INTERNATIONAL UNIVERSITY, IRAN

MS., GUILAN UNIVERSITY, IRAN

Ph.D., UNIVERSITY OF MASSACHUSETTS AMHERST, MA, USA

Directed by: Professor Byung Kim

Large Molecule bioanalysis and biosensor development are essential techniques that are required in many applications, including biotherapeutic development, in vitro diagnostic, biomarker detection, and early detection. These techniques should be highly specific and sensitive enough to identify and quantify an analyte of interest with minimum sample pretreatment requirements.

This work explores the development and application of chip-scale bioassays based on surface-enhanced Raman scattering (SERS). It introduces sensing techniques to quantify various disease biomarkers, specifically pancreatic cancer. Blood is the best source of information about our body's function. There are many biomarkers in the blood, and each biomarker's high expression level can be referred to as a specific disorder. In this work, we have developed sensitive detecting methods to quantify these biomarkers. We successfully validated this method with human serum samples. Due to its capability to detect multiple biomarkers, the proposed bioanalytical technique can enhance the specificity of the approach enabled by machine learning based data classification algorithm.

TABLE OF CONTENTS

Page

LIST OF TABLES

Table Page

LIST OF FIGURES

Figure Page

CHAPTER 1

INTRODUCTION

1.1 Dissertation organization

This work explores the development and application of chip-scale bioassays based on surface-enhanced Raman scattering (SERS). It introduces a sensing technique to quantify various cancer biomarkers, specifically pancreatic cancer. A general introduction, including basic knowledge of Raman spectroscopy, SERS, and immunoassay, is presented in this chapter. In Chapters 2 and 3, a method for quantification of pancreatic cancer biomarkers is introduced. Chapter 2 presents the effects of gold particle-size and substrate materials on the amplification of Raman signals. The expression level of three pancreatic cancer biomarkers was measured using intensity-based SERS immunoassay. Chapter 3 investigates the efficiency of a SERS-based immunoassay technique in detecting tumor-derived EVs in the serum of cancer patient samples and its ability to differentiate between PC and CP patients. In Chapter 4, a SERS-based protein biomarker detection platform in a microfluidic chip is investigated to detect several protein biomarkers of OVC, PC, and pancreatitis (CA19- 9, HE4, MUC4, MMP7, and mesothelin). Chapter 4 also explores the impact of two machine learning algorithms (Decision tree and K nearest neighbor classification) on the assay's specificity and improving the chance of recognition for one specific disorder among diseases with overlapped protein biomarkers changes. In Chapter 5, a novel SERS-based frequency-shift immunoassay is reported for the detection of cancer markers in human serum. The expression level of five biomarkers has been measured in the serum of pancreatic and ovarian cancer patients and compared to that of healthy individuals.

1.2 Raman Spectroscopy

Raman spectroscopy was discovered in 1928 by C.V. Raman spectroscopy is a highly specific technique that can identify our targeted molecules through their specific molecular structure, and fingerprint information can be served in their Raman spectra. Raman occurs because of molecular vibration. Vibration can change the molecule's binding structure's polarizability, resulting from a molecule binding structure and light interaction. Raman signal is intrinsically weak, and that is because a few photons (1 in 10^7) scatter with a small difference in wavelength compared to incident photons wavelength. Raman spectroscopy measures the numbers of those photons with different wavelength compared to the original photons. This shift in wavelength (Raman shift) of inelastically scattered radiation can provide chemical and structural information of our target molecule [1,2]. Due to weak signal, Raman spectroscopy has not been widely used in biomolecular studies until 1974 when significant enhancement of the signal observed and discovered by Fleischman et al. in Jeanmarie and Van Duyne, and it is known as Surface-enhanced Raman Spectroscopy [3,4].

1.3 Surface Enhanced Raman Spectroscopy

Surface-Enhanced Raman Spectroscopy (SERS) is vibrational optical spectroscopic technique based on significant enhancement of inelastic scattering of molecules which absorbed on a gold or silver nanostructure. While there have been a huge number of studies trying to explain the SERS phenomenon it is generally agreed that SERS enhancement is largely due to electromagnetic (EM) enhancement.

This Electromagnetic enhancement effect is based on the amplification of the EM field due to resonance excitations of localized conduction-electron oscillations at the metallic nanostructure surface[2]. In other words, free electrons in a nanostructure metal absorb the energy and start to

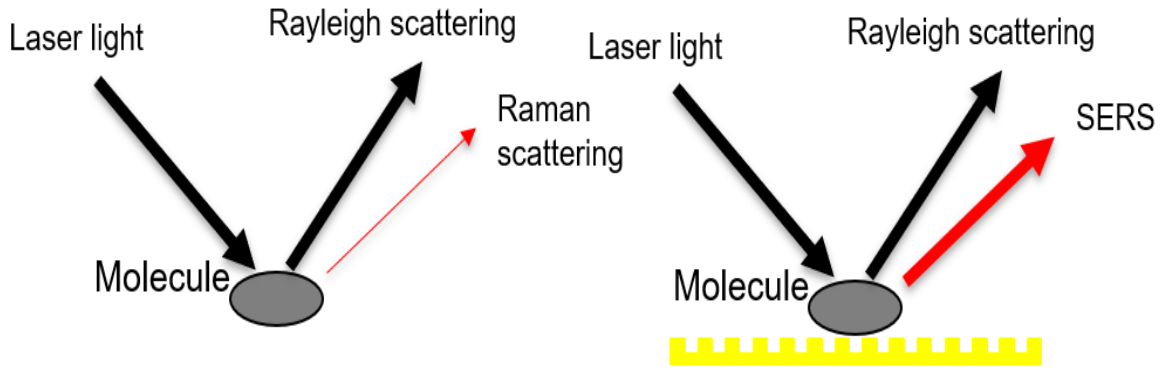

Figure 1: Raman Spectroscopy vs. SERS

oscillate with a resonance frequency determined by the dielectric function of the metal, the surface plasmon resonance. Thus, there is a huge enhancement in the incident field, which leads to the enhancement of scattered fields in shifted frequency. The average SRES enhancement factor is about 10^5 but even values about 10^{11}-10^{14} can be achieved in very sensitive and engineered approaches. These results of the SERS introduced a promising way of using this technique to observe very low concentrations of molecules on nanoparticles and nanostructured surfaces.

1.4. Immunoassay

Immunoassay plays a critical role in various bioanalytical applications, such as early detection, biotherapeutic development, biopharmaceutical analysis. It is a selective method that measures molecules' presence in a solution using an antibody or an antigen. Sandwich immunoassay conventionally uses two antibodies to bind to different binding sites (epitopes) of the antigen. One type of antibody that is used in sandwich immunoassay serves as a capture antibody. The capture antibody is responsible for capturing the antigen from the matrix and immobilizing it on the binding surface. The first step in an immunoassay is the immobilization of the captured antibody on the surface and segregating the target antigen. Then the detection antibody would

be tagged with the appropriate label[5]. SERS-based immunoassay is employed to segregate target protein among other proteins and, at the same time, provide high SERS intensity. Intrinsic label-free detection of proteins with SERS-based immunoassay is not effective due to lack of sensitivity and specificity. Without segregation and purification steps, final intensities are affected by the compositions, other proteins, and salts in the solution.

The most commonly used platform for SERS-based immunoassay is that the target antigen is selectively sandwiched between gold surface coated with antibody, and gold nanoparticles, which are functionalized with antibody and Reporter. Extrinsic Raman labels (ERLs) are designed to bind selectively to a captured antigen and to increase Raman scattering, and provide a strong Raman spectroscopic signal.

CHAPTER 2

DETECTION OF PANCREATIC CANCER PROTEIN BIOMARKERS USING A SERS-BASED IMMUNOASSAY

2.1 Abstract

Early diagnosis of pancreatic cancer is critical to reduce the mortality rate of this disease. Current biological analysis approaches cannot robustly detect several low abundance pancreatic cancer biomarkers in sera, limiting the clinical application of these biomarkers. This study demonstrates a novel system for multiplex detection of pancreatic biomarkers CA19-9, MMP7 and MUC4 in sera samples with high sensitivity. Measuring the levels of these biomarkers in pancreatic cancer patients, pancreatitis patients, and healthy individuals reveals the unique expression pattern of these markers in pancreatic cancer patients, suggesting the great potential of using this approach for early diagnostics of pancreatic cancers

2.2 Introduction

Pancreatic cancer (PC) remains to be one of most deadly cancers with a five years' survival rate of 8% [6,7], which has not been improved over the past 40 years. The high mortality rate of PC is mainly due to the lack of early symptoms, and absence of specific biomarkers and diagnostic platform for early detection. As a result, most pancreatic cancer patients are diagnosed in late stages with advanced diseases, which prevent effective surgical interventions and/or chemotherapy. Currently, biopsy and standard imaging approaches like MRI, CT Scan and endoscopy are routinely used for diagnosing PC in high-risk patients (e.g., those with pancreatitis). However, these approaches often fail since the location of pancreas sits across the back of the

abdomen, behind the stomach[8]. In addition, the high cost of these methods prevents them from being standard screening tests for normal adults.

Detecting biomarkers in body fluid is a cheaper and potentially more effective approach for PC diagnostics. CA19-9 antigen is currently the most common and only validated serum marker for the prognosis and diagnosis of PC. However, CA19-9 cannot be used as a screening test for PC because it fails to distinguish PC with several benign diseases like liver cirrhosis, cholangitis, and chronic pancreatitis (false positive) and has low expression level in Lewis negative diseases (false negative)[9,10]. Furthermore, CA19-9 cannot be found in 10% of the population because their body do not synthesize CA19-9[11,12]. Thus, there is an urgent need for identifying novel PC biomarkers to assess patient prognosis. Several emerging biomarkers, including MUC4[13,14], and MMP7[15-17] have been identified as potential biomarkers of PC. However, the low abundance of these proteins in serum limits their applications for PC diagnostics, and the sensitivity and specificity of these markers have not been thoroughly examined.

Surface Enhanced Raman Spectroscopy (SERS) can provide an intrinsic fingerprint information of samples with high sensitivity[2]. SERS is a vibrational optical spectroscopic technique based on significant enhancement of inelastic scattering of molecules absorbed on gold or silver nanostructures[2,18]. In the past decades, SERS technique has been widely employed to detect and analyze chemical structure of various materials[19-21]. SERS-based detection of low abundance biomarkers has attracted much attention in recent years. Although various types of gold and silver particles and multifarious substrates have been exploited to improve sensitivity and specificity, broad applications of SERS in the detection of biomolecules have not been realized[7,22-25].

In this work, we examined the possibility of using SERS-based immunoassay to detect CA19-9, MUC4, and MMP7 simultaneously for evaluating the risk of PC. We first systematically examined the effects of gold particle size, gap distance between immobilized particle and underlying substrate, and substrate materials on the amplification of Raman signals. We next developed a micropatterning approach to precisely control the address of capture antibody for multiplex detection of PC biomarkers in sera. The sensitivity of the platform was first evaluated by quantification of different concentration of spiked proteins in the pooled human sera. The usefulness of this platform is further evaluated by detecting levels of different biomarkers in sera samples collected from normal adults, patients with pancreatitis, and patients with pancreatic cancer. Our results demonstrated the advantages of using gold nanoshells and micropatterning for high-sensitivity, low-cost, multiplex detection of biomarkers and provided a streamlined process for multiplex detection.

2.3 Experimental Setup

2.3.1 Reagent

Gold Nanoparticles (60 nm in diameter, 2.6×10^{10} particles/ml) were purchased from Ted Pella. Gold Nanoshells (660 nm resonant, 151 nm diameter, 3.7×10^{10} particles/ml and 800 nm resonant, 163 nm diameter, 3.9×10^{10} particles/ml) were purchased from NanoComposix. Sodium chloride, StartingBlock and borate buffer (50mM) were obtained from ThermoFisher Scientific. Dithiobis-(succinimidyl proprionate) (DSP), dimethylsulfoxide (DMSO), 4-Nitrobenzenethiol (4-NBT), acetonitrile, phosphate buffered saline (PBS), and bovine serum albumin (BSA) were acquired from Sigma Aldrich. Pooled human serum was acquired from Innovative Research.

In our SERS-based immunoassay, three different sets of monoclonal antibodies were used to modify the capture substrate and extrinsic Raman labels (ERLs), and corresponding recombinant proteins were used to validate the immunoassay. Lyophilized MMP7 mAb along with recombinant human MMP7 as an antigen (~28 kDa) were purchased from R&D Systems. CA19-9 antibody along with Lyophilized CA19-9 recombinant protein (~40 kDa) were purchased from LifeSpan Bioscience and monoclonal anti-MUC4 and human MUC4 peptide as an antigen were obtained from Abcam.

Four different substrates were used in our assay. Gold nanopillar substrates were purchased from Silmeco; gold deposited paper substrates were purchased from Diagnistic anSERS Co; gold coated silicon substrates were purchased from Sigma Aldrich; gold coated microscope slides were purchased from Ted Pella.

2.3.2 Preparation pf ERL

As illustrated in Fig. 2, antibody-conjugated ERLs were prepared based on standard protocols as reported by Porter, Lipert et al. [26]. Specifically, modified gold nanoparticles and gold nanoshells as ERLs are exploited to provide more intense Raman signal and immunopositivity. In this paper, all of gold particles were modified with two different thiols, DSP and 4-NBT.

DSP has both disulfide and succinimidyl functionalities for chemisorption onto the gold and facile covalent binding of antibodies to the gold particles and substrate; however, DSP does not show intrinsically intense Raman signal. 4-NBT, on the other hand, has been used to provide intense Raman signal due to aryl nitro group with an intrinsically strong Raman active vibrational mode. 4-NBT also contains a disulfide group for spontaneous chemisorption to the gold particles [27]. Preparation of ERLs is described as follows: 1.0 mL suspension of gold nanoparticles or gold nanoshells, 40 μL of 50 mM borate buffer, 2.0 μL of 1.0 mM DSP in DMSO and 8.0 μL of 1.0

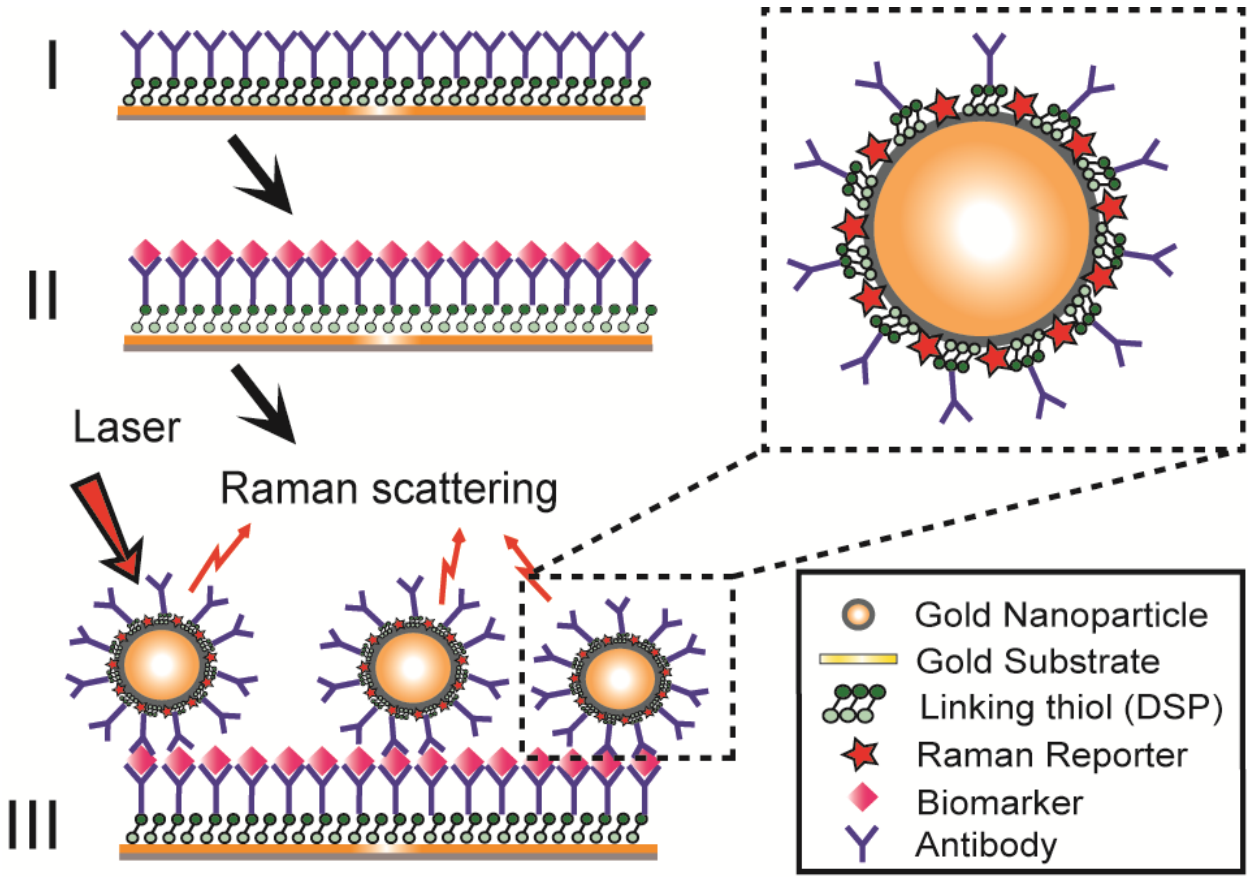

Figure 2. A SERS-based immunoassay for biomarker quantification: (I) Functionalizing gold substrate with thiol and antibody; (II) Capturing desired antigens from the serum; (III) Loading antibody-conjugated ERL, Gold nanoparticles were modified with antibody and Raman reporter

mM 4-NBT solution in acetonitrile were mixed and left to react for 8 h. To discard excess thiols, the suspension was centrifuged at 2000g for 10 min and supernatant was removed with a syringe. Gold nanoparticles/nanoshells were resuspended in 2.0 mM borate buffer. ERL preparation was continued by adding 20 µg of MMP7, MUC4 or CA19-9 primary antibodies to the suspension and incubating for 16 h at 4 ºC. Next, 100 µL of 10% BSA was added to the suspension for stabilizing the suspension and blocking nonspecific binding sites and unreacted succinimidyl. After 8 h, functionalized ERLs were rinsed three times by centrifugation. The ERL pellet was resuspended in 1.0 mL of 2 mM borate buffer containing 1% BSA. The pellet was then resuspended in 0.5 mL

of 2.0 mM borate buffer containing 1% BSA. Finally, suspension was modified with 50 mL of 10% NaCl for stabilization, and then passed through a 0.22 µm syringe filter to remove any large aggregate.

2.3.3 Optimization of ERL's Raman Signal

To maximize Raman enhancement factor of ERL for this application, various combination of most commonly used substrates and nanoparticles were tested and compared. ERLs were prepared using gold nanoparticles, and gold nanoshells with 660 nm and 800 nm resonant wavelength. Also, four different kind of substrates, glass substrate, gold deposited paper substrate, gold nanopillar substrate and gold coated silicon substrate, were coated with DSP. SEM image of gold nanoparticle on gold coated silicon substrate can be found in Fig. 3. 20 µL of each 4-NBT

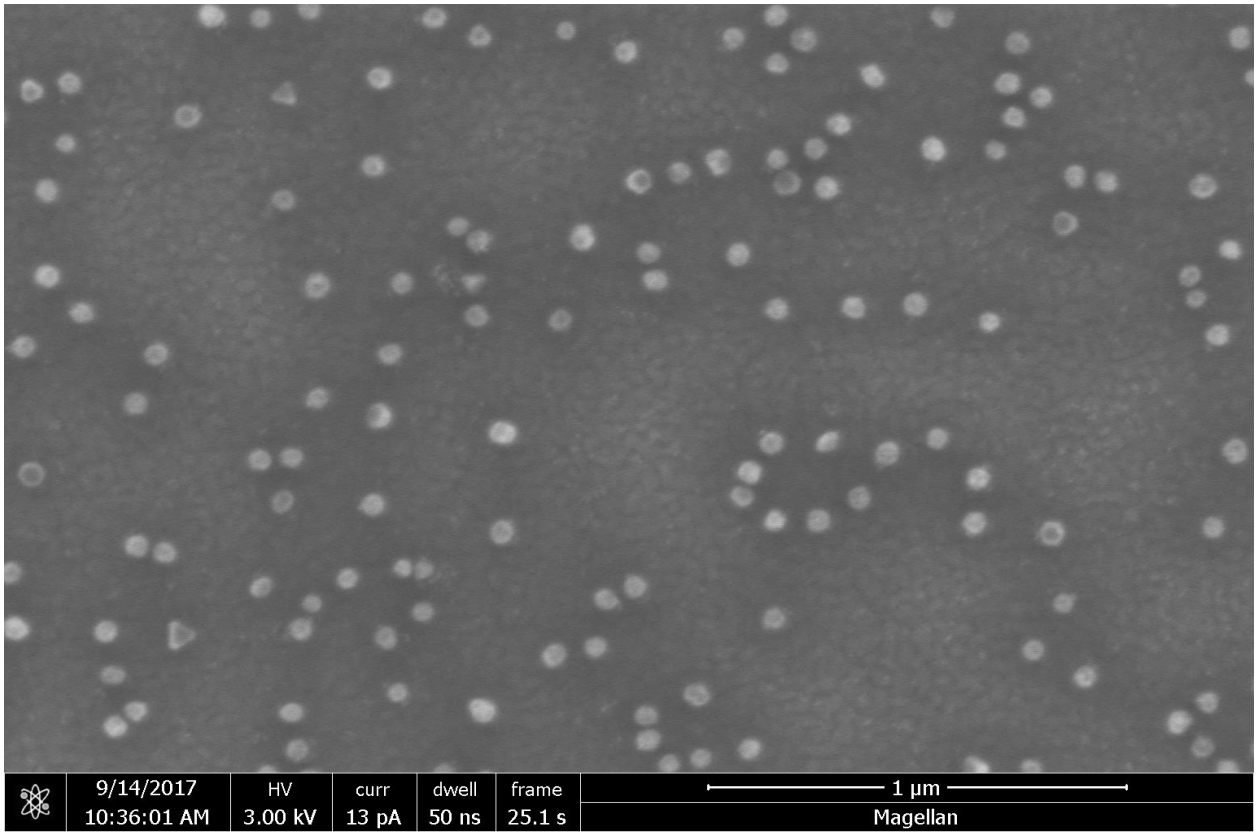

Figure 3 SEM image of gold Nanoshell on gold coated silicon wafer

functionalized nanoparticle solution was then pipetted on these four substrates. After 8 h of incubation, the samples were dried with a stream of air. Each substrate was then placed under Raman system and spectra were collected from these twelve-different conditions.

2.3.4 Functionalizing capture substrate and immunoassay procedures

As shown in Fig. 4, substrates were immersed in 1mM DSP in ethanol for 16 h and then rinsed with ethanol and dried under stream of air. As a result, gold substrates are coated with a layer of DSP. To confine the substrates and form the addressed arrays, we used a patterned stamp made of polydimethylsiloxane (PDMS). PDMS stamps were fabricated by pouring a 10:1 (w/w) mixture of Sylgard 184 elastomer and curing agent and mixture were cured for 1 hour at 80ºC. The PDMS stamp was first patterned with a 3×15 array of punched holes (diameter d = 3 mm) and then immersed in 2 mM ODT for 1 min. ODT is a water-soluble sulfur compound, which can bind to gold surface and form a strong hydrophobic layer. Dried PDMS stamp was then pressed on to the gold substrate to transfer ODT to gold substrates. As a result, addresses surrounded with hydrophobic ODT monolayer were formed to confine droplets of aqueous samples.

Antibodies conjugation to each of three substrates were conducted as follow; addresses were modified with MMP7, CA19 and MUC4 primary antibody. (Fig. 4). For each capture address 10 µL, 100 µg* mL^{-1} antibodies were used. All coated substrates were reacted with antibodies for 8 h in a humidity chamber. Thus, a capture antibodies layer was formed by attaching to succinimidyl ester of DSP on the substrate. Antibodies were then aspirated by rinsing with 10mM PBS. Rinsing was performed by reverse pipetting for five times with the same pipette tip to avoid contamination. Next, 20 µL of StartingBlock blocking buffer was added to each address to react for 16 h, then the capture substrates were ready to use.

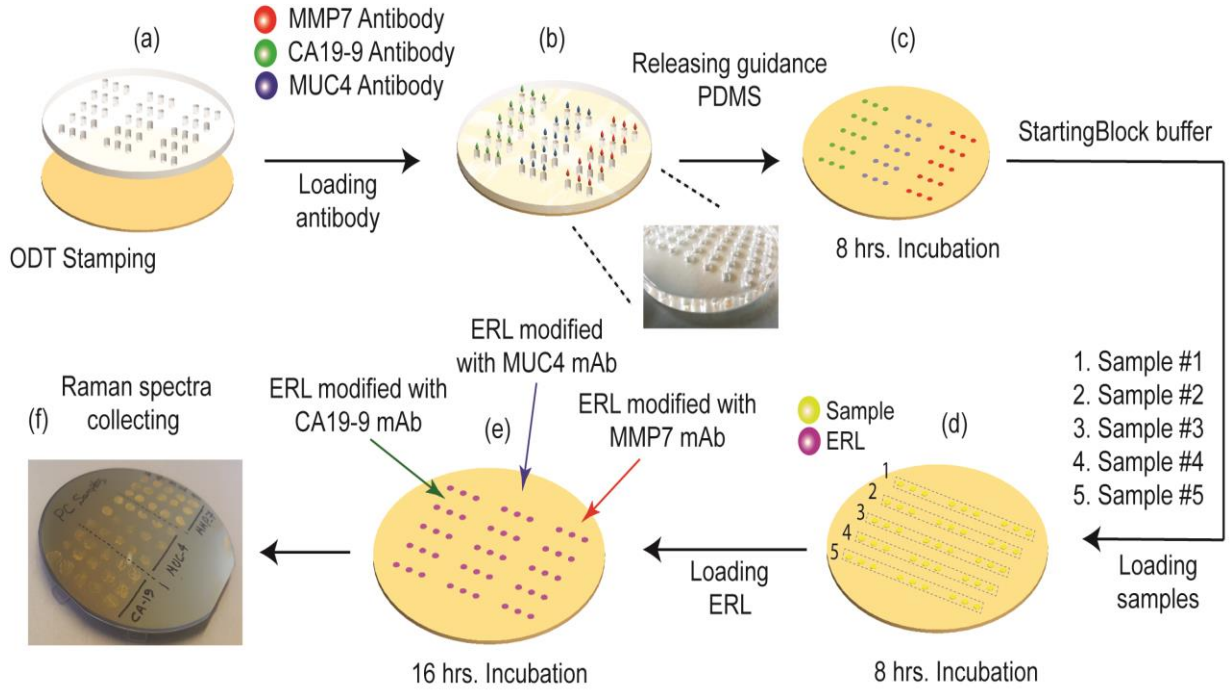

Figure 4. A micropatterning approach for the multiplex detection of MMP7, MUC4 and CA19-9 levels in serum samples using the SERS-based immunoassay. (a) The PDMS stamp was first patterned with a 3×15 array of punched holes (diameter d = 3 mm) and then immersed in 2 mM ODT for 1 min, dried PDMS stamp was then pressed on to the gold substrate. (b) 10 µl, 100 $\mu g\ ml^{-1}$ antibodies were loaded in to the capture addresses. (c) The addresses were then exposed with blocking buffer, (d) serum samples and (e) ERL. (f) Finally, Raman signals from 5 random positions were collected from each capture address.

After ERL and capture substrates functionalization, the substrates should be loaded with samples. For protein spiking assay, captured substrates were exposed to 20 µL of different concentrations of MMP7, MUC4 and CA19-9 recombinant proteins. Concentrations between 20 µg/ml down to 2 ng/ml were spiked in pooled human sera. For clinical samples, 20 µL of undiluted sera were applied and left in humidity chamber. After 8 h incubation, each sample area was rinsed with buffer (2 mM borate, 150 mM NaCl) via reversed pipetting. Captured antigens were then labeled by exposing addresses with 20 µL of related ERL suspension for 16 h in humidity chamber (Fig. 4). Finally, the substrates were rinsed with buffer (2 mM borate, 150 mM NaCl), and dried with a stream of air, and analyzed by the Raman device.

2.3.5 ELISA quantification

The micro-ELISA plate has been pre-coated with a CA19-9 antibody specific to Human CA-19-9. The standard sample was centrifuged at 10000xg for one minute and serially diluted to 200, 67, 22, 7.4, 2.5, 0.8, and 0.27 ng/mL. 100 uL of each concentration of standard samples were added in designated wells. The plate was covered with the sealer and was subsequently incubated for 90 minutes at 37 °C. The plate was then was washed and blotted. Standards or samples are plated in wells and combined with the specific antibody. Immediately 100 uL of Biotinylated Detection antibody was added to each well covered with the plate sealer and gently mixed up. After a 1-hour incubation, the solution was washed and blotted from each well, followed by adding 100 uL Avidin Horseradish Peroxidase (HRP) conjugate solution to each well. Free components were washed away. The substrate solution (TMB) was then added to each well. Only those wells that contain Human CA19-9, biotinylated detection antibody, and Avidin-HRP conjugate appeared blue in color. In the next step, the enzyme-substrate reaction was terminated by the addition of the stop solution, and the color turned yellow. The optical density (OD) was measured spectrophotometrically at a wavelength of 450 nm ± 2 nm. The OD value is proportional to the concentration of CA19-9. The concentration of CA19-9 in the samples and individuals can be calculated by comparing the OD of the samples to the standard curve.

2.3.6 SERS readout instrument

All the measurements and Raman spectra collection were performed with portable BWS415 i-Raman from B&W TEK Co. The incident laser light was focused to 85 μm spot size on the substrate normal incidence. The working distance is 5.9 mm. The light source has a power of 499.95 mW, and an excitation wavelength of 785 nm, and the same objective was used to collect

the scattered radiation. The antigen concentration was quantified using ($v_s(No_2)$) of 4-NBT intensity at the 1336 cm^{-1} position averaged over five readouts on each address. For reproducibility, three addresses were measured for each concentration.

2.3.7 Patient sample collection

Under an IRB approved protocol, patients with pancreatic cancer, benign pancreatic disease and normal control patients were identified from the UMass Memorial Medical Center Chemotherapy Infusion Center and Gastroenterology Clinics. Patients were identified from review

Table 1 Clinical sample characteristics.

Serum Sample	Sex/Age	Sample Characteristics
PC #1	F/38	Metastatic pancreatic adenocarcinoma
PC #2	F/58	Metastatic pancreatic adenocarcinoma
PC #3	M/61	Metastatic pancreatic adenocarcinoma
PC #4	F/88	Locally advanced pancreatic cancer
PC #5	M/57	Metastatic pancreatic adenocarcinoma
Pancreatitis #1	M/41	Acute pancreatitis- gallstone disease
Pancreatitis #2	F/55	Chronic pancreatitis- autoimmune
Pancreatitis #3	M/61	Chronic pancreatitis- alcohol related
Pancreatitis #4	F/43	Chronic pancreatitis-hereditary, cystic fibrosis gene mutation
Pancreatitis #5	M/55	Chronic pancreatitis- alcohol related
Control patients	M:F 3:2/ Age 53-75 Average 62	

of the weekly schedules and consecutive patients were enrolled to avoid bias. Patient gender, age and clinical sample characteristics are shown in table 1. Sera samples (4 ml serum per patient) were collected and immediately processed/frozen for analysis.

2.4 Result and Discussions

2.4.1 Material and platform optimization

We first identified the combination of nanoparticles and substrates that most drastically amplify the SERS signals. As descripted in section 2.3.2 and 2.3.3, we tested the effects of nanoparticles-substrates coupling on the amplification of 4-NBT SERS signals. As shown in Fig.5,

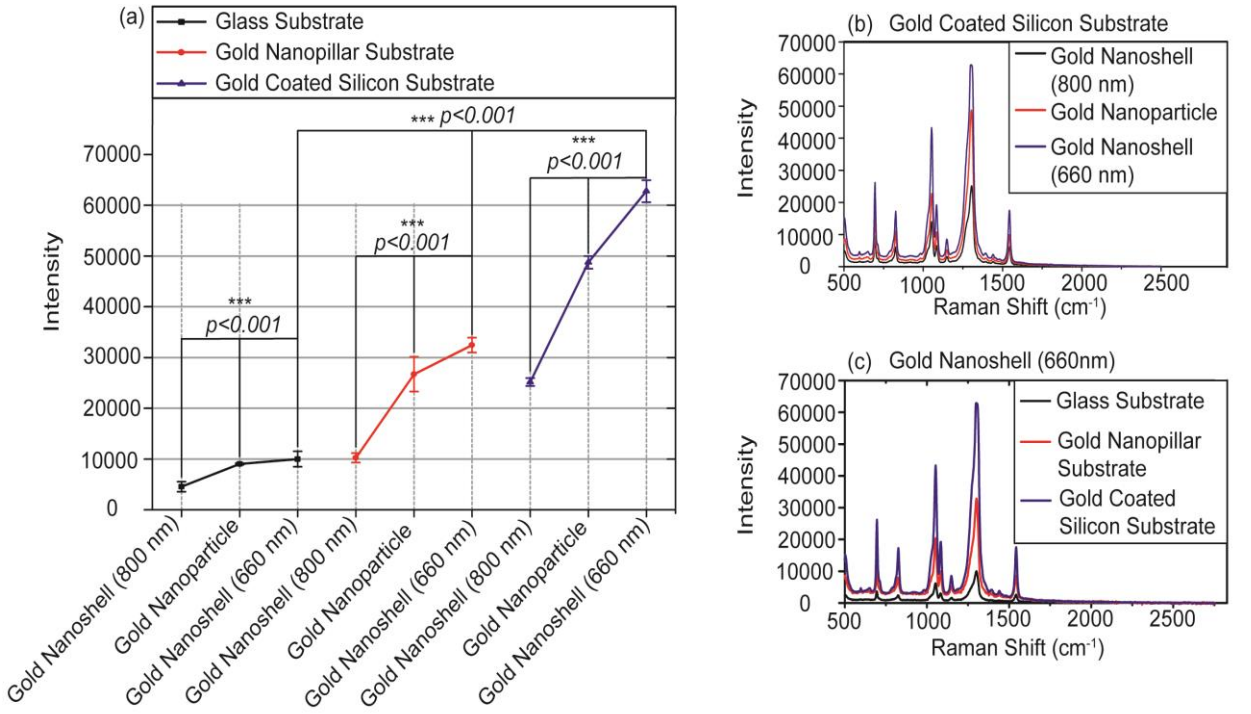

Figure 5. Comparison of the SERS signal enhancement using different combinations of gold nanoparticles and substrates. (a) A plot showing the Raman intensities of 4-NBT (1336 cm^{-1}) enhanced by gold nanoparticles – gold substrate combinations. Each point represents 5 random readout. *P* values were calculated using one-way ANOVA test. ***, $P < 0.001$. (b) A plot showing the complete Raman spectrum acquired from gold coated silicon wafer coupled with different nanoparticles. (c) A plot showing the complete Raman spectrum acquired from gold nanoshells with resonant wavelength of 660 nm coupled with different substrates.

we found that gold nanoshell with resonant wavelength of 660 nm provided highest amplification of the SERS signals, regardless of the substrates used. Moreover, substrates also have a very significant effect. Despite of nanoparticles tested, gold coated silicon substrate consistantly achived the higheset signlaing enhancement as compared with the glass substrate or gold nanopillar substrate. Thus, we will use gold nanoshells with resonant wavelength of 660 nm coupled with gold coated sillicon substrate in our following studies.

We reasoned that the observation here can be attribute to the shifting of surface plasmon resonance (SPR) of the suspended gold nanoparticles towards longer wavelength when immobilized on gold substrates. As reported previously[1,28,29] , the SERS signal is maximized when SPR is shifted between excitation source λ_{ex} (785 nm for our Raman device) and the scattered radiation λ_{sc} (877 nm for 4-NBT). It is known that the gap distance between nanoparticles and substrates can serve as an important factor for changing the maximum SPR and consequently SERS intensity [30]. Our results suggest that a smooth gold surface (coated on silicon) can more

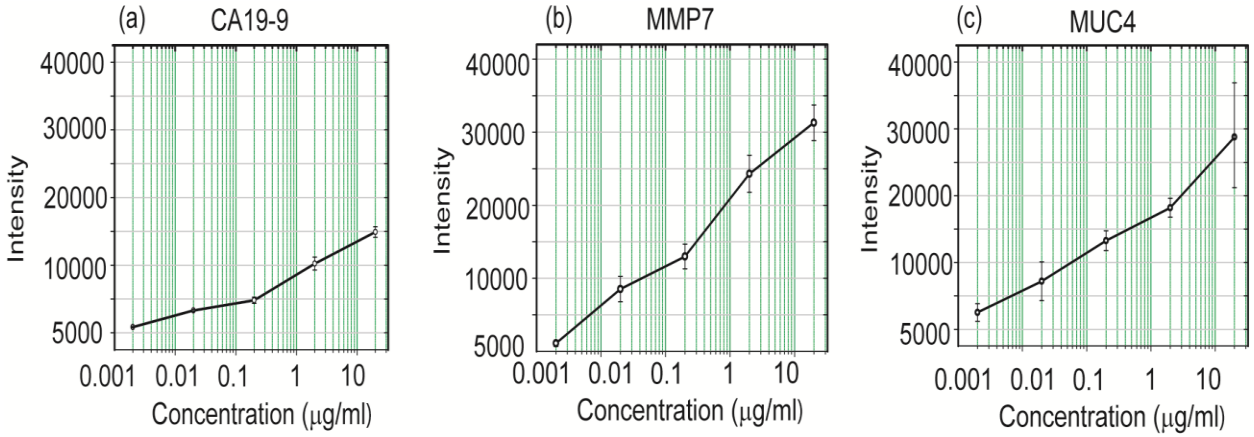

Figure 6 The calibration curve for detecting (a) CA19-9, (b) MMP7 and (c) MUC4 using the SERS-based immunoassay. Corresponding proteins were spiked in buffer solution with concentration increasing from 2 ng* mL^{-1} to 20 μg* mL^{-1}. Error bars Error bars show the standard deviation. Five random spots were measured at each single address, and three addresses were measured for each concentration.

significantly enhance SERS signals compared with rough surfaces (deposited on paper or gold nanopillars), likely through SPR shifting of 660 nm gold nanoshells.

2.4.2 Detection of spiked PC biomarkers in pooled human sera

We next prepared antibody-conjugated ERLs to determine the detection limit of three potential PC biomarkers, MUC4, MMP7 and CA19-9, using the SERS based approach. We spiked corresponding recombinant proteins in the pooled human serum with a serial dilution. As shown in Fig. 6, as spiked protein concentration increased from 2 ng* mL^{-1} to 20 µg* mL^{-1}, SERS signals also steadily increased as a function of analyte concentration. These results suggest that our platform has potential to detect under 2 ng* mL^{-1} concentration of each measured PC biomarker. This detection sensitivity should be sufficient to distinguish those biomarkers in healthy individuals and PC patients based on reported ranges [15,31-34].

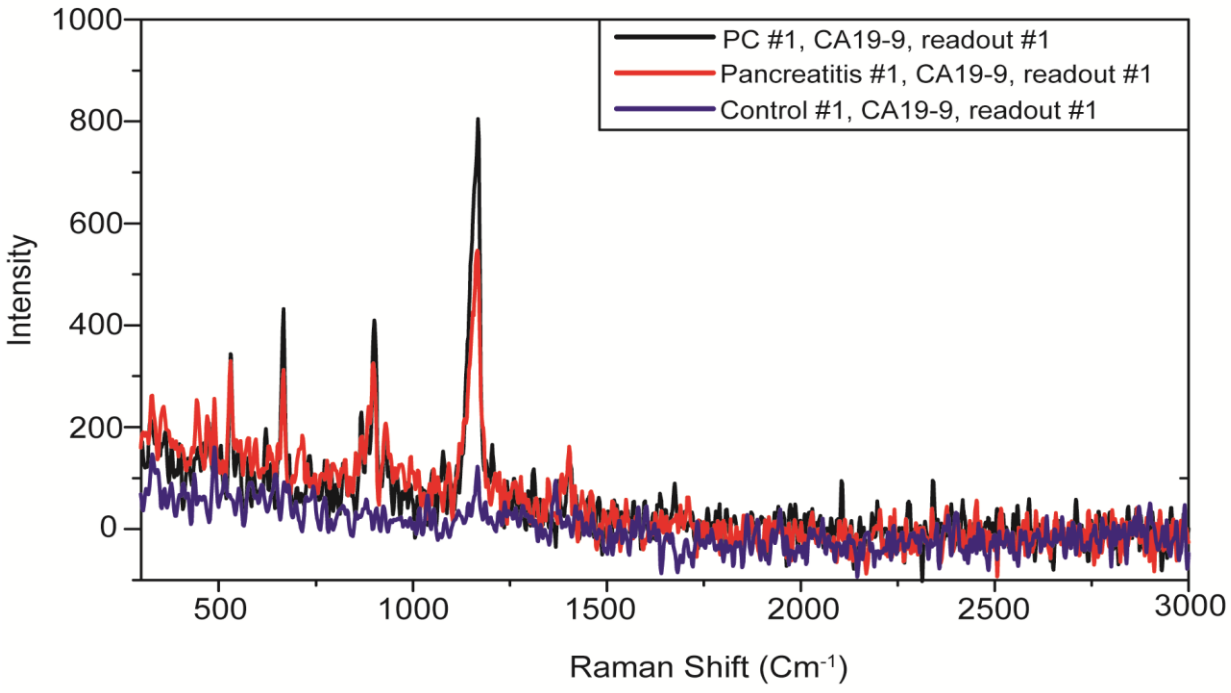

Figure 7 First readout of SERS spectra for detection of CA19-9 in PC#1, Pancreatitis #1 and control #1

2.4.3 Detection of PC biomarkers in patient sample

We further evaluated whether this SERS based immunoassay can detect these biomarkers in PC patients. A total of 15 sera samples were collected, from five normal individuals, five patients with various types of pancreatitis but not PC, and five PC patients. As an example of biomarker's spectra which can be detected by assay, few SERS readouts are demonstrated in Fig. 7. As shown in Fig. 8 and appendix figure 1, significantly higher levels of MUC4, MMP7, and CA19-9 were detected in PC patients compared with normal controls and pancreatitis patients, while a marginal increase of these markers were found in pancreatitis patients.

To evaluate the sensitivity and robustness of this assay, we further calculated the Z-score of each marker, which is determined by the following equation [35].

$$Z_i = \frac{x_i - \bar{\mu}}{\sigma} \qquad (1)$$

Where the x_i is sample's intensity, $\bar{\mu}$ and σ are mean and population standard deviation of normal controls.

As shown in Fig. 8c, CA19-9 appears to have the best predicting capability because its averaged Z-score for PC patients is 2.96 folds larger than that of pancreatitis patients. Averaged Z-scores of MMP7 and MUC4 for PC patients are 2.78 and 2.2 folds larger than that of pancreatitis patients. Although CA19-9 shows a high sensitivity for diagnosing PC patients, its level also elevates significantly in patients with pancreatitis, as illustrated in Fig. 8b&c. It is notable that 6% to 9% of pancreatic resection for suspected PC are done inappropriately for pancreatitis, partially due to the lack of selectivity of CA 19-9[15,36]. Our results here highlight the importance of

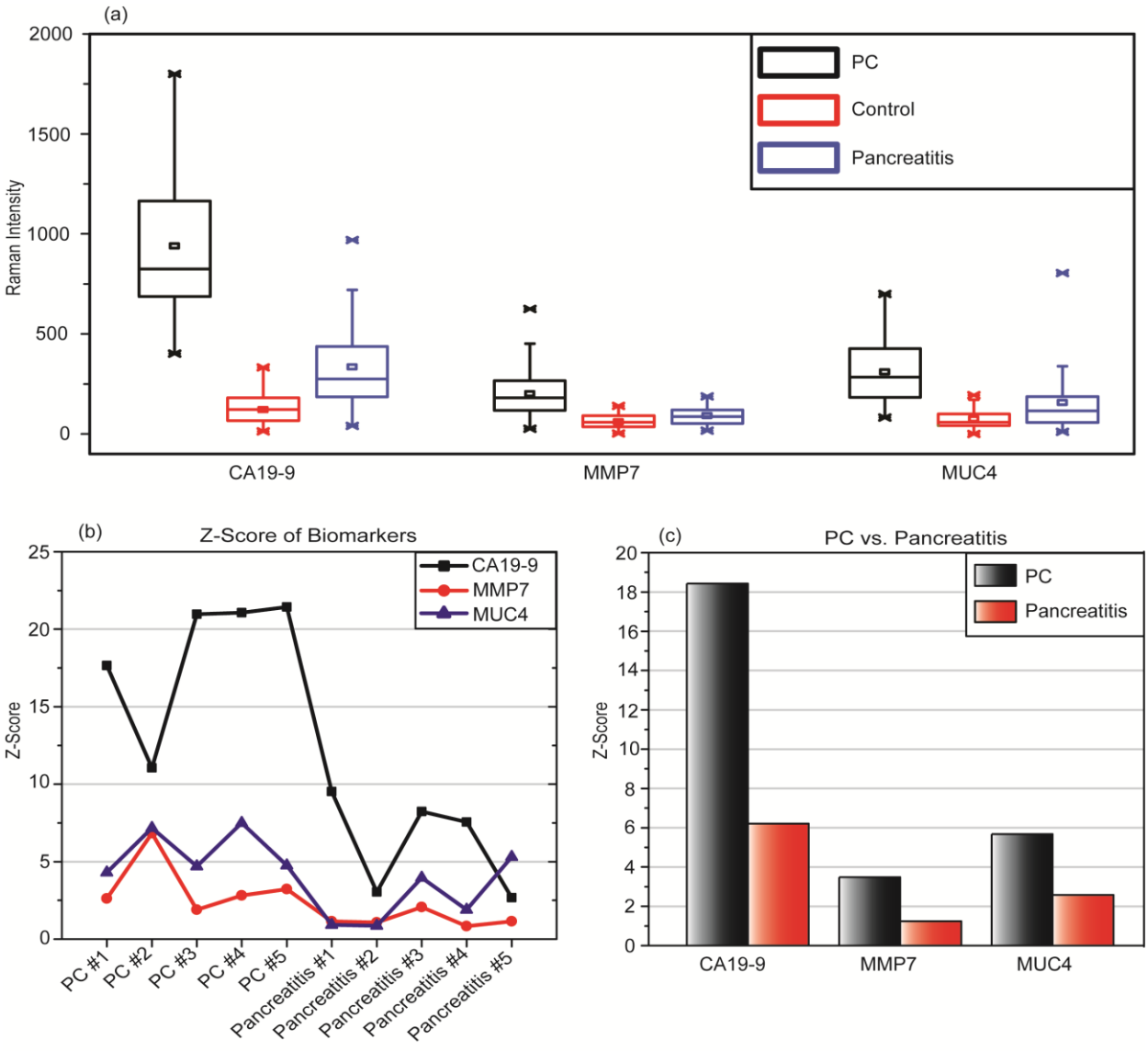

Figure 8. Multiplex detection of MMP7, MUC4 and CA19-9 levels in serum of normal, PC and pancreatitis samples (total of 15 sera samples) using the SERS-based immunoassay. (a) Raman intensities of 4-NBT (1336 cm^{-1}) corresponded to MMP7, MUC4 and CA19-9 in serum samples. Each box represents 15 readouts. (b) Z- scores for each biomarker in PC and pancreatitis serum samples based on mean of total controls. (c) PC vs. pancreatitis Z-

simultaneous detection of other PC biomarkers including MUC4 and MMP7, whose level do not increase in pancreatitis patients but elevate significantly in PC patients.

Notably, one patient (PC #2) has a relatively low level of CA19-9, while the MUC4 and MMP7 level are significantly higher than the pancreatitis group. These results suggest a heterogeneous

expression of different PC biomarkers in patient sera depending on the development stages of the disease and highlight the necessity of multiplex detection. Several pancreatitis patients (#1, #3, #4 and #5) have relatively higher-level expression of these biomarkers, and carefully following up disease development might be necessary based on the test results.

2.4.4 SERS vs. ELISA

To evaluate performance of the proposed technique, the assay was performed using the most common immunoassay technique in the industry, ELISA. Enzyme-Linked Immunosorbent Assay (ELISA) is a common immunoassay, in which antibodies, peptides, proteins, and small biomarkers can be detected and quantified using a multi-well plate. The assay uses a solid-phase type of enzyme immunoassay to detect a protein's presence in a liquid sample using antibodies directed against the protein to be measured.

Sandwich Immunoassay is a type of assay that requires a compatible antibody pair that recognizes different antigenic targets (epitopes) on the same antigen. The first antibody, called the capture antibody, is coated on the plate and used to immobilize the antigen upon binding with the sample during incubation. The free antigen is removed by a washing step, and then a detection antibody is added to bind the captured antigen and enable subsequent detection.

The amount of a target protein within a sample could be precisely determined by setting up a standard curve of the known target protein concentrations using a purified antigen. The preparation of the ELISA standard curve is critical for accurate sample quantification. Estimation of the analyte concentration depends upon the construction of a standard curve, that is prepared by making serial dilutions of the protein standard within a range of concentrations close to the expected concentrations of the unknown samples. The concentration of the unknown samples is determined by interpolation, which relies on a properly generated standard curve. The standard

Plate Maps

Plate 1 of 1	1	2	3	4	5	6	7	8	9	10	11	12
A	200 ng/ml		PC #1			OPC #1			Control #1			
B	66.6 ng/ml		PC #2			OPC #2			Control #2			
C	22.2 ng/ml		PC #3			OPC #3			Control #3			
D	7.4 ng/ml		PC #4			OPC #4			Control #4			
E	2.46 ng/ml		PC #5			OPC #5			Control #5			
F	0.82 ng/ml											
G	0.274 ng/ml											
H	0 ng/ml											
Plate	Elisa 96 well plates											
Capture ug/mL and Detection ug/mL	1 ug/mL Detectio mAb / Biotinylated 1.0 ug/mL mAb											

Raw Data

Plate 1 of 1	1	2	3	4	5	6	7	8	9	10	11	12
A	3.87	3.75	3.131	3.004	2.989	2.87	2.799	2.667	1.33	1.311	1.298	
B	3.12	3.12	2.78	2.701	2.712	1.653	1.676	1.701	1.688	1.705	1.71	
C	2.67	2.61	3.761	3.765	3.841	2.23	2.198	2.311	1.21	1.199	1.229	
D	2.13	2.11	3.423	3.394	3.401	2.01	2.126	2.11	1.891	1.86	1.811	
E	1.67	1.62	3.478	3.402	3.455	1.76	1.681	1.679	1.001	1.114	1.109	
F	0.988	0.97										
G	0.342	0.34										
H	0.05	0.05										
Plate	Elisa 96 well plates											
Capture ug/mL and Detection ug/mL	1 ug/mL Detectio mAb / Biotinylated 1.0 ug/mL mAb											

Analysed

Plate 1 of 1	1	2	3	4	5	6	7	8	9	10	11	12
A	3.8		3.04			2.78			1.31			
B	3.1		2.73			1.68			1.70			
C	2.6		3.79			2.25			1.21			
D	2.1		3.41			2.08			1.85			
E	1.6		3.45			1.71			1.07			
F	1.0											
G	0.3											
H	0.1											
Plate	Elisa 96 well plates											
Capture ug/mL and Detection ug/mL	1 ug/mL Detectio mAb / Biotinylated 1.0 ug/mL mAb											

Figure 9 Plate map, raw data, and the analyzed data for measuring the concentration of CA19-9 in serum samples of standard samples, five pancreatic cancer patients, five pancreatitis patients, and five control samples.

curve should be prepared using purified protein. Fig. 9 shows a plate map, raw data, and the analyzed data for measuring the concentration of CA19-9 in serum samples of standard samples, five pancreatic cancer patients, five pancreatitis patients, and five control samples. As shown in

the Fig. 9, the optical density, which is considered as assay signals in this experiment, decreased from 3.87 to 0.05 by serial dilution of standard samples. the control sample is a buffer that doesn't contain any biomarkers, and the corresponding signal is considered as background noise.

The data was analyzed using a weighted 4-parameter curve. The X-axis is the concentration, and the Y-axis is the adjusted absorbance. This 4-parameter logistic model allows us to extend the range of the standard curve since the range is not limited to a linear, symmetrical region and is only limited by the minimum and maximum detectable dose. The standard curve is weighted so that those standard responses that are more reliable have a greater influence on the computed standard curve than those which are less reliable. The immunoassay dose-response curve is described by the weighted model-based curve equation given below:

$$y = \frac{a - d}{\left(1 + \left(\frac{x}{c}\right)^{b}\right)^{g}} + d \qquad (2)$$

Where:

x = standard concentration

y = response

a = Y value corresponding to asymptote at high values of X-axis

b = Directs the shape of the curve, how rapidly the curve makes its transition from the asymptote at the center of the curve.

c = X value corresponding to the midpoint between a and d

d = Y value corresponding to asymptote at low values of X-axis

Using the 4-parameter logistic model the OD and the concentration of pancreatic cancer patient samples, pancreatitis samples, and healthy individuals were measured and reported in table 2

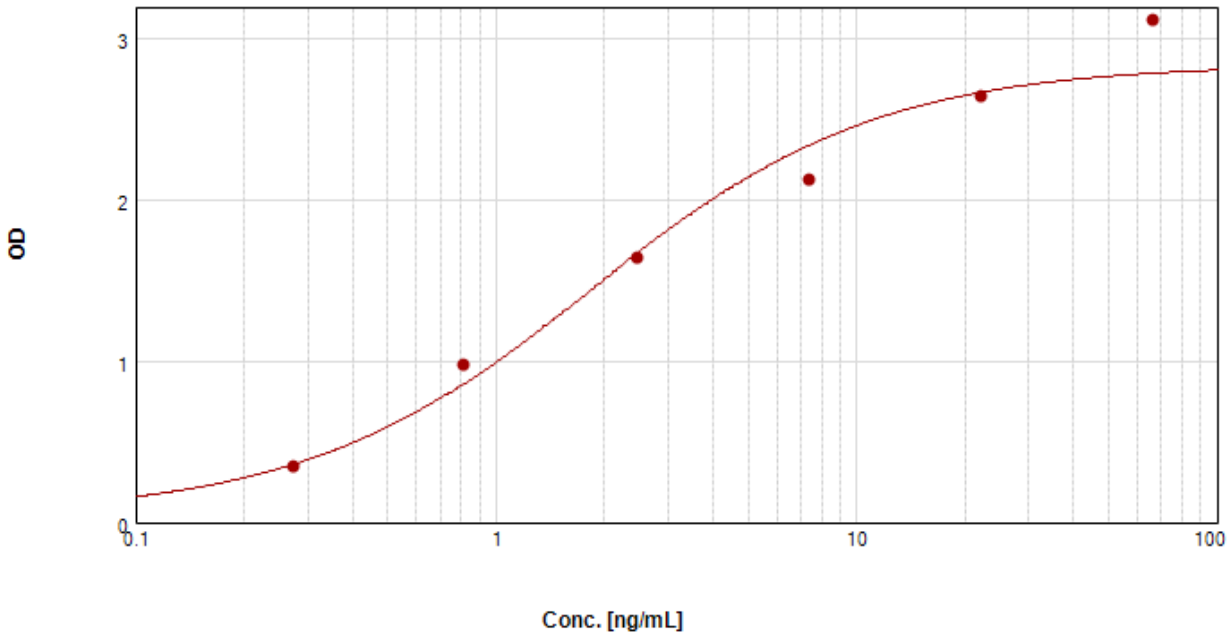

Figure 10 Standard curve of CA19-9 using weighted 4-parameter logistic model.

Table 2 Optical densities and corresponding concentrations of patient samples.

Samples	Optical Density (OD)	Conc. (ng/mL)
PC #1	3.04	45.47
PC #2	2.73	24.92
PC #3	3.79	193.3
PC #4	3.41	92.05
PC #5	3.45	99.26
OPC #1	2.78	27.35
OPC #2	1.68	3.168
OPC #3	2.25	9.73
OPC #4	2.08	7.059
OPC #5	1.71	3.36
Control #1	1.31	1.53
Control #2	1.7	3.32
Control #3	1.21	1.24
Control #4	1.85	4.5
Control #5	1.07	0.94

Here, we compared the ELISA and SERS results of the quantified CA19-9 in the serum of pancreatic cancer, pancreatitis, and control samples. For measuring the concentration of the target biomarker, SERS uses the relative SERS intensity while ELISA uses optical density (OD). Fig. 11 shows the measured values of CA19-9 in all samples using ELISA and SERS approach. The plot indicates good coordination between the data measured with ELISA and SERS. In both methods, the highest signals were measured for pancreatic cancer samples, where PC#1 has the lowest and PC#3-5 have the highest signals. For the signals measured for pancreatitis and control samples,

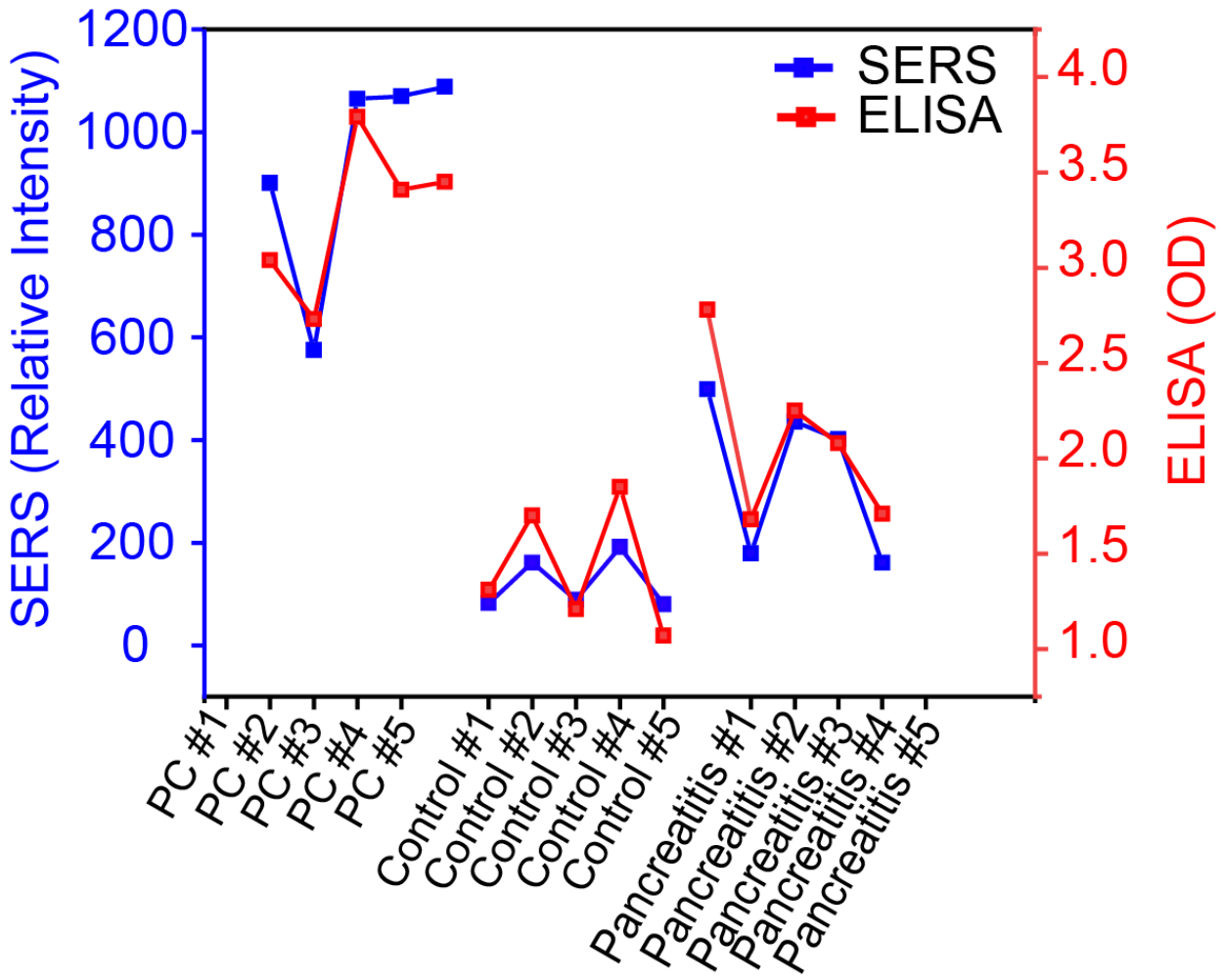

Figure 11 Comparison between SERS and OD signals, which are acquired from five pancreatic cancer patients, five pancreatitis patients, and five control samples.

significant similarity can be observed in the trend of the signals where pancreatitis #1 has the highest signal, and the control sample has the lowest signal.

2.5 Conclusion

This study demonstrated that immobilization of functionalized gold nanoshells with resonance wavelength of 660 nm on the gold coated silicon substrate lead to a significant improvement of SERS signals. Using a multiplex, high-throughput SERS-based immunoassay platform, we successfully detected three PC biomarkers, CA19-9, MMP7 and MUC4, in spiked sera samples at the concentration as low as 2 ng* mL^{-1}. Also, for the first-time, simultaneous detection of these three biomarkers was accomplished using a micropatterning approach for PC and pancreatitis patient samples. Our findings demonstrate the great promise of using SERS as a low-cost, high-sensitivity, and high-throughput approach for the emerging liquid biopsy diagnostics.

2.6. Acknowledgements

This work is supported by a IALS Seed Grant from the University of Massachusetts Amherst.

CHAPTER 3

SERS-BASED IMMUNOASSAY DETECTION OF TUMOR-DERIVED EXTRACELLULAR VESICLES TO DIFFERENTIATE PANCREATIC CANCERS FROM CHRONIC PANCREATITIS

3.1 Abstract

Pancreatic cancer (PC) is an aggressive malignancy with an exceptionally high mortality rate because it lacks effective early diagnosis methods. To improve the ability to diagnose PC, the identification of biomarkers that can differentiate PC patients from both normal controls (NC) and those with chronic pancreatitis (CP) is vital. This study demonstrates the detection of extracellular vesicles (EVs) as an excellent resource of diagnostic biomarkers in serum samples from NC individuals, and CP and PC patients using a SERS-based immunoassay technique. The assay uses the Au-CD81-EVs-EphA2-Au complex to capture PC tumor-derived EVs specifically and produces highly localized regions of intense field enhancement (hot spots) concurrently. Applying a machine learning algorithm to the analysis of the expression level of EVs biomarkers in PC, CP and NC individuals, the sensitivity and specificity were measured as 0.95 and 0.96 respectively. Measuring PC tumor-derived EVs' expression levels in serum of PC patients, CP patients, and NC individuals suggests the great potential of using this biomarker to differentiate pancreatic cancers from chronic pancreatitis.

3.2 Introduction

Cancer is a leading cause of death worldwide that accounted for 18.1 million new cases and 9.6 million deaths in 2018[37]. Among all types of cancer, pancreatic cancer (PC) has the highest

mortality rate, with a five-year survival rate of 8% that has not improved over the past 40 years[6,7]. Most patients are found to be in an advanced stage with metastasis at the time of diagnosis[38]. An early, accurate, and sensitive diagnosis can lead to effective cancer management by decreasing the treatment cost, enhancing the overall survival rate substantially[39], and enhancing cancer treatment efficacy significantly[40].

One of the principal challenges in pancreatic cancer diagnosis is to distinguish pancreatic cancer (PC) patients from chronic pancreatitis (CP) patients and healthy individuals[41-43]. CP and PC present with similar symptoms and signs frequently, which makes differential diagnosis difficult[44-46]. The expression level of the only approved serum marker for PC's diagnosis and prognosis (CA 19-9) can be elevated in both PC and CP patients[47,48]. Notably, 6%–9% of pancreatic resections for suspected PC are performed inappropriately in cases of pancreatitis, attributable in part to CA 19-9's lack of selectivity [49,50]. Various studies have attempted to solve this dilemma; however, effective diagnostic methods to detect PC and differentiate it from CP remain insufficient[51]. Thus, biomarkers in biofluids and convenient diagnostic methods that can be employed effectively for the differential diagnosis of CP and PC are needed for effective therapy and to reduce cancer mortality. In addition to protein biomarkers, extracellular vehicles (EVs) that are secreted from cancer cells represent a good source of such biomarkers.

EVs are a heterogeneous group of cell-derived membranous structures. These particles can be released from a cell naturally but cannot replicate. Most cells secrete abundant EVs into the extracellular space, and therefore, can be found in biological fluids[52-54]. Further, EVs are involved in multiple physiological and pathological processes and carry a cargo of proteins, nucleic acids, lipids, and metabolites[55,56]. EVs play an active role in tumor initiation, progression, and metastasis[57-59] because of their ability to communicate between cells using their cargo of protein

and nucleic acids[60-62]. Therefore, circulating tumor-derived EVs can be considered excellent potential cancer biomarkers for liquid biopsy and cancer detection[63-66]. More importantly, PC-derived EVs represent a likely source for a biomarker that can discriminate between PC and CP patients. Cancer cells express differentially multiple factors present in circulating EVs that are secreted by pancreatic tumors and not present in patients with CP[67,68]. In recent years significant efforts have been dedicated to developing novel biosensors for EV detection based on microfluidics, nanomaterials, or plasmonics[69-73]. However, the majority of these platforms are only proof of concept.

Among many approaches to detect cancer biomarkers in serum, Surface Enhanced Raman Spectroscopy (SERS) is an emerging technology that provides highly sensitive intrinsic fingerprint information on biomarkers[2,74-76]. Quantification of biomarkers based on SERS intensity is affiliated with experimental parameter factors that prevent biomarkers standard detection. This method is cumbersome, and immobilization of functionalized gold particles (NPs) are often associated with technical issues such as the inhomogeneous distribution of NPs on substrates during multiple manual washing steps. During the past two decades, SERS has become one of the most attractive analytical tools for immunoassay[77-79]. A SERS immunoassay is usually developed with a sandwich structure, in which two types of antibodies are used as capture and detection components[80].

Employing EVs as a cancer biomarker requires a detection technique that differentiates between normal and tumor-derived EVs. Specific detection of tumor-derived EVs among normal EVs has been challenging during past decades because of the small number of tumor-derived EVs in body fluids, which has prevented its clinical applications, such as early detection. It has been difficult to detect tumor-derived EVs with conventional methods, as they require EV purification

and subsequent analysis to quantify the relative abundance of the candidate diagnosis[81]. This study investigates the efficiency of a SERS-based immunoassay technique in detecting tumor-derived EVs in the serum of cancer patient samples and its ability to differentiate between PC and CP patients.

3.3 Experimental Details

3.3.1 Reagent

Gold nanoparticles (60 nm in diameter, 2.6X1010 particles ml−1) were purchased from Ted Pella. Sodium chloride, StartingBlock, and borate buffer (50mM) were obtained from ThermoFisher Scientific. Dithiobis-(succinimidyl propionate) (DSP), dimethylsulfoxide (DMSO), 4-Nitrobenzenethiol (4-NBT), acetonitrile, phosphate buffered saline (PBS), and bovine serum albumin (BSA) were acquired from Sigma Aldrich.

In our SERS-based immunoassay, CD81 and EphA2 antibodies were used to modify the capture substrate and gold nanoparticles, respectively. CD81 monoclonal antibody was purchased from Abcam, and EphA2 monoclonal antibody was obtained from ThermoFisher.

3.3.2 Functionalizing the substrate and capturing nonspecific EVs

The optimization of Extrinsic Raman Labels (ERL) has been described previously[82] and chapter 2.3.2. As a part of the method development, we optimized the signal and enhancement factor by examining the effects of gold particle size and type, the gap distance between the immobilized particle and the underlying substrate, and substrate materials on the amplification of Raman signals. The enhancement factor of our optimized sandwich immunoassay platform was estimated to be ~10^{7}[82]. We demonstrated that the immobilization of functionalized gold

nanoparticles with a resonance wavelength of 540 nm and a diameter of 60 nm on the gold-coated silicon substrate leads to a significant improvement of SERS signals.

Sandwich immunoassay conventionally uses two antibodies to bind to different binding sites (epitopes) of the antigen. One type of antibody that is used in sandwich immunoassay serves as a capture antibody. The capture antibody is responsible for capturing the antigen from the matrix and immobilizing it on the binding surface. CD81 is a recognized EV-marker protein for capturing EV and is expressed on EVs of all pancreatic cell lines of the capture antibody[83,84]. We therefore used antibodies that were enriched on EV membranes against CD81 to capture all EVs (including normal and tumor-derived) present in the serum sample. The self-assembled monolayers of thiols on gold surfaces are one of the most popular model systems for immunoassays. DSP is a thiol

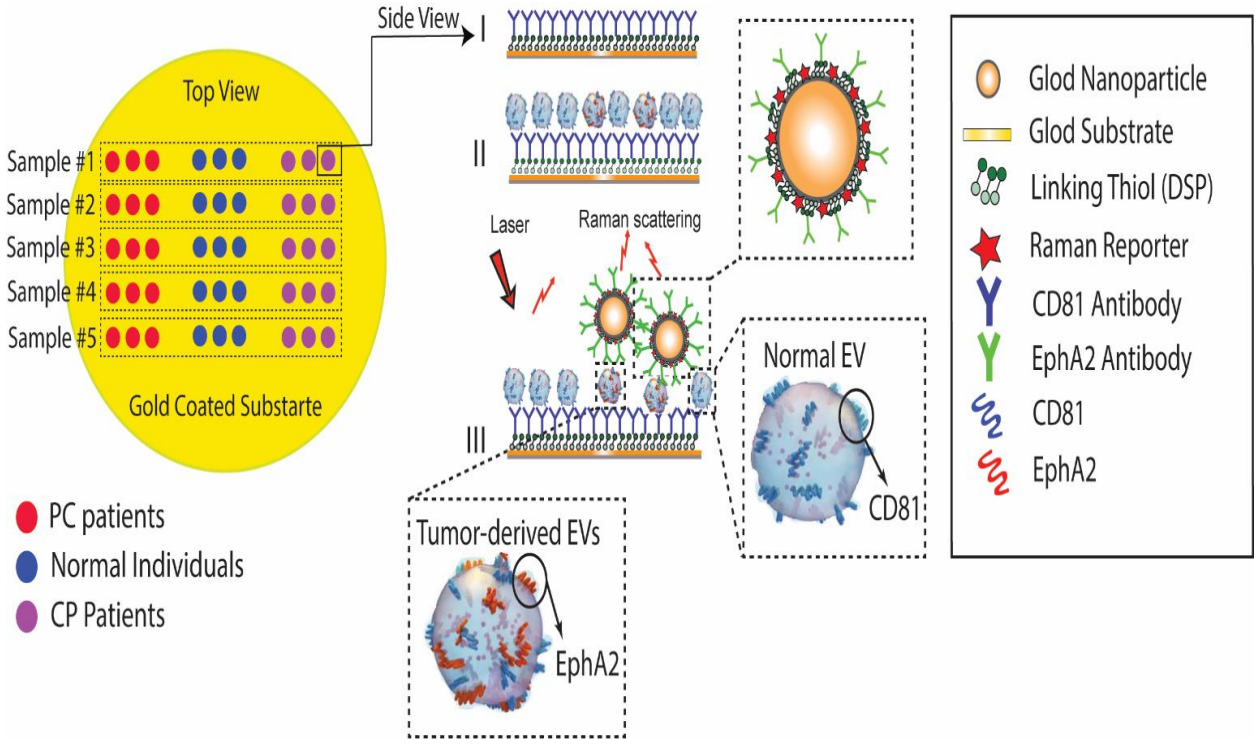

Figure 12 A SERS-based immunoassay for PC tumor-derived EVs quantification: (I) Functionalizing gold substrate with thiol and CD81 antibody; (II) Capturing normal and tumor-derived EVs present in the serum sample. (III) Loading EphA2-NPs-Reporter to enhance Raman signal and selectively label tumor-derived EVs

molecule that was used in the experiment to immobilize the CD81 antibody on the gold-coated substrate. The strength of the gold–sulfur (Au–S) interaction that is formed between thiol and gold surfaces provides spontaneous binding of DSP to the gold surface. DSP also has succinimidyl functionalities to facile covalent binding of antibodies to the substrate.

The DSP coated substrate was then modified with the CD81 antibody (Fig.12). 10 µl of 10 µgml−1 antibodies were used for each capture address. DSP coated substrate was then reacted with the antibody for 2 hours. Thus, a capture antibodies layer was formed by attaching to succinimidyl ester of DSP on the substrate. The antibody was then rinsed by PBS. Next, 10 µL of StartingBlock blocking buffer was applied to each address to react for 10 hours; then, the capture substrates were ready to use.

After the ERL and capture substrates functionalization, the substrates should be loaded with samples. 20 µL of undiluted clinical sera samples, were applied on the substrate, and after 6 hours of incubation, it was rinsed with buffer (2 mM borate, 150 mM NaCl). Captured antigens were then labeled by applying each address with 10 µL of ERL suspension for 10 hours. Finally, the substrates were rinsed with buffer (2 mM borate, 150 mM NaCl) and analyzed by the Raman device.

3.3.3 Preparation of ERL and labeling tumor-derived EVs

In this study, functionalized gold nanoparticles were designed to bind to the PC tumor-derived EVs specifically. Gold nanoparticles were used as carrier components for EphA2 and SERS labels. EphA2 antibody was immobilized on the gold particles using DSP to detect overexpressed antigen markers on the tumor-derived EVs. Therefore, modified nanoparticles specifically discriminate between tumor-derived EVs, which have high expression of EphA2 on their membrane, and normal EVs, which were already captured on the substrate using CD81, a

common protein marker on all secreted EVs. 4-NBT was used as a reporter molecule to provide intense Raman signal due to its aryl nitro group with an intrinsically strong Raman active vibrational mode. 4-NBT also contains a disulfide group for spontaneous chemisorption to the gold particles.

Details of the procedure for the preparation of functionalized gold nanoparticles are as follows. 1.0 mL suspension of gold nanoparticles, 40 mL of 50 mM borate buffer, 2.0 mL of 1.0 mM DSP in DMSO, and 8.0 mL of 1.0 mM 4-NBT solution in acetonitrile were mixed and left to react for 8 hours. To discard excess thiols, the suspension was centrifuged at 2000g for 10 minutes, and the supernatant was removed with a syringe. Gold nanoparticles were resuspended in 2.0 mM borate buffer. ERL preparation was continued by adding 20 mg of EphA2 antibodies to the suspension and incubating for 8 hours at 4°C. Next, 100 mL of 10% BSA was added to the suspension to stabilize the suspension and block nonspecific binding sites and unreacted succinimidyl for 8 hours. After the interaction between ERL and the blocking buffer, the solution needs to be rinsed three times. For the rinsing process, the suspension was centrifuged, and after decanting the clear supernatant, the loose red sediment was resuspended in 1.0 mL of 2.0 mM borate buffer containing 1% BSA. The triple rinsed ERL pellet was then resuspended in 0.5 mL of 2.0 mM borate buffer containing 1% BSA to obtain a final solution with the desired concentration of gold nanoparticles. Finally, the suspension was modified with 50 mL of 10% NaCl for stabilization and then passed through a 0.22 mm syringe filter to remove any large aggregates. The substrate modified with antibody was exposed to 20 μl of different serum samples. After 2 hours of incubation, each sample area was rinsed with buffer (2 mM borate, 150mM NaCl) via reversed pipetting. Captured EVs were then labeled by loading 20 μl of modified gold nanoparticle suspension for 8 hours in the humidity chamber. In the end, the substrates were rinsed

with buffer (2 mM borate, 150mM NaCl) and dried with a stream of air, and finally analyzed by the Raman device.

3.3.4 SERS readout instrumentation and quantification

All the measurements and Raman spectra collection were performed with portable BWS415 i-Raman from B&W TEK Co. The incident laser light was focused on 85 µm spot size on the normal substrate incidence. The working distance is 5.9 mm. The light source has a 499.95 mW power and an excitation wavelength of 785 nm, and the same objective was used to collect the scattered radiation.

Fig. 13 shows the method used to quantify biomarkers' expression levels. An SEM image of captured EVs-ERL is shown in Fig. 13.a, where the EVs-ERL complexes are formed using

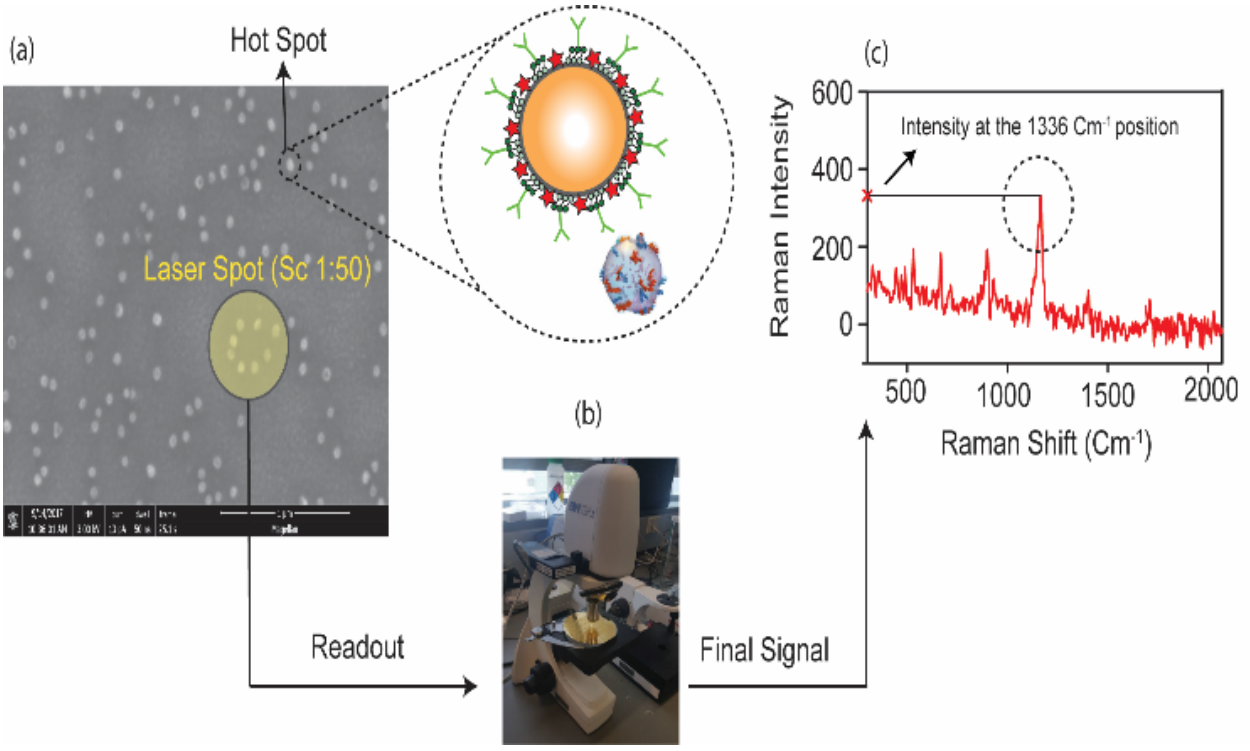

Figure 13 EVs quantification method (a) SEM image of captured ERL-EVs on the gold coated substrate (b) collecting the SERS signal using Raman spectroscopy (c) The EVs concentration was quantified using ($v_s(No_2)$) of 4-NBT intensity at the 1336 cm^{-1}.

sandwich immunoassay and hot spots that help enhance the signal. The hot spots are the junctions between gold nanoparticles and a gold substrate, where certain resonances in highly spatially localized regions are the source of an extremely enhanced local field[85]. The EVs concentration was quantified using ($v_s(No_2)$) of 4-NBT intensity at the 1336 cm^{-1}, which has the maximum intensity among all of the 4-NBt signal peaks (Fig. 13.c). As an example of the biomarker's spectra, the SERS readout is illustrated in Fig 13.c. For reproducibility, three addresses were measured for each concentration, and a total of 10 readouts on each sample's biomarker were obtained.

3.3.5 Patient sample collection and samples characteristics

Under an IRB approved protocol, patients with PC, CP, and NC patients were identified from the UMass Memorial Medical Center Chemotherapy Infusion Center and Gastroenterology Clinics. Patients were identified from a review of the weekly schedules, and consecutive patients were enrolled to avoid bias. Patient gender, age, and clinical sample characteristics are presented in table 3. Sera samples (4 ml serum per patient) were collected and immediately processed/frozen for analysis.

Table 3. Clinical Sample Characteristics

Serum Sample	Sex/Age	Sample Characteristics
PC #1	F/38	Metastatic pancreatic adenocarcinoma
PC #2	F/58	Metastatic pancreatic adenocarcinoma
PC #3	M/61	Metastatic pancreatic adenocarcinoma
PC #4	F/88	Locally advanced pancreatic cancer
PC #5	M/57	Metastatic pancreatic adenocarcinoma
CP #1	M/41	Acute pancreatitis- gallstone disease
CP #2	F/55	Chronic pancreatitis- autoimmune
CP #3	M/61	Chronic pancreatitis- alcohol related
CP #4	F/43	Chronic pancreatitis-hereditary, cystic fibrosis gene mutation
CP #5	M/55	Chronic pancreatitis- alcohol related
Control	M:F 3:2/ Age 53-75 Average 62	

3.4 Result and discussion

3.4.1 Detection of PC tumor-derived EVs in patient samples

Several protein markers can be found conventionally on the standard EVs' membrane. As an example, CD9, CD63, and CD81 are EV-enriched membrane biomarkers present on EVs derived from most cells[86,87]. However, only a few proteins on the EVs membrane represent cancer-associated biomarkers. Through comprehensive analysis of EVs from normal and tumor-derived pancreatic cell lines, Ephrin type-A receptor 2 (EphA2) has been identified as a good candidate biomarker that was enriched selectively on pancreatic cancer cells' EVs[88,89]. In this analysis, 128 membrane proteins were investigated, of which only 26 were expressed on the EVs of at least 2 of the 3 PC cell lines. According to the Oncoming database, of these 26 membrane proteins, only

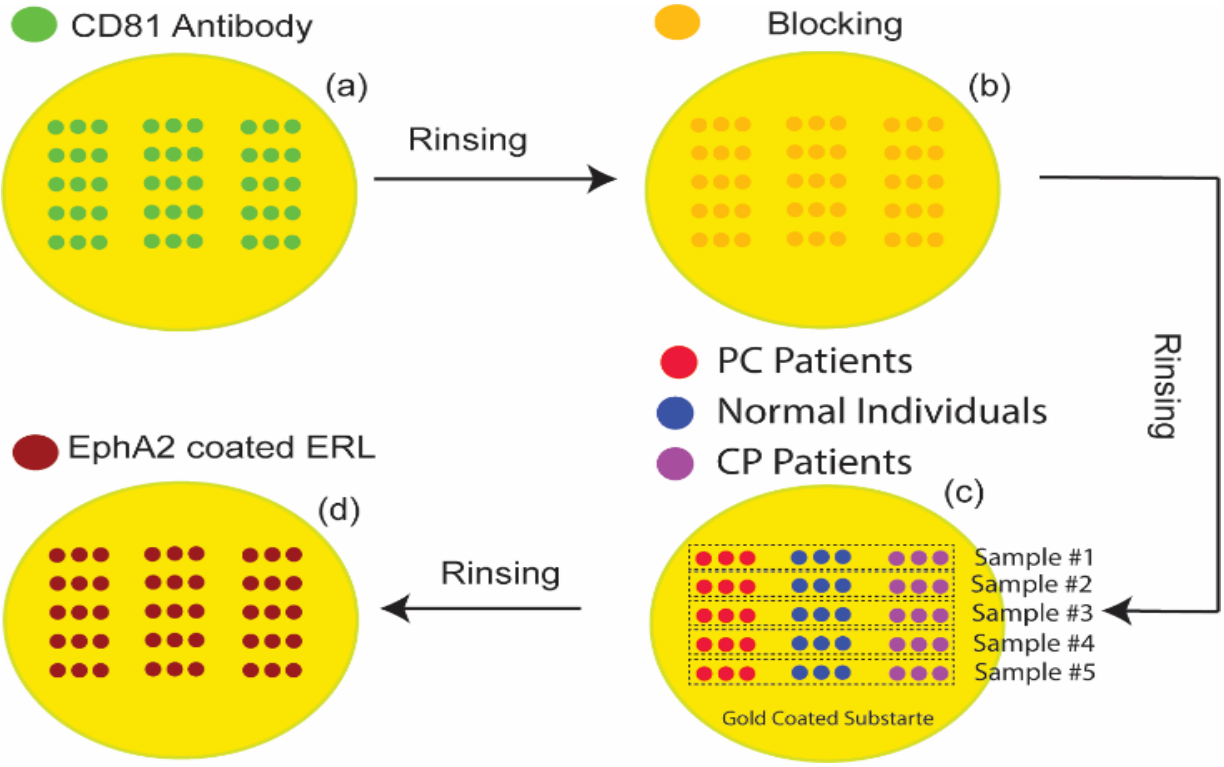

Figure 14 Experimental setup for detection of PC tumor-derived EVs in levels in serum samples of PC, CP and NC individuals. For reproducibility, three addresses were measured for each concentration and a total of 10 readouts on each sample's biomarker were obtained.

EphA2 exhibited significantly higher expression in human PC tissue samples than CP or NC pancreatic tissue samples[90,91]. EphA2 plays a critical role in PC progression, metastasis, and prognosis.[81]

Serum samples from five healthy individuals, five CP patients, and five PC patients were analyzed and compared to evaluate the specificity of the proposed SERS-based CD81-EphA2 complex in detecting PC tumor-derived EVs. Serum samples from these three groups were selected to determine the PC specificity of the EphA2-EV (CD81-EphA2) and general-EV (CD81) detection and quantification systems. Fig. 14 demonstrates the experimental setup for the quantification of PC tumor-derived EVs in serum samples of PC, CP, and NC.

As shown in Fig. 15a and b, significantly higher levels of PC tumor-derived EVs were detected in PC patients compared to CP patients and NC individuals. There was a significant mean

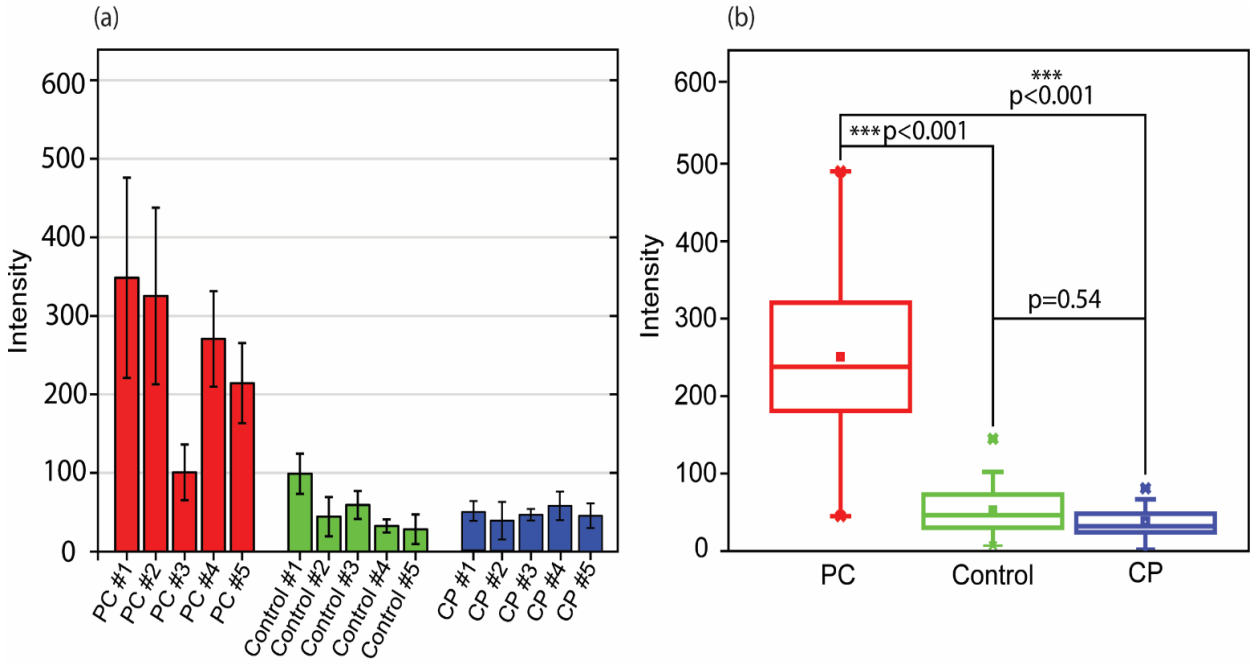

Figure 15 Quantification of tumor-derived EVs in serum samples of PC, CP and NC individuals (total of 15 sera samples) using the SERS-based immunoassay. (a) Raman intensities of 4-NBT (1336 cm−1) corresponded to number of captured tumor-derived EVs in serum samples. (b) Plot box of expression level of tumor-derived EVs in PC, CP and NC individuals. P values were calculated using one-way ANOVA test. ***, P < 0.001. Tukey's post hoc test revealed significant mean differences between PC and CP samples (p < .001) and between PC and NC (p < .001). The difference between CP and NC samples was non-significant.

difference for the concentration of EVs biomarker between the three groups ($F(2,72) = 59.15$, $p<.001$). Tukey's post hoc test revealed significant mean differences between PC and CP samples ($p < .001$) and between PC and NC ($p < .001$). The difference between CP and NC samples was non-significant.

To investigate whether the proposed EphA2-EV immunoassay technique has the potential to detect early PC cases, we analyzed the EphA2-EV signal in the serum sample of PC patient #1, which was diluted with different factors (1:2, 1:3, 1:4, and 1:5). As can be seen in Fig. 16, the signals recorded for PC patient #1 were 348, 162, 71, 52, and 40 for the dilution factors of 1:1, 1:2, 1:3, 1:4, and 1:5, respectively. We can see a robust trend in which a diminished signal is associated with a decreasing concentration of an analyte in the serum sample. These results

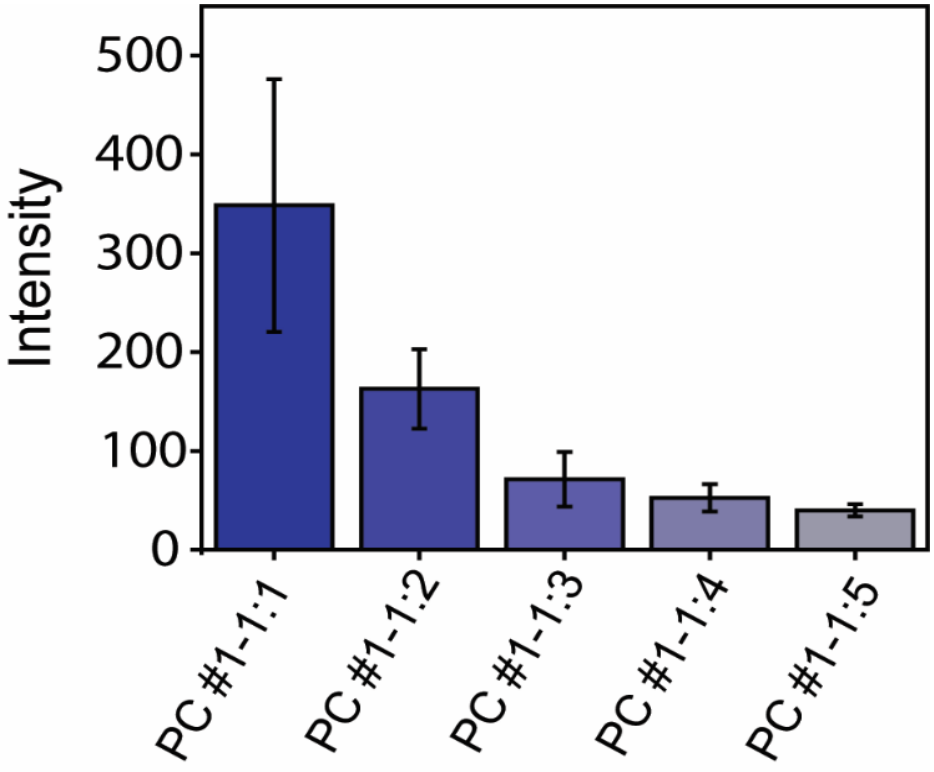

Figure 16 The SERS signals recorded for PC patient #1 which was diluted with different factors (1:2, 1:3, 1:4, and 1:5).

indicate an association between circulating EphA2-EV and PC, including early-stage PC, suggesting EphA2-EV's potential utility as an early detection marker.

3.4.2 Differentiating pancreatic cancer from chronic pancreatitis

To evaluate the ability to discriminate between PC and CP patients, the Z-score ratio between these two groups can be calculated accordingly. The calculations of the Z-score of each biomarker can be determined by the following equation[92].

$$Z_i = \frac{x_i - \bar{\mu}}{\sigma} \qquad (3)$$

Where the x_i is sample's intensity, $\bar{\mu}$ and σ are population mean and standard deviation of NC. Calculation of Z-Score for PC and CP patients is a statistical measurement that compares patients' results to a healthy population and gives an idea of how far your data is from the mean of NC.

In the previous chapter (2.4.3), we calculated the Z-Score for three PC protein biomarkers, CA19-9, MMP7, and MUC4. In that analysis, CA19-9 appeared to have the best ability to discriminate between PC and CP patients. For CA19-9, the mean Z-score for PC patients was 3-

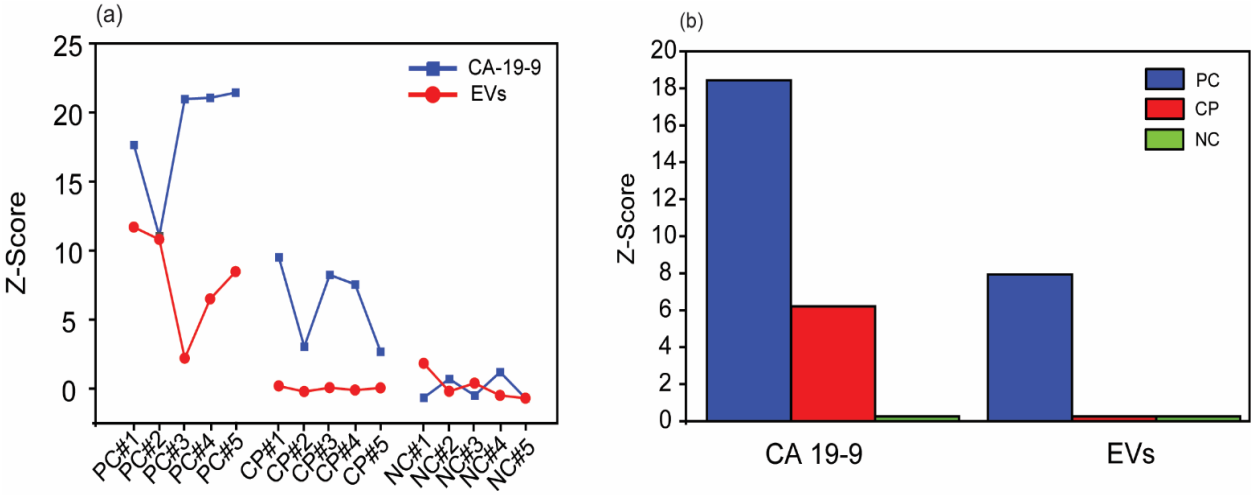

Figure 17 (a) Z-scores for CA19-9 protein biomarker and tumor-derived EVs in PC, CP and NC serum samples based on mean of total NC. (b) PC versus CP and NC Z-scores.

fold larger than that of CP patients, while the mean Z-scores of MMP7 and MUC4 for PC patients were 2.78 and 2.2-fold larger than that of CP patients. Fig. 17 compares the Z score of CA19-9, the only approved PC biomarker, and that of PC tumor-derived EVs. It can be seen from Fig. 17 that although CA19-9 shows a better sensitivity in diagnosing PC patients compared to EVs, it also increases significantly in CP patients. However, the Z-score ratio of PC to CP for EV biomarkers is substantially large value, indicating that it is the biomarker that discriminates best between these two patient populations.

3.4.3 Data Analysis

3.4.3.1 Classification Algorithms

Each measurement for each biomarker in each sample is the intensity of the peak value in Raman spectrum. Dataset includes five samples in each of classes PC, CP and NC individuals. 10 measurements of EVs expression measured for each patient, totaling to 150 data points. Classification tree is employed to predict the condition of patients. Details of this approach can be found in the previous work. Since the size of the dataset is limited, five-fold cross-validation is utilized to estimate the generalization error, in which the dataset is randomly partitioned into five equal subsets. In each run, four subsets are used to train the model, and the other held-out subset is used to test the performance of the trained model. The outcome of these five tests for the sensitivity and specificity of the model are averaged and reported as the performance of the model. In order to avoid over-fitting, the maximum depth of the decision tree is set to two.

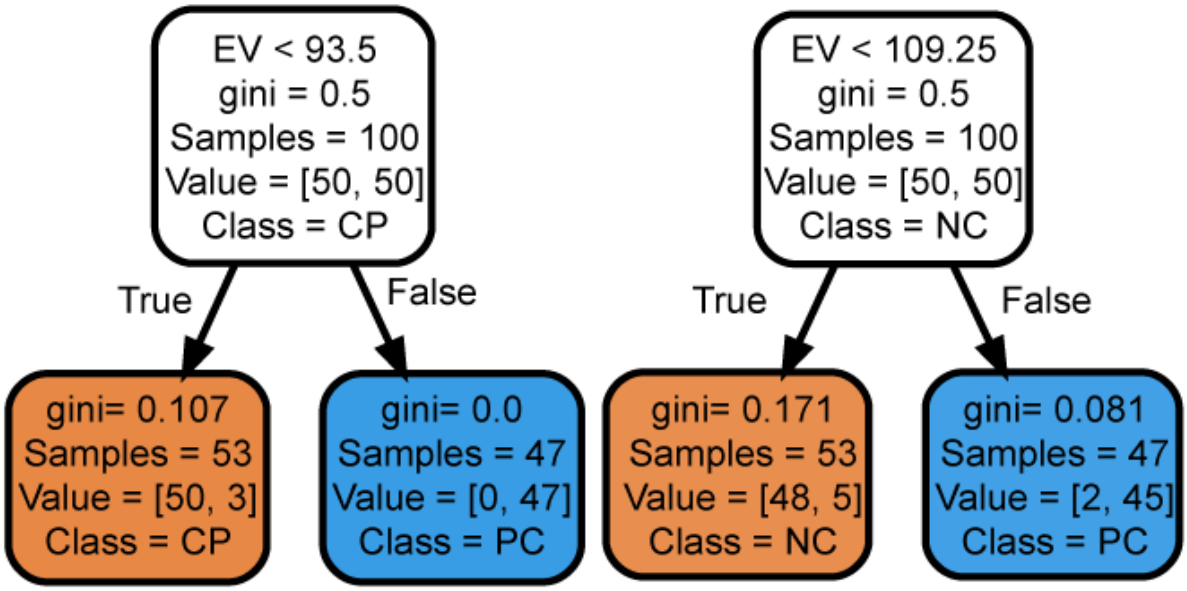

Figure 18: The classification tree trained with whole dataset of peak-value Raman shifts with depth = 2.

3.4.3.2 Classification Algorithms

To evaluate the performance of each model the sensitivity, specificity, and accuracy are computed similar to our previous publication. To measure the stability of the performance of the proposed model the data is divided into training and testing data with 5-fold cross validation.

$$Sensitivity = \frac{True\ Positive}{Positive} = \frac{True\ Positive}{True\ Positive + False\ Negative} \quad (4)$$

$$Specificity = \frac{True\ Negative}{Negative} = \frac{True\ Positive}{True\ Negative + False\ Positive} \quad (5)$$

Using 5-fold cross validation, the performance of the proposed method is computed as follows; Sensitivity = 0.95, Specificity = 0.96.

3.4 Conclusion

In this study, we detected tumor-derived EVs in PC patients' sera samples successfully, while there was no evidence of elevated tumor-derived EVs in patients with CP. The EphA2-EV signal was significantly higher in PC patients' serum samples than in samples from CP patients or NC individuals ($p < 0.001$).

The SERS-based immunoassay approach described in this study offers a rapid, purification-free measurement of circulating EVs in small sample volumes that require minimal sample preparation. Our finding indicated that EphA2-EV levels in serum matrix are excellent classifiers to differentiate PC cases from CP and healthy individuals and offer significantly better performance compared to conventional protein biomarkers such as CA19-9, MMP7, and MUC4.

3.5 Acknowledgment

This work is supported by a IALS Seed Grant from the University of Massachusetts Amherst.

CHAPTER 4

MACHINE LEARNING ALGORITHMS ENHANCING THE SPECIFICITY OF CANCER BIOMARKERS DETECTION BASED ON SERS IMMUNOASSAYS IN MICROFLUIDIC CHIPS

4.1 Abstract

The specificity is a challenge in liquid biopsy and early diagnosis of various diseases. There are only a few biomarkers that have been approved for the use of cancer diagnostics; however, these biomarkers suffer from the lack of high specificity. Moreover, determining the exact type of disorder for patients with positive liquid biopsy test is difficult, especially when the aberrant expression of one single biomarker can be found in various other disorders. In this study, a SERS-base protein biomarker detection platform in a microfluidic chip and two machine learning algorithms (K-Nearest Neighbor and Classification Tree) are used to improve the reproducibility and specificity of the SERS-based liquid biopsy assay. Applying machine learning algorithms to the analysis of the expression levels data of 5 protein biomarkers (CA19-9, HE4, MUC4, MMP7, and mesothelin) in pancreatic cancer patients, ovarian cancer patients, pancreatitis patients, and healthy individuals improves the chance of recognition for one specific disorder among aforementioned diseases with overlapped protein biomarkers changes. Our results demonstrate a convenient but highly specific approach for cancer diagnostics using serum samples.

4.2 Introduction

Early diagnosis would significantly decrease the mortality from cancer prior to the onset of metastasis with removal surgery or even at the early initiation of metastasis with current common therapies such as chemotherapy and cytotoxic drug[93-96]. Liquid biopsy is an emerging

non-invasive diagnosis approach which can be used as an inexpensive early detection tool and alternative to cumbersome imaging and tissue biopsy techniques [97,98]. The high cost and invasive nature of conventional tissue biopsies prevent them from being standard screening tests for normal adults. Recent studies demonstrated that liquid biopsies have potentials to diagnose adenovirus infection [99], lung cancer [100], breast cancer [101], lung cancer [100], breast cancer [101] and ovarian cancer (OVC) [102].

One of the major challenges that bottleneck the broad applications of the liquid biopsy in cancer screening is the lack of specificity. So far, only few protein biomarkers have been approved by the FDA for the use of cancer diagnostics. However, these biomarkers are often non-specific to a certain type of cancer. For example, CA19-9 is the only validated serum biomarker for pancreatic cancer (PC). However, CA19-9 also elevates in patients with OVC[103] and chronic pancreatitis[104]. Similarly, human epididymis protein 4 (HE4), an approved serum biomarker for OVC [105,106], also overexpressed in patients with PC[107,108], endometrial cancer [109], and lung cancer[110,111]. MMP-7[16,17,112], MUC-4[13,14] and mesothelin [113,114] are some other examples of potential biomarkers for PC that also have been identified as potential biomarkers for OVC[115-117]. Thus, relying on a single biomarker for cancer diagnostics has limited success.

Current strategies to improve the specificity of liquid biopsy is to detect various types of biomarkers not limiting to proteins, but also including microRNAs, circulating tumor DNA, etc.[118,119]. Although this approach significantly improves the detection specificity, multiple detection methods such as immunoassays and PCR are required, limiting its application in resource-limited settings.

We recently reported a Surface Enhanced Raman Spectroscopy (SERS)-based immunoassay for detecting several biomarkers of PC in sera[82]. SERS can provide intrinsic

fingerprint information of samples with high sensitivity[74]. The SERS technique has evolved as one of the most suitable candidates for the multiplex detection[120,121], due to the sharp and narrow spectra and multiple signatures of Raman spectra[122]. SERS has been widely used for the detection of cancer biomarkers[123,124]. Although SERS is a promising way for biomarker detection, a quantitative assessment of SERS is difficult, partially due to the poor reproducibility[125,126]. This is because SERS-based immunoassays using conventional immobilization of functionalized gold particles (NPs) are often associated with technical issues such as the inhomogeneous distribution of NPs on substrates during multiple manual washing steps[126]. It has been suggested that a highly sensitive and reproducible SERS-based analysis can be addressed if a continuous flow and homogeneous mixing conditions are maintained[125].

In this work, we reported a SERS-base multiplex protein biomarker detection platform in a microfluidic chip to detect several protein biomarkers of OVC, PC, and pancreatitis (CA19-9, HE4, MUC4, MMP7, and mesothelin). The microfluidic platform significantly improved the reproducibility of the assay, and multiplex detection can improve the specificity for cancer detection. We further employed machine learning algorithms to predict the type of disease and find critical biomarkers among multiple biomarkers to distinguish between diseases with similar biomarkers (PC, OVC, and pancreatitis). Decision tree and K nearest neighbor classification methods are used in this analysis. Together, we demonstrated a convenient but highly specific approach for cancer diagnostics using serum samples.

4.3 Experimental Setup

4.3.1 Reagent

Gold Nanoshells (660 nm resonant, 151 nm diameter, 3.7×10^{10}Particles/ml and 800 nm resonant), was purchased from NanoComposix. Sodium chloride, StartingBlock, and borate buffer (50mM) were obtained from ThermoFisher Scientific. Dithiobis-(succinimidyl propionate) (DSP), dimethylsulfoxide (DMSO), 4-Nitrobenzenethiol (4-NBT), acetonitrile, phosphate buffered saline (PBS), and bovine serum albumin (BSA) were acquired from Sigma Aldrich.

In our microfluidic SERS-based immunoassay, five different sets of monoclonal antibodies were used to modify the capture substrate and extrinsic Raman labels (ERLs). HE4 antibody was purchased from Proteintech, anti-mesothelin antibody and monoclonal anti-MUC4 were obtained from Abcam, Lyophilized MMP7 mAb was purchased from R&D Systems. The CA19-9 antibody was purchased from LifeSpan Bioscience.

4.3.2 Preparation of ERL

The preparation of antibody conjugated ERLs has been described previously in chapter 2.3.2 and also is illustrated in Fig. 19. Specifically, modified gold nanoshell as ERL is exploited to provide more intense Raman signal and immunopositivity. In this work, gold particles were modified with two different thiols, DSP and 4-NBT. DSP has both disulfide and succinimidyl functionalities for chemisorption onto the gold and facile covalent binding of antibodies to the gold particles and substrate; however, DSP does not show intrinsically intense Raman signal. 4-NBT, on the other hand, has been used to provide intense Raman signal due to aryl nitro group with an intrinsically strong Raman active vibrational mode. 4-NBT also contains a disulfide group for spontaneous chemisorption to the gold particles[27]. Preparation of ERLs is described as follows:

1.0 mL suspension of gold nanoshells, 40 µL of 50 mM borate buffer, 2.0 µL of 1.0 mM DSP in DMSO and 8.0 µL of 1.0 mM 4-NBT solution in acetonitrile were mixed and left to react for 8 h. To discard excess thiols, the suspension was centrifuged at 2000g for 10 min, and the supernatant was removed with a syringe. Gold nanoshells were resuspended in 2.0 mM borate buffer. ERL preparation was continued by adding 20 µg of MMP7, MUC4, HE4, Mesothelin or CA19-9 primary antibodies to the suspension and incubating for 16 h at 4oC. Next, 100 µL of 10% BSA was added to the suspension for stabilizing the suspension and blocking nonspecific binding sites and unreacted succinimidyl for 8 hours. After interaction between ERL and blocking buffer, the solution needs to be rinsed three times. For the rinsing process, the suspension was centrifuged, and after decanting the clear supernatant, the loose red sediment was resuspended in 1.0 mL of 2.0 mM borate buffer containing 1% BSA. The triple-rinsed ERL pellet was then resuspended in 0.5

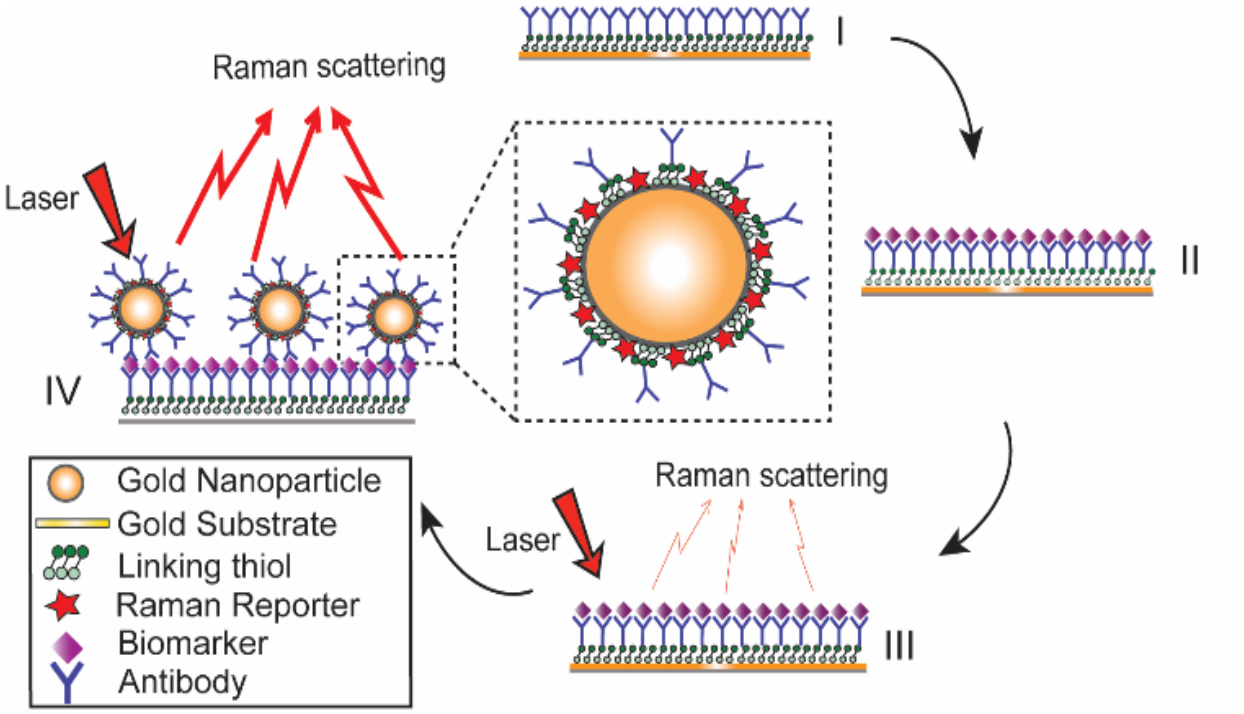

Figure 19: A SERS-based immunoassay for biomarker quantification: (I) Functionalizing gold substrate with thiol and antibody; (II) Capturing desired antigens from the serum; (III) Raman signal is weak without ERL (IV) Loading antibody-conjugated ERL to enhance Raman signal, Gold nanoparticles were modified with antibody and Raman reporter

mL of 2.0 mM borate buffer containing 1% BSA to have a final solution with the desired concentration of gold nanoparticles. Finally, the suspension was modified with 50 µL of 10% NaCl for stabilization and then passed through a 0.22 µm syringe filter to remove any large aggregate.

4.3.3 Functionalizing Capture Substrate and Microfluidic Immunoassay Procedures

The optimization of ERL's Raman signal has been described in chapter 2.4.1. We systematically examined the effects of gold particle size, the gap distance between the immobilized particle and the underlying substrate, and substrate materials on the amplification of Raman signals and demonstrated that immobilization of functionalized gold nanoshells with a resonance wavelength of 660 nm on the gold coated silicon substrate leads to a significant improvement of SERS signals. Thus, we will use gold nanoshells with a resonant wavelength of 660 nm coupled with the gold coated silicon substrate in our following studies.

As shown in Fig. 20 substrate was immersed in 1 mM DSP in ethanol for 10 h and then rinsed with ethanol and dried under a stream of air. As a result, a layer of DSP is formed on the gold substrate. The microfluidic method is used to provide on-chip flow with sequential injections. Polydimethylsiloxane (PDMS) replica molding from a 3D printed mold was used to fabricate a microfluidic device. PDMS stamps were fabricated by pouring a 10:1 (w/w) mixture of Sylgard 184 elastomer and curing agent and mixture were cured for 1 h at 80 °C. Patterned PDMS was then attached to the DSP coated gold substrate. Capture addresses were filled with 20 µL, 100 µg* mL-1 antibody as the first injection. DSP coated substrate was then reacted with the antibody for 6 h. Thus, a capture antibodies layer was formed by attaching to succinimidyl ester of DSP on the substrate.

4.3.4 SERS Readout Instrumentation

All the measurements and Raman spectra collection were performed with portable BWS415 i-Raman from B&W TEK Co. The incident laser light was focused to 85 µm spot size on the substrate normal incidence. The working distance is 5.9 mm. The light source has a power of 499.95 mW, and an excitation wavelength of 785 nm and the same objective was used to collect the scattered radiation. The antigen concentration was quantified using $(v_s(No_2))$ of 4-NBT intensity at the 1336 cm^{-1}. For reproducibility, three addresses were measured for each concentration and total of 10 readouts on each sample's biomarker.

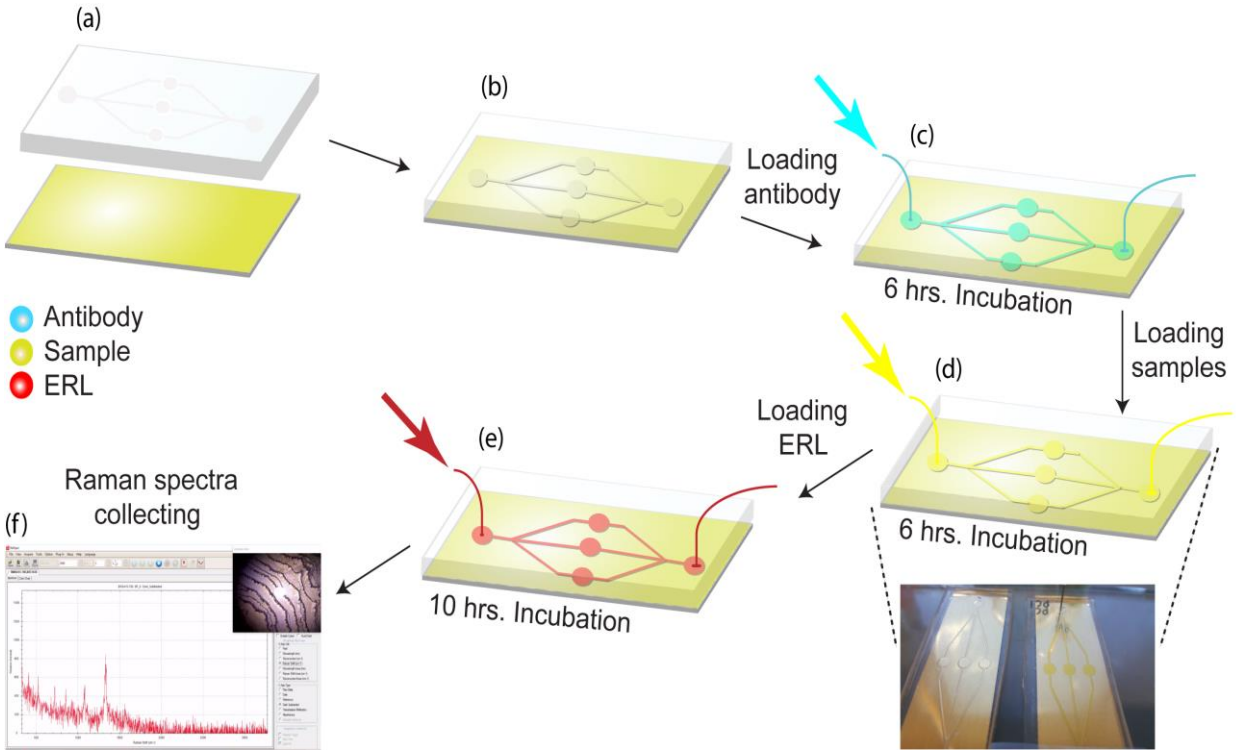

Figure 20 A microfluidic SERS-based immunoassay approach for the multiplex detection of CA19-9 levels in serum samples (a) PDMS replica molding from a 3D printed mold was used to fabricate a microfluidic device. PDMS replicated with one closed and open surface. (b) Patterned PDMS is attached to gold coated microscope slide. (c) 10 µl, 100 µ$g\ mL^{-1}$ CA 19-9 antibody were loaded in to the capture addresses, the addresses were then exposed with blocking buffer (d) serum samples and (e) ERL. (f) Finally, Raman signals from 10 random positions were collected from each capture address.

4.3.5 Patient Sample Collection and Samples characteristics

Under an IRB approved protocol, patients with pancreatic cancer, benign pancreatic disease, and normal control patients were identified from the UMass Memorial Medical Center Chemotherapy Infusion Center and Gastroenterology Clinics. Patients were identified from a review of the weekly schedules, and consecutive patients were enrolled to avoid bias. Patient gender, age, and clinical samples characteristics are shown in able 4.

Sera samples (4 mL serum per patient) were collected and immediately processed/frozen for analysis. Five ovarian cancer samples were purchased from Innovative Research.

Table 4: Clinical Sample Characteristics

Serum Sample	Sex/Age	Sample Characteristics
PC #1	F/38	Metastatic pancreatic adenocarcinoma
PC #2	F/58	Metastatic pancreatic adenocarcinoma
PC #3	M/61	Metastatic pancreatic adenocarcinoma
PC #4	F/88	Locally advanced pancreatic cancer
PC #5	M/57	Metastatic pancreatic adenocarcinoma
Pancreatitis #1	M/41	Acute pancreatitis- gallstone disease
Pancreatitis #2	F/55	Chronic pancreatitis- autoimmune
Pancreatitis #3	M/61	Chronic pancreatitis- alcohol related
Pancreatitis #4	F/43	Chronic pancreatitis-hereditary, cystic fibrosis gene mutation
Pancreatitis #5	M/55	Chronic pancreatitis- alcohol related
OVC#1	F/57	Endometrioid adenocarcinoma of the ovary
OVC#2	F/59	Adenocarcinoma, invasive of the ovary
OVC#3	F/62	Serous carcinoma of the ovary
OVC#4	F/50	Adenocarcinoma, mucinous type of the ovary
OVC#5	F/59	Endometrioid carcinoma of the ovary
Control	M:F 3:2/ Age 53-75 Average 62	

4.4 Results and discussion

4.4.1 Microfluidic and assay reproducibility

To investigate the effect of microfluidic approach on the reproducibility of the Raman signal, CA19- 9 in serum samples of PC/pancreatitis patients and healthy individuals were detected, and the Raman intensities obtained from the on-chip assay is compared with conventional assay using either a handheld Raman probe or a Raman microscope (Fig. 21a). Notably, the measurement variation of the microfluidic assay reduced to about 50% of the variation of the conventional assays (Fig. 21b). For reproducibility, each microfluidic unit contained three addresses to capture one single biomarker from one serum sample. Thus, for each serum sample (including control, PC, ovarian cancer, and pancreatitis), five microfluidic units were used to detect five different biomarkers (CA19-9, HE4, Mesothelin, MMP7, and MUC4). Total of 10 Raman signals were collected from each microfluidic unit.

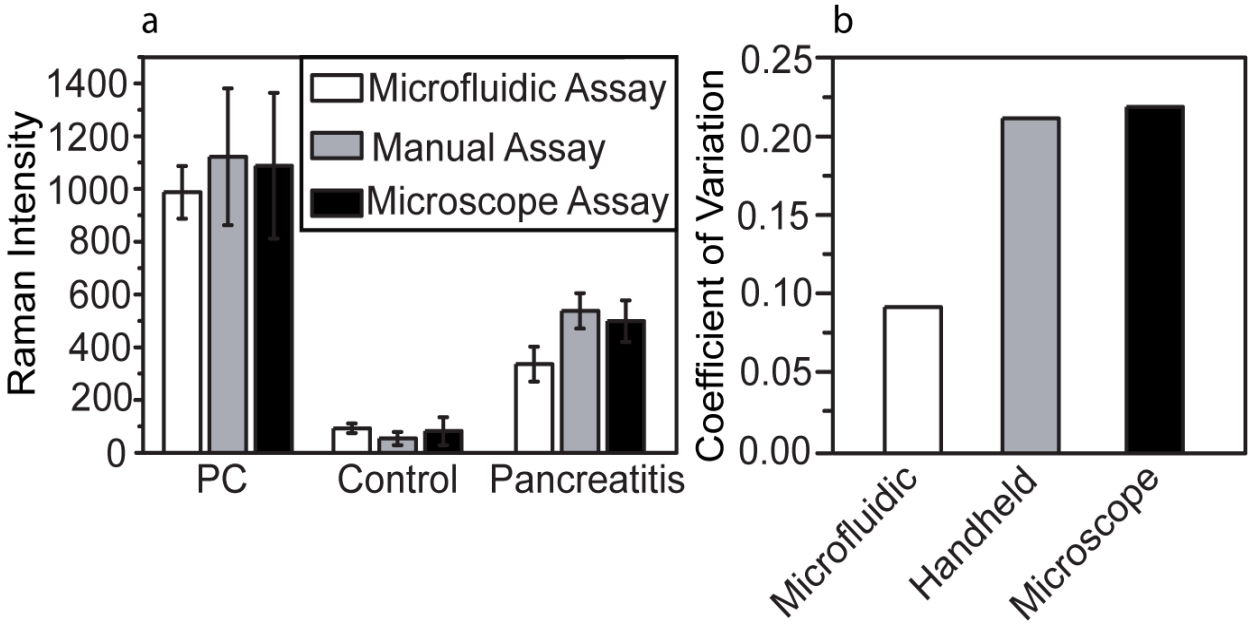

Figure 21 (a) Raman intensity obtained using different approaches. (b) Coefficient of variation (CV) of different approaches, which is calculated by the ratio of the standard deviation to the mean.

4.4.2 Detection of Ovarian and Pancreatic Cancer Biomarkers in Patients Samples

In chapter 2.4.2 the quantification of different concentration of spiked proteins in the pooled human sera was evaluated as a proof of concept. We further used microfluidic SERS-based immunoassay to detect five potential biomarkers (CA19-9, HE4, Mesothelin, MMP7, MUC4) from a total of 20 sera samples including five from normal individuals, five from patients with various types of pancreatitis but not PC, five from PC patients and five from ovarian cancer patients. Raman spectra of five selected biomarkers in clinical sera samples are shown in Fig. 22.

It appears that CA19-9 is the most sensitive biomarker with the highest expression level in almost all patient samples, and other biomarkers, by themselves, cannot distinguish the PC and OVC. Thus, to fully leverage the data obtained from multiple biomarkers for a more accurate prediction, more comprehensive data analysis is needed.

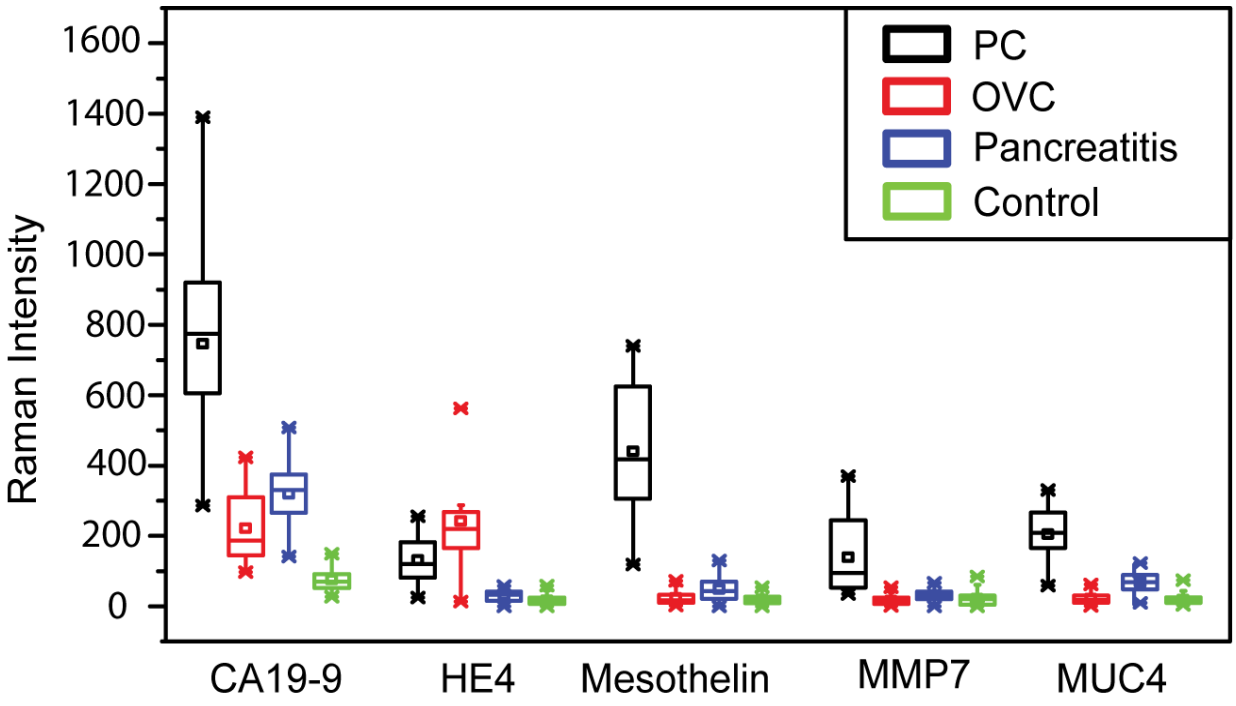

Figure 22 Multiplex detection of CA19-9, HE4, Mesothelin, MMP7 and MUC4 levels in serum of normal, PC, ovarian cancer and pancreatitis samples (total of 20 sera samples) using the microfluidic SERS-based immunoassay. Raman intensities of 4-NBT (1336 cm^{-1}) corresponded to CA19-9, HE4, Mesothelin, MMP7 and MUC4 in serum samples. Each box represents 50 readouts.

4.4.3 Data Analysis

We next sought to use machine earning based approach to analyze the Raman intensity data we obtained to provide a better prediction of the condition of patients. We first processed the raw Raman spectrum data to reduce the noise level. As the background noise level in SERS signals is relatively low compared with the strongly enhanced peak signals, we applied a simple Fast Fourier Transform (FFT) to the Raman intensity data three times to reduce the noise and smooth the Raman spectrum. The original and denoised spectra of CA19-9 for a pancreatic cancer sample are plotted in Fig. 23(a), (b) respectively. Fig. 23(c) also demonstrates the original and denoised spectrum together for a better comparison. The processed Raman spectrum of each measurement of biomarker b on patient i is denoted by $R_{i,s}^{b}(\tilde{\nu})$, as a function of wavelength discretized with 1783 points. Measured biomarkers include CA19-9, HE4, Mesothelin, MMP7, and MUC4.

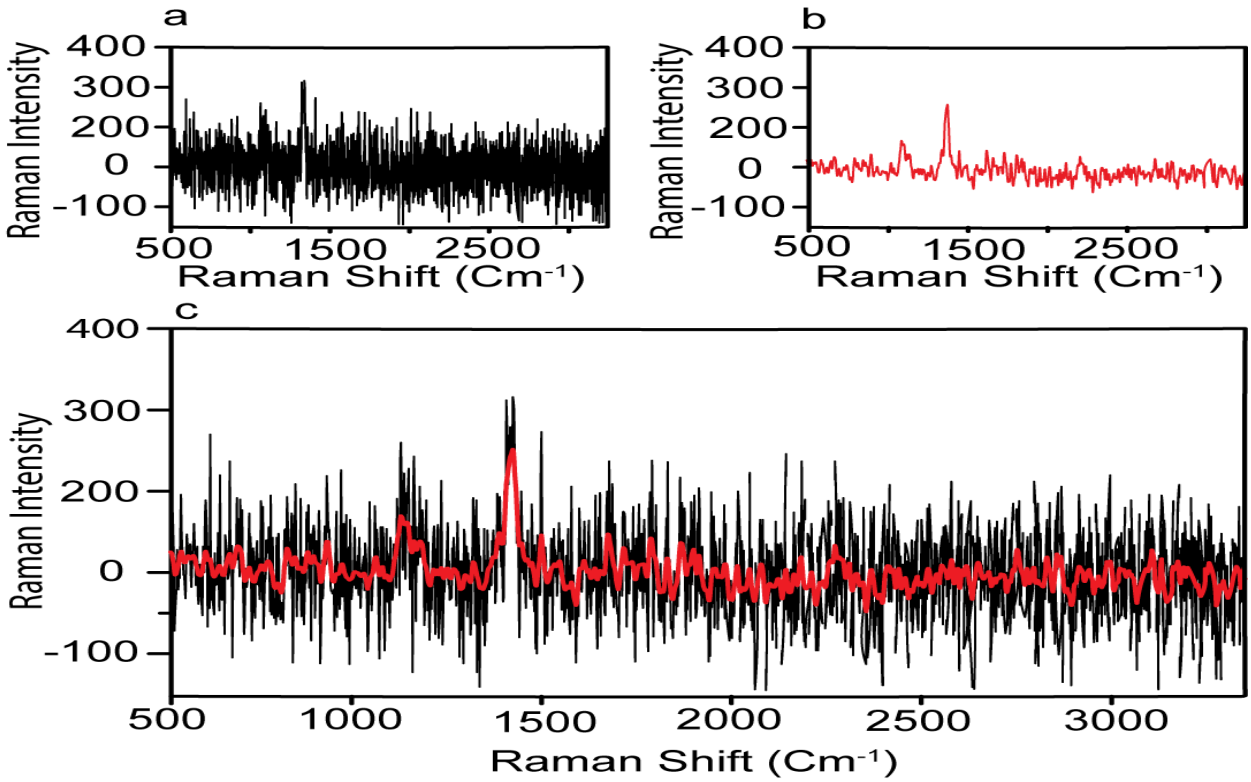

Figure 23 Pre-processing of Raman spectrum. (a) The measured Raman spectrum; (b)The denoised spectrum using FFT filter; (c) the original and denoised spectrum together.

Performing ten measurements for each of the 20 individual samples and five biomarkers, the dataset includes 1000 Raman spectra $R_{i,s}^{b}(\tilde{v})$.

Two supervised algorithms are employed to classify the condition of the patients. First, the Raman spectra peak values $R_{i,s}^{b}(\tilde{v})$ are used for decision tree classifiers, which are fast, simple, and provide useful information about the importance of biomarkers. However, since a single peak value at $\tilde{v}_r = 1500cm^{-1}$, the resonance wavelength of Raman reporter, is used for classification, it is vulnerable to noise. Therefore, the full spectrum of Raman spectra $R_{i,s}^{b}(\tilde{v})$ are then analysed using K-Nearest Neighbor (K-NN) classifiers, which are easy to implement and robust to spike noise. However, K-NN does not scale favorably when the size of the dataset increases. In this case, the artificial neural network may be used to learn the pattern of Raman spectra for different biomarkers/diseases, in order to classify patients efficiently. Since the size of our dataset is not too large yet, we have employed K-NN classifiers at this stage for the full spectrum analysis.

4.4.3.1 Classification Algorithms

4.4.3.1.1 Classification Tree

Classification trees (CT), considerably advanced in[127] assigns class labels to samples using a conjunction of rules organized into a tree structure classifier. The inputs of the algorithm are vectors $X_i = (x_1, x_2, \dots, x_k)$, $i = 1,2, \dots, N$, where k is the number of features and N is the number of the training dataset. The rule of each decision node m, in the form of $x_d < t_m$ or $x_d = t_m$, tests a single feature x_d of the sample against a threshold t_m to assign it to the left or right sub-tree. Classification trees are usually constructed using recursive partitioning algorithms, in which all possible partitioning based on a single feature are evaluated and the one with the best score is selected. The scoring of the partitioning may be performed using the Gini impurity[127] or

information gain. Assuming that the training dataset at node m is represented by Tr_m of size N_m, and each partitioning candidate is denoted by $\theta(j, t_m)$ consisting of feature j and threshold t_m, the impurity at m is computed as follows:

$$G(Tr, \theta) = \frac{\eta_{left}}{N_m} H\left(\mathrm{Tr}_{\mathrm{left}}(\theta)\right) + \frac{\eta_{\mathrm{right}}}{\mathrm{N_m}} H\left(Tr_{right}(\theta)\right) \quad (6)$$

where $H(\,)$ is the impurity function, η_{left} is the size of the dataset in the left sub-tree, and η_{right} is the size of the dataset in the right sub-tree with partition θ. The best partition θ∗ minimizes the function $G(Tr, \theta)$. Gini impurity and cross-Entropy are the two-common choices for the impurity function H. The Gini impurity is computed using:

$$H(Tr_m) = \sum_l p_{ml}(1 - p_{ml}) \quad (7)$$

where p_{ml} is the proportion of class l observations at node m. The cross-Entropy or information gain is calculated by:

$$H(Tr_m) = -\sum_l p_{ml} log\ (1 - p_{ml}) \quad (8)$$

In this paper, Gini impurity is utilized.

Data Preparation for CT

The peak values of $r_{i,s}^b = R_{i,s}^b(\tilde{\nu}_r)$ at the resonance wavelength of Raman reporter $\tilde{\nu}_r = 1336cm^{-1}$ for measurement s of each biomarker b and patient i are first extracted. Then, the average over the measurements for each biomarker, $r_i^b = avg_s(r_{i,s}^b)$, is computed and used as the features of the input dataset. Therefore, the input data for patient i takes the form:

$$X_i = \left(r_i^{CA19-9}, r_i^{MUC4}, r_i^{Mesothelin}, r_i^{HE4}, r_i^{MMP7}\right) \quad (9)$$

4.4.3.1.2 K-Nearest Neighbor (KNN) Algorithm

The K-NN algorithm is a supervised learning method for classifying data points based on the proximity or similarity of them to the previously observed data. The algorithm accepts a new patient's data and compares it with a training set of previously classified patients with various medical conditions. The algorithm then utilizes the K-NN technique to classify patients as having or not having a specific condition. K-NN is easy to implement, adaptive to relatively noisy training sets, and naturally handles multi-class classification problems. K-NN has been extensively used in the medical field with a relatively high rate of success compared to other methods like Linear Discriminant Analysis (LDA) [128,129].

The basic underlying hypothesis of K-NN is that if two data-points have a high degree of similarity, there is a high probability that they belong to the same class. In other words, the probability of two data points belonging to the same class is proportional to their degree of proximity or similarity. There are various measures for quantifying similarity for the K-NN classifier, however, in our work we use Euclidean distance as our measure of similarity. In order to diagnose a new patient, we first calculate the Euclidean distance between the patient's data-point and all the data-points in the training set. We then sort the distances in increasing order and keep the top k points with the shortest distance to the patient's data. Since we already have the diagnosis on all the k points from the training set, the majority value among the k diagnoses will be used as the diagnostic predictor for the new patient.

The K-NN algorithm works based on a similarity measure between the data-points. There are various measures of similarity used in the literature to capture different properties of data[130]. In this work, we use the simplest and most straightforward measure of similarity which is the

Euclidean distance. The Euclidean distance between two points p and q in an n-dimensional space $\mathbb{R}^n$ is defined as:

$$D(p,q) = \sqrt{(q_1 + p_1)^2 + (q_2 + p_2)^2 + \cdots + (q_n + p_n)^2} = \sqrt{\sum_{i=1}^{i=N} (p_i - q_i)^2} \qquad (10)$$

Data Pre-processing for K-NN

The most prevalent method in the literature for analyzing Raman spectroscopy data is to use the peaks of the spectra. However, this method is very sensitive to noise in the data since a single noisy fluctuation in one of the points of the spectrum could change the result of the classification model. In this work, we introduce a novel method for analyzing Raman spectral data for cancer diagnosis by using the whole spectrum. As we will discuss in the results section, this method outperforms our decision tree algorithm which uses only the peaks of Raman spectral data. This is in part because we are extracting more information from the spectra and this extracted information is more robust to noise in the experimental setup.

For measurement s of patient i for biomarker b, our Raman spectra $R_{i,s}^{b}$ is a vector of 1783 intensities. This 1783-dimensional vector could be regarded as a point in a 1783-dimensional space. Therefore, we can define a similarity metric for the spectral data of a patient based on the Euclidian distance between the vectors of specific biomarkers. In addition, in order to use the entire data for all the biomarkers for each patient, we can create a large vector by appending all the vectors corresponding to different biomarkers and creating a larger vector.

$$R_{i,s} = [R_{i,s}^{CA19-9}, R_{i,s}^{MUC4}, R_{i,s}^{Mesothelin}, R_{i,s}^{HE4}, R_{i,s}^{MMP7}) \qquad (11)$$

Given this high dimensional vector which contains the whole information of all the Raman spectral data for all biomarkers for a sample of a patient, first, we calculate the Euclidean distance

between this new sample and the rest of the previously known training dataset. We then create a list containing all the distances:

$$Distances = [D(R_{test,}R_{1,1})\ D(R_{test,}R_{1,1}) \ldots . D(R_{test,}R_{i,s})\ \ldots$$
$$D(R_{test,}R_{i,s}) \ldots . D(R_{test,}R_{n,10})] \qquad (12)$$

Where i corresponds to the i-th patient and s corresponds to measurement s of the i-th patient. (In this work, we had 10 measurements for each patient) in the training data. The next step in the algorithms follows by sorting this list of distances and choosing the k shortest distances from the list. These k instances correspond to k pre-classified samples in the training set. The final stage of the algorithm is performed by taking a majority vote over the classes corresponding to these k samples and determining the diagnosis for the unknown test sample.

4.4.3.2 Performance Evaluation

To evaluate the performance of each model the sensitivity, specificity, and accuracy are computed. The sensitivity is the ratio of positive samples that are correctly classified as positive, i.e., the proportion of patients that are classified with the correct type of cancer. The specificity is the ratio of negative samples that are correctly classified as healthy, i.e., the proportion of normal individual that are classified as healthy. The accuracy is the proportion of samples that are correctly classified[131]. To measure the stability of the performance of the proposed model the data is divided into training and testing data with 5-fold cross validation.

$$Sensitivity = \frac{True\ Positive}{Positive} \qquad (13)$$

$$Specificity = \frac{True\ Negative}{Negative} \qquad (14)$$

$$Accuracy = \frac{True\ Positive\ + True\ Negative}{Positive + Negative} \qquad (15)$$

4.4.3.3 Data Analysis Result

First, the data analysis results using classification trees is presented to show the effectiveness of multiplex biomarker method. Next, the results of full spectrum analysis using K-NN approach is presented. Python scikit-learn[132] tool is used for all the analysis performed in this paper

3.4.3.3.1 Peak-Value Analysis

Classification trees are used to analyze the peak-value dataset of Raman shift measurements. Since the size of the dataset is limited, a specific test set is not held out to evaluate the performance of the classification. Instead, five-fold cross-validation is utilized to estimate the generalization error, in which the dataset is split into five equal subsets. Four subsets are used to train the model, and the other held-out subset is used to test the performance of the trained model. This train-test approach is performed five times, and in each test, one subset is held out. The outcome of these five tests for the sensitivity and specificity of the model are averaged and reported as the performance of the model. In order to avoid over-fitting, the depth of trees is limited to two.

Table 5 The sensitivity and specificity for each panel of patients using classification trees with 5-fold cross-validation with depth ¼ 2 for increasing number of biomarkers

	Normal		Pancreatic cancer		Pancreatitis		Ovarian cancer	
Biomarker(s)	Specificity	Sensitivity	Specificity	Sensitivity	Specificity	Sensitivity	Specificity	Sensitivity
CA19-9	1	0.8	0.73	0.2	0.87	0.4	0.8	0.8
CA19-9 + HE4	1	0.8	0.87	0.8	0.73	0.6	0.93	0.4
CA19-9 + HE4 + mesothelin	0.67	0.8	0.87	0.2	0.93	0.6	1	0.8
CA19-9 + HE4 + mesothelin + MMP7	0.93	0.8	0.87	1	0.93	0.4	0.93	0.8
CA19-9 + HE4 + mesothelin + MMP7 + MUC4	1	0.8	0.93	0.8	0.93	1	0.93	0.8

The performance of the classification trees with 5-fold cross-validation with depth = 2 for an increasing number of biomarkers are presented in table 5. The sensitivity and specificity for each panel of normal adults, Pancreatic cancer patients, Pancreatitis patients, and Ovarian cancer patients in the table demonstrate that the accuracy of the early cancer perdition is improved by employing multiplex biomarkers. Finally, we used the whole dataset to train the classification tree shown in Fig. 24. This plot shows that the most important biomarkers in diagnosis are HE4, CA19-9, and MUC, as expected. Note that the whole dataset is used to train this model. Therefore, the

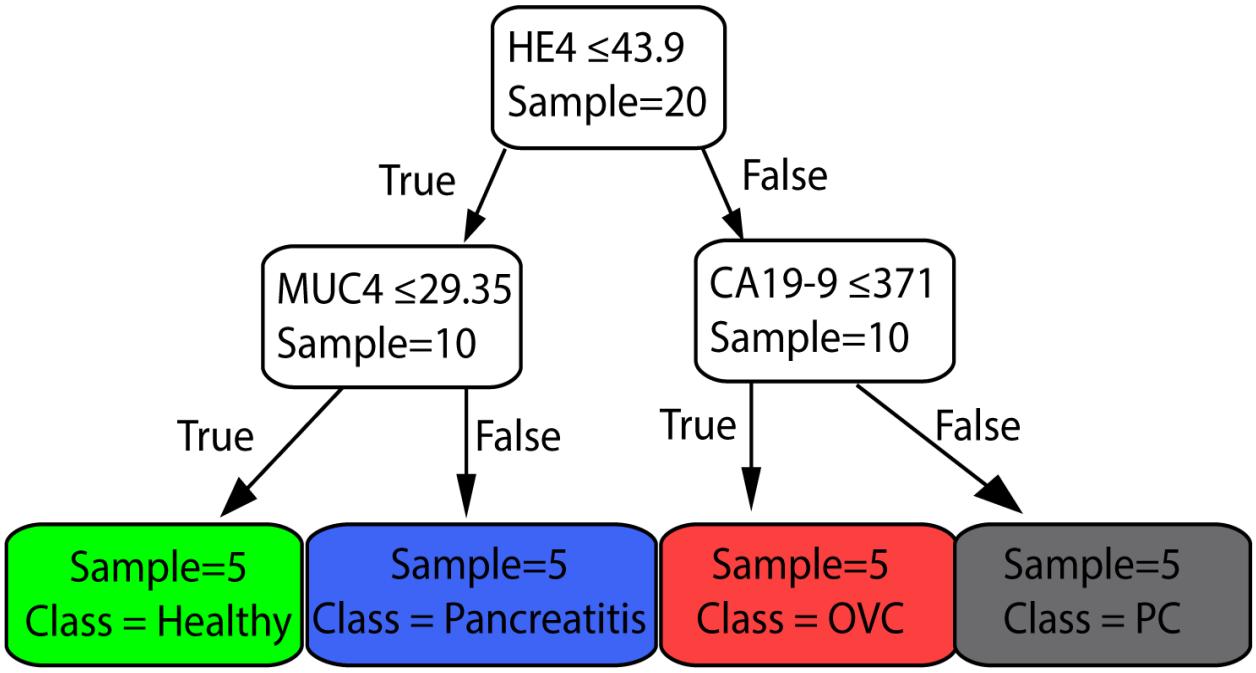

Figure 24 The classification tree trained with whole dataset of peak-value Raman shifts with depth = 2. This shows that the most important biomarkers in diagnosis are HE4, CA19-9, and MUC4.

same data cannot be used to evaluate the performance of the model. It could be used to predict the healthiness of future patients.

4.4.3.3.2 Full Spectrum Analysis

In order to achieve better accuracy, we have applied K-NN classifier with k = 5, which employs the full spectrum of all biomarkers. The whole dataset includes 200 vectors $R_{i,s}$ of the format in Eq. (7), which is randomly splitted in 20% for training data $R_{i,s}^{train}$ and 80% for test data $R_{i,s}^{test}$. Using this setup, we achieved sensitivity of 86%, specificity 93%, and accuracy of 91% to predict the class of each measurement $R_{i,s}^{test}$ in the test data. If we use the majority vote of the 5 measurements to diagnose the patient, the prediction would always be correct. Since the dataset size is limited, we cannot compute a more accurate estimation of the test error for this classifier.

The general setting of a K-NN classifier is very hard to visualize due to the high number of dimensions in the algorithm. In order to visualize how our K-NN algorithm works, we simplify our model to only two biomarkers. Fig. 25 depicts the Scatter plot of the distance of a sample test data-point from all other data-points in the training set. The x-axis denotes the distance between the test data-point and all the training set data-points for the HE4 biomarker, $D(R_{test}^{HE4}, R_{train}^{HE4})$. The Y-axis denotes the distance between the test data-point and all the training set data-points for the CA19-9 biomarker, $D(R_{test}^{CA19-9}, R_{train}^{CA19-9})$. The point (0,0) in the plot, which is not shown, is where the test data-point resides. This is because the test data-point is regarded as the center for calculating all the corresponding distances. As it can be seen in the Fig. 25, all 5-nearest neighbors of the test patient's data points are diagnosed as PC. Therefore, we conclude that the unknown data point should be diagnosed as PC, which is a correct diagnosis for the test sample.

In our case, we can clearly observe that when we translate our problem into K-NN, a small sample of our small dataset encapsulates lots of information about the spatial patterns between different classes. This means that there is a clear spatial separation between different classes in the defined high-dimensional space. In addition, it is worth noting that the smallness of our dataset is a limitation to any statistical analysis technique. Thus, we need to assess different statistical techniques with respect to their robustness. As mentioned earlier, using the smallest subset of our data (20%) as the training set for our K-NN model yields very accurate results which shows its

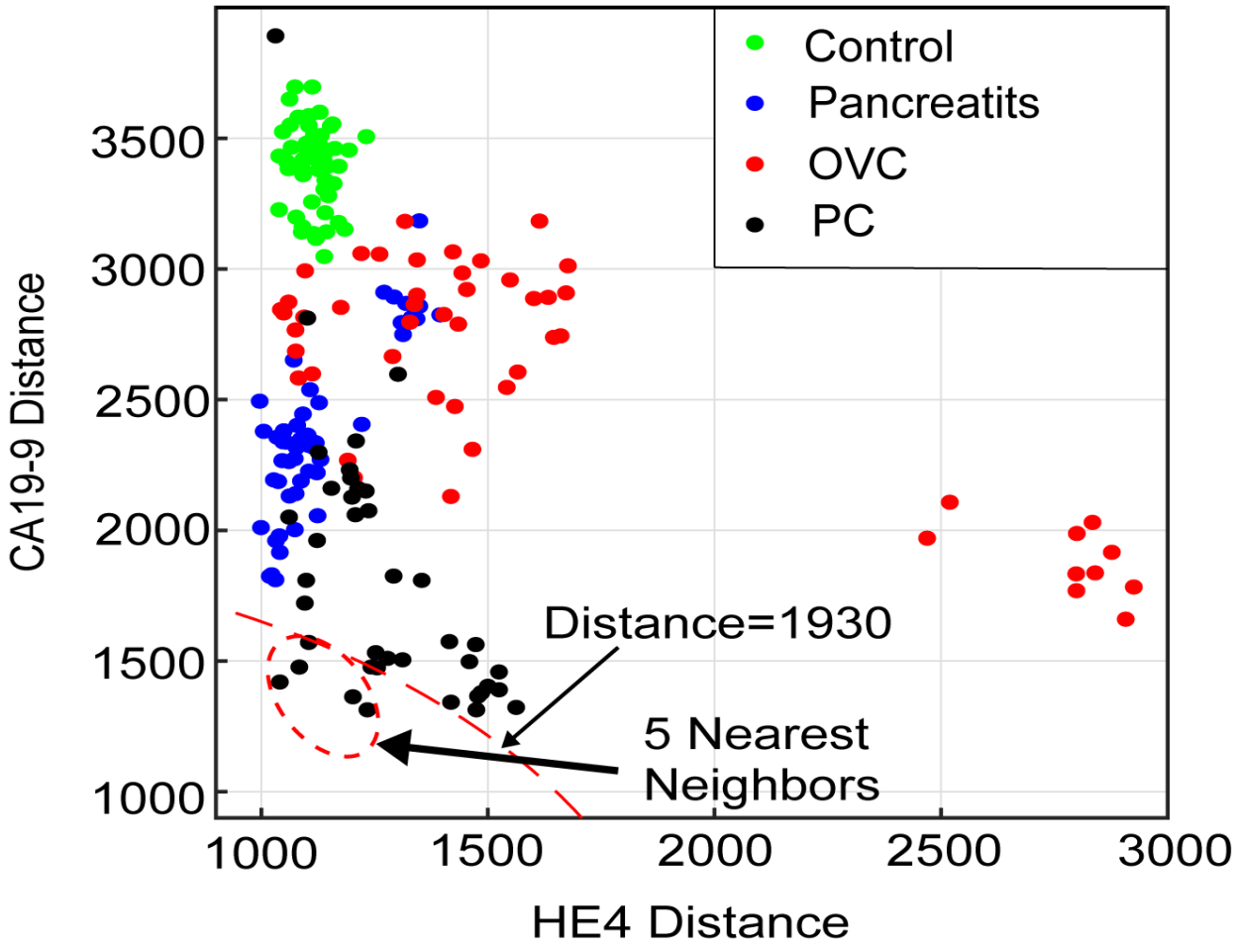

Figure 25 Scatter plot of the distance of a sample test data-point from all other data-points in the training set. In this case *k* in our K-NN algorithm is set to 5. The point (0,0), which is not shown, is where the test point resides. Looking at the 5-nearest neighbours, one quickly concludes that the test sample should be diagnosed as PC, which in this case is a correct diagnosis.

robustness to the size of the training set. In our future work, we plan to increase the size of our dataset and perform state of the art machine learning techniques such as deep neural networks for statistical analysis.

In order to evaluate the effectiveness of adding new biomarkers to our classification problem, we make use of a conventional machine learning concept called Receiver Operating Characteristic (ROC) curve. In a ROC curve, true positive rate (TPR) is plotted against the false positive rate (FPR) at various threshold settings. The trained machine learning classifier outputs

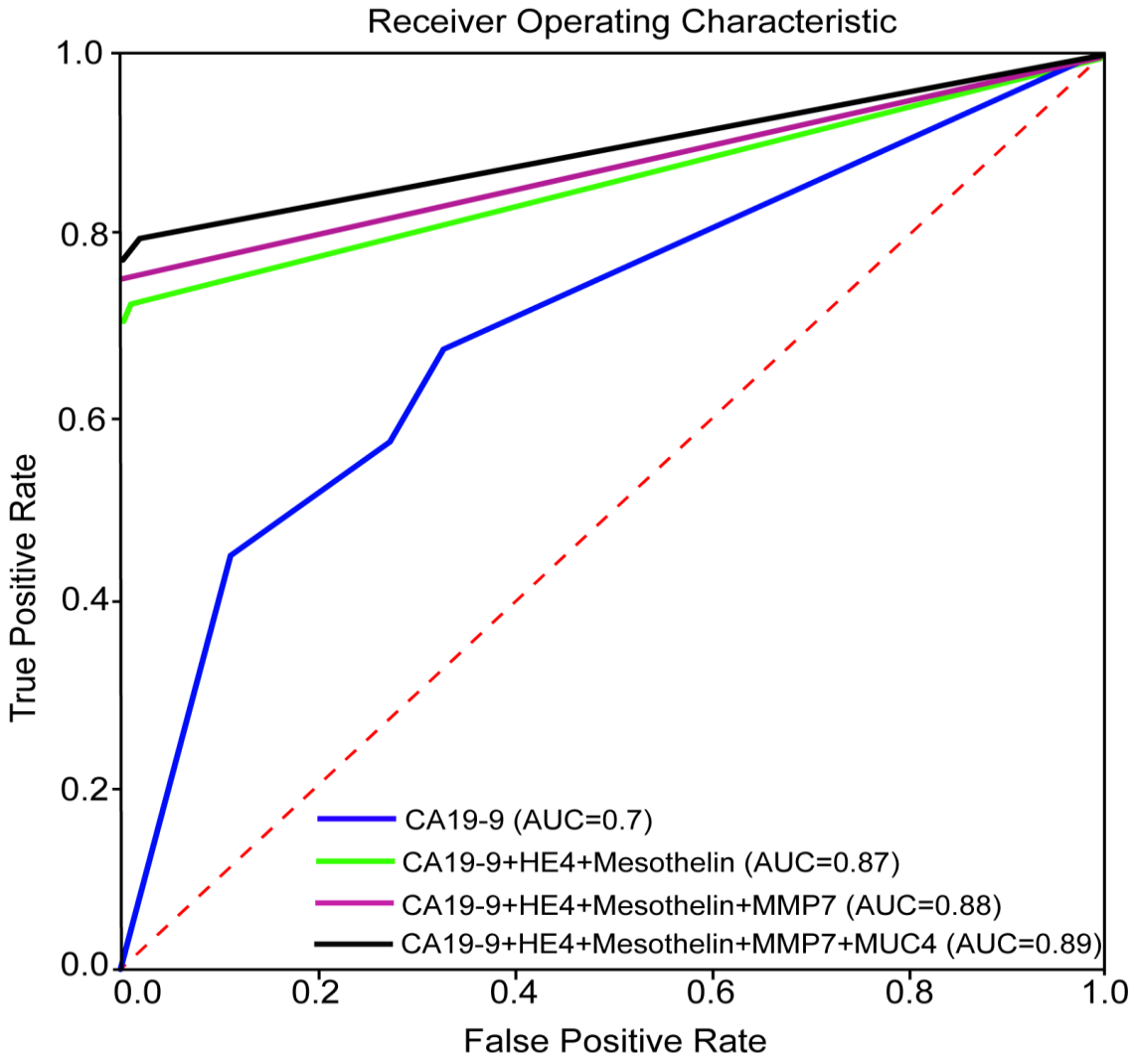

Figure 26 ROC curve for various combinations of biomarkers for the k-nearest neighbour model with k=3 and 80 percent of the data as the training set and 20 percent as the test set.

the probability that a given test sample is positive. To plot the ROC curve, we start by sorting all the test samples based on the predicted probability of being a positive sample. We then decrease the threshold gradually from 1 until it is equal to the highest probability and see if the corresponding sample test is a true positive or a false positive. If we have a true positive/false positive for our first sample, we draw a unit vertical/horizontal line starting from the point (0,0). We then continue decreasing the threshold to arrive at the next sample in our sorted list and continue to draw vertical/horizontal unit length lines for true positives/false positive. It has been shown that the area under the ROC curve (AUC) is equal to the probability that a classifier will rank a randomly chosen positive instance higher than a randomly chosen negative one (assuming 'positive' ranks higher than 'negative'). AUC is a standard metric for evaluating machine learning classifiers. A perfect predictor has AUC of 1. On the other hand, a random prediction model gives us AUC of 0.5. To this end, the K-NN model is trained with 80 percent of the data using K=3 and tested with the other 20 percent of the data. This arrangement is chosen to demonstrate the effect of biomarkers more clearly. Fig. 26 shows the ROC curve for various combinations of biomarkers. As it can be seen in the Fig. 26, adding biomarkers significantly increases our prediction accuracy.

4.5 Conclusion

Multiplex detection of five biomarkers which elevate in both PC and ovarian cancer was accomplished with microfluidic SERS-based immunoassay approach.We employed decision tree classification and nearest neighbor method to evaluate the importance of different biomarkers and estimate the specificity and accuracy of the prediction. The result from data analysis demonstrated that multiplex detection of protein biomarkers (CA19-9, HE4, MUC4, MMP7, and mesothelin) in cancer patients and diseases with similar protein biomarkers significantly increased specificity and

prediction accuracy. It is also observed that HE4 and MUC4 biomarkers improved the specificity of diagnosis, in addition to CA19-9 biomarker.

4.6 Acknowledgment

This work is supported by the IALS Seed Grant from the University of Massachusetts Amherst

CHAPTER 5

A MAGNETIC ENHANCED RAMAN FREQUENCY SHIFT IMMUNOASSAY USING GOLD-COATED NANOPILLAR SUBSTRATE FOR QUANTIFICATION OF PROTEIN BIOMARKERS

5.1 Abstract

In this work, a SERS-based frequency-shift immunoassay is reported for the detection of cancer markers in human serum. The expression level of five cancer biomarkers (CA-125, CA19-9, CEA, OPN, Prolactin) have been measured in the serum of pancreatic and ovarian cancer patients and compared to that of healthy individuals. These measurements indicate that serum from cancer patients produced a larger change in SERS frequency shift compared to that in sera from healthy individuals. The population means of pancreatic, ovarian, and healthy individuals are different for all of the tested biomarkers. This study demonstrates that employing magnetic beads can increase the sensitivity of the frequency shift immunoassay. Applying a machine learning algorithm to the analysis of the expression level of protein biomarkers in pancreatic, ovarian cancer patients, and healthy individual samples showed that the sensitivity, specificity, and accuracy were 0.93, 0.97 and 0.96, respectively.

5.2 Introduction

Among many approaches to detect protein biomarkers in serum, Surface Enhanced Raman Spectroscopy (SERS) is an emerging technology that provides intrinsic fingerprint information of samples with high sensitivity[2,74]. Gold/silver nanoparticles and substrates with nanostructures need to be coupled to amplify inelastic scattering signals of targeted molecules and reach the desired sensitivity[133,134]. However, SERS technology has not yet been extensively used for cancer

biomarker detection in the clinic; even it demonstrates higher sensitivity than enzyme-linked immunosorbent assay (ELISA) in some cases[34,135]. While most current studies focus on developing new materials to achieve higher signal enhancement, the major challenges that prevent the wide spreading application of SERS are the lack of standardized testing materials and reproducible SERS based immunoassay approach[125,136,137]. This is because SERS-based immunoassays using conventional immobilization of functionalized gold particles (NPs) are often associated with technical issues such as the inhomogeneous distribution of NPs on substrates during multiple manual washing steps[126]. Also, quantification of biomarkers based on SERS intensity is affiliated with some experimental parameters including integration time, laser power, laser focus, amount of Raman reporters, and other environmental factors which prevent standard detection of biomarkers.

Biomarkers quantification based on frequency shift was first introduced by Olivo and coworkers[138,139] and investigated by other study [140]. This SERS nanostress sensing is a novel readout method which is supported by the observation that the Raman frequencies of an antibody-conjugated SERS-active molecule can be affected when binding it to its targeted antigen. The mechanical perturbations of the linker molecule in the conjugated antibody/linker construct are responsible for the observed shifts[138]. However, the main obstacle in these studies is the limited sensitivity, which is due to the relatively small shift of frequencies. The range of frequency shifts for low concentration analyte has been observed to be near 1-2 cm^{-1}. By considering the fact that many Raman spectroscopy systems, especially portable and handheld devices, have the meager spectral resolution ($\sim 3 - 10\ cm^{-1}$), detection of the broad range of biomarker's concentration is almost impossible unless using the advanced and expensive Raman spectroscopy systems with the small spectral resolution ($\sim 0.3\ cm^{-1}$).

In this work, we developed a novel magnetic enhanced Raman frequency shift immunoassay using gold-coated nanopillar substrate to amplify the SERS signals produced by Raman reporters and improved the assay sensitivity by two orders of magnitude. Advantages of these approaches are 1) heterogeneous distribution of NPs can be prevented by excluding the nanoparticle-based Extrinsic Raman Labels (ERLs) from the assay. 2) The frequency shift will be quantified which should significantly increase the reproducibility of the assay by reducing the assay dependency to the experimental parameters. 3) In conventional ERLs SERS-based immunoassay, Raman reporters are located ~15-30 nm far from the surface of metal nanostructure because of utilizing ERLs and two antibodies in the assay, however, most substantial enhancement commonly occurs when Raman reporter molecules have been located proximately to the roughened metal surface (<7nm)[141,142]. In our assay, optimal enhancement can be achieved by direct binding of Raman reporter which also serves as linker molecule to the SERS active substrates. 4) Significant enhancement occurs when the assay is accompanied by magnetic forces; as a result, sensitivity of the platform is significantly improved.

5.3 Experimental Setup

5.3.1 Reagents

Gold coated nanopillar substrates were purchased from Silmeco, 4-Aminothiophenol (4-ATP), 1-ethyl-3-(3- dimethylaminopropyl)carbodiimide (EDC), N hydroxysuccinimide (NHS), Glycin were obtained from Sigma Aldrich. Magnetic beads were purchased from Expedeon. Neodymium magnet was purchased from CMS Magnetics, INC. Monoclonal anti-MUC4 and human MUC4 peptide as an antigen were obtained from Abcam.

5.3.2 Functionalization Capture Substrate and Immunoassay Procedures

It has been shown that gold-coated nanopillar substrate can provide very high enhancement factor with good reproducibility due to leaning effect of nanopillar[143]. In this study, gold-coated silicon wafer with standing vertical silicon pillars in the range 50–80 nm wide and 600 nm heights has been used to capture and detect antigen (Fig. 27).

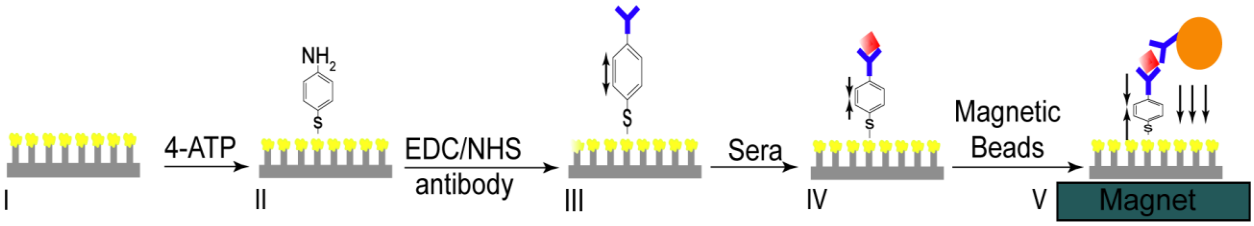

Figure 27: A schematic showing the magnetic enhanced SERS-based Raman frequency shift immunoassay. (I) Gold coated nanopillar substrate; (II) functionalizing the substrate with linker reporter molecule; (III) Stretching of linker molecule (4-ATP) due to intermolecular repulsion between immobilized MUC4 antibodies; (IV) Relaxation of the linker molecule (4-ATP) owing to hydrophobic interactions between bound antigens; (V) compressing the linker molecular using functionalized magnetic beads and magnetic force.

As illustrated in Fig. 28, the gold-coated nanopillar substrate was first coated with 4-ATP via Ag-S bonding by immersing the substrate in 10mM 4-ATP for 1 hour. After removing unbound 4-ATP molecules with ethanol and PBS, the carboxyl groups on capture antibodies was activated by EDC/NHS (EDC =171mM/NHS = 427.5mM) to bind to 4-ATP. 5µL of EDC/NHS solution was added to MUC4 antibody diluted in 0.5mL of PBS and was allowed to react for 15 minutes. The activated antibody was applied on the functionalized substrate and was incubated for 2 hours. The substrate was then washed with PBS, and the unspecific binding was blocked by soaking the substrates in 1mM EDC/NHS-activated glycine solutions for 6 hours. The substrate then was ready to use. Different concentration of MUC4 recombinant protein at 10, 100, and 1000 ng/mL were spiked in normal serum samples and then applied on the functionalized substrates to react for 2

hours. Finally, the substrates were thoroughly washed with PBS, dried with the air stream and analyzed by the Raman device.

5.3.3 Magnet Enhancement

As shown in Fig. 27, the magnetic field was generated by using a magnet bar and the gold coated nanopillar substrate was directly placed on the flat surface of the magnet. The magnet is a grade N45 permanent neodymium magnet which can hold up to 33 lbs. It is magnetized through the 1/4" thickness so the north and south poles are on the flat surfaces. The Magnetic beads allow antibodies to be covalently attached to 500nm particles. 50µL of the 0.4mg ml^{-1} MUC4 antibody was added to the magnetic beads. The beads were reconstituted by gently and thoroughly pipetting up and down. The tube was then placed on the magnet bar for 5-10 seconds to collect the particles

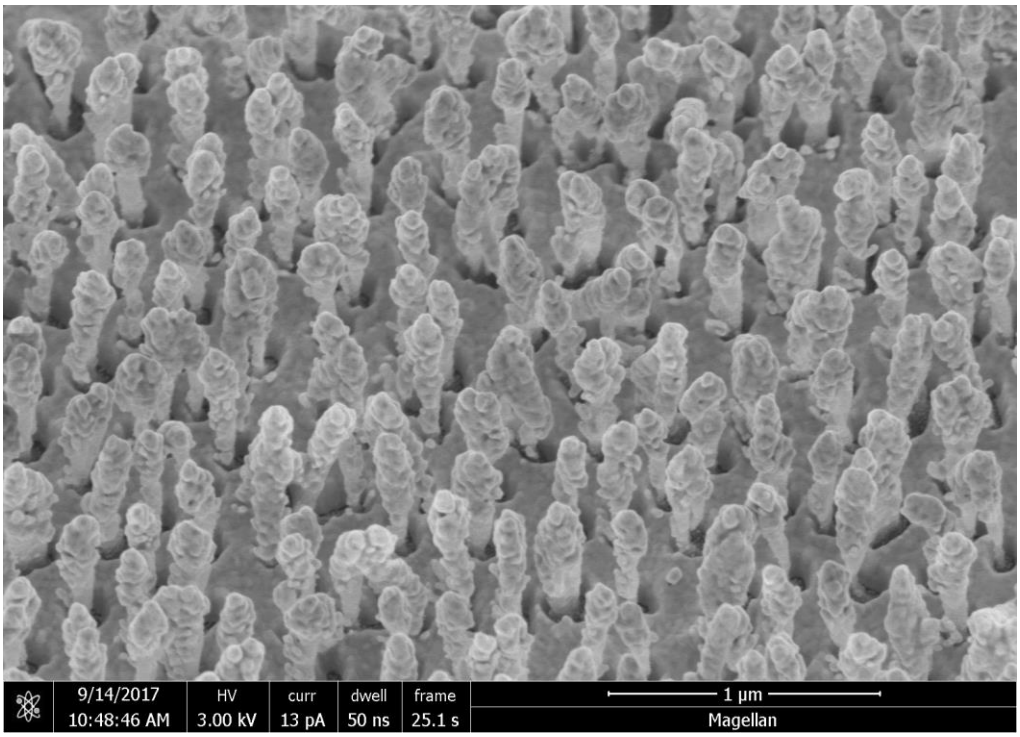

Figure 28 SEM image of gold-coated silicon substrate

and remove supernatant. The beads were washed by adding 200 µL of washing buffer to the tube and mix thoroughly for 15 seconds. The tube was again placed on the magnetic bar for 5-10

seconds to collect the particles and discard the supernatant. The solution was then rinsed one more time. Next, 200 µL of blocking buffer was added to the suspension for stabilizing the suspension and blocking nonspecific binding sites. The solution was left to react for 30 minutes at room temperature and was placed on the magnetic bar for 5-10 seconds to collect the particles and discard the supernatant. The washing step was repeated twice. The pellet was then resuspended and mixed thoroughly in 25 µL of storage buffer. At the end of the protocol, the tube contained 1×10^{10} particles/ml in the 25µL. The prepared magnetic beads were then applied on the captured antigens and the magnetic force was applied through magnet to further compress the reporter 4-ATP by placing the magnets on the bottom of the substrates.

5.3.4 Multiplex Detection

We subsequently investigate whether multiplexed detection of two biomarkers can be achieved using two bifunctional reporters, 4-ATP and 6-MP. Fabrication of mixed Anti-CA19-9/4-ATP and Anti-HE4/ 6MP was conducted as follows. Gold-coated nanopillar SERS-active substrates were cleaned thoroughly with ethanol. These substrates were then immersed in a 100 nM 4-ATP solution prepared in ethanol for one hour to form a submonolayer of 4-ATP. The substrates were then removed from the solution and washed thoroughly with ethanol to remove unbound 4-ATP, followed by rinsing with PBS. Anti-HE4 was then conjugated to the 4-ATP submonolayer in a similar manner. Anti-HE4-conjugated 6-MP was prepared by mixing diluted anti-HE4 solution (1 µL of anti-HE4 stock in 0.5 mL of PBS) with 100 µM 6-MP. This step was followed by activation with EDC/NHS (171 mM/427.5 mM) for eight hours at room temperature. The mixture was then applied onto the anti-Ca19-9/4-ATP-coated SERS-active substrate and reacted for two hours at room temperature. Finally, the conjugated substrates were removed from the mixture and washed thoroughly with PBS. The substrates were then blocked with 0.1 mM

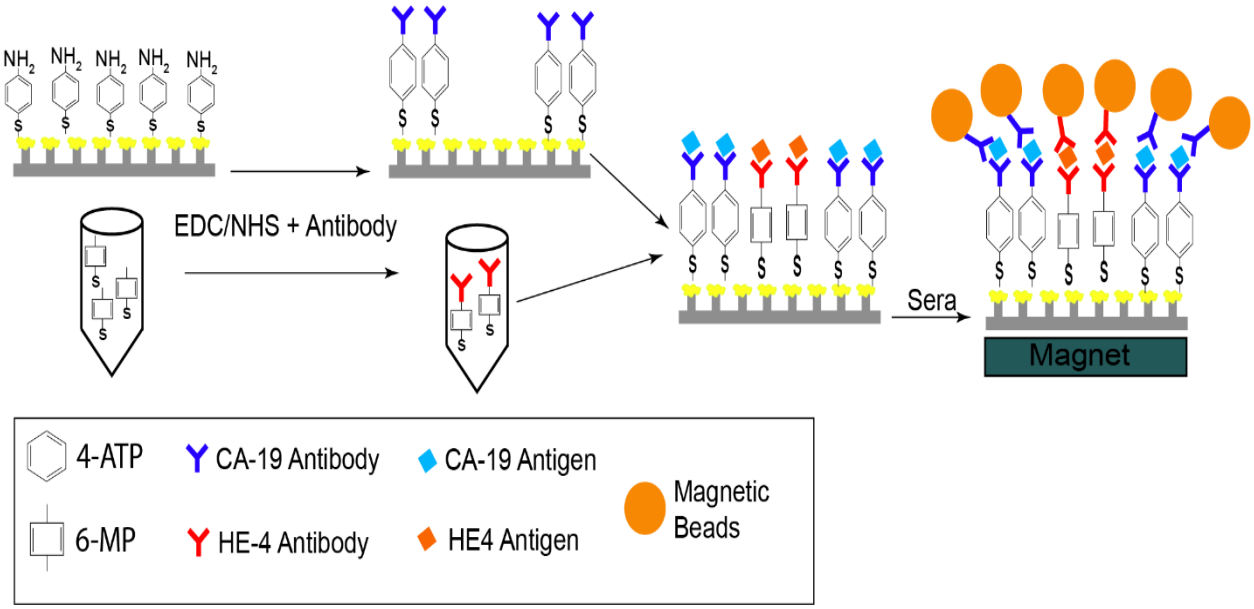

Figure 29. Multiplex detection of CA19-9 and HE4 using magnetic-enhanced frequency shift detection.

EDC/NHS-activated glycine prepared in PBS for about eight hours. Upon completion of the incubation, the substrates were thoroughly washed with PBS. The steps of the multiplex detection of cancer biomarkers using magnetic-enhanced frequency shift detection is shown in Fig. 29.

5.3.5 SERS Readout Instrumentation

All the measurements and Raman spectra collection were performed with portable BWS415 i-Raman from B&W TEK Co. The incident laser light was focused to 85 µm spot size on the substrate normal incidence. The working distance is 5.9 mm. The light source has a power of 499.95mW, and an excitation wavelength of 785nm and the same objective was used to collect the scattered radiation. In this study, the antigen concentration was quantified using two approaches. For intensity-based quantification, $v_s(No_2)$ of 4-NBT intensity at the 1336cm^{-1} position averaged over five readouts on each substrate. The shifts on the peak near 1580cm^{-1} corresponding to the symmetric aromatic C-C stretch (ν(CC)) of 4-ATP were used for

shift-based quantification and also averaged across five measurements from a monolayer of a Raman reporter (4-ATP) recorded at different places on one substrate.

5.4 Result and Discussions

5.4.1 Detection of spiked antigen and patient sample's biomarker in the absence of magnetic field

We first sought to determine which intensity peak of the Raman reporter 4-ATP has the most significant frequency shift upon antigen binding. There are multiple Raman intensity peaks for 4-ATP which occur at 639, 705, 1007, 1081, 1179, 1427 and 1586 cm^{-1}. Table 6 shows the peak assignments of the linker molecule 4-ATP. As shown in Fig. 30, among these peaks, wavenumber down-shifts upon binding to the MUC4 antibody and up-shifts as a function of exposure to MUC4 solutions of different concentration were observed at only 1077.5 cm^{-1} and 1583 cm^{-1}. Our experimental results demonstrated that 1583 cm^{-1} peak is more sensitive than 1077.5 cm^{-1} for detection of the spiked antigen in serum sample.

Table 6: Vibrational assignment of linker molecule 4-ATP

Wavenumber (CM^{-1})	*Vibrational assignment*
639	$\gamma(CCC)$
705	$\pi(CS) + \pi(CH) + \pi(CC)$
1007	$\gamma(CCC) + \gamma(CC)$
1081	$\nu(CS)$
1179	$\delta(CH)$
1427	$\nu(CS) + \delta(CH)$
1586	$\nu(CC)$

Without antigen binding, the reporter molecules are stretched mechanically which caused by intermolecular repulsion between the immobilized MUC4 antibodies and steric hindrance[138], while hydrophobic interactions between bound antigens allowing more efficient packing and make these molecules to relax. As a result, a shift of Raman frequency can be observed, which is quantitatively correlated with the concentration of the targeted antigen (Fig 31.a). As spiked protein concentration decreased from 1000ng ml^{-1} to 10ng ml^{-1}, SERS signals also steadily

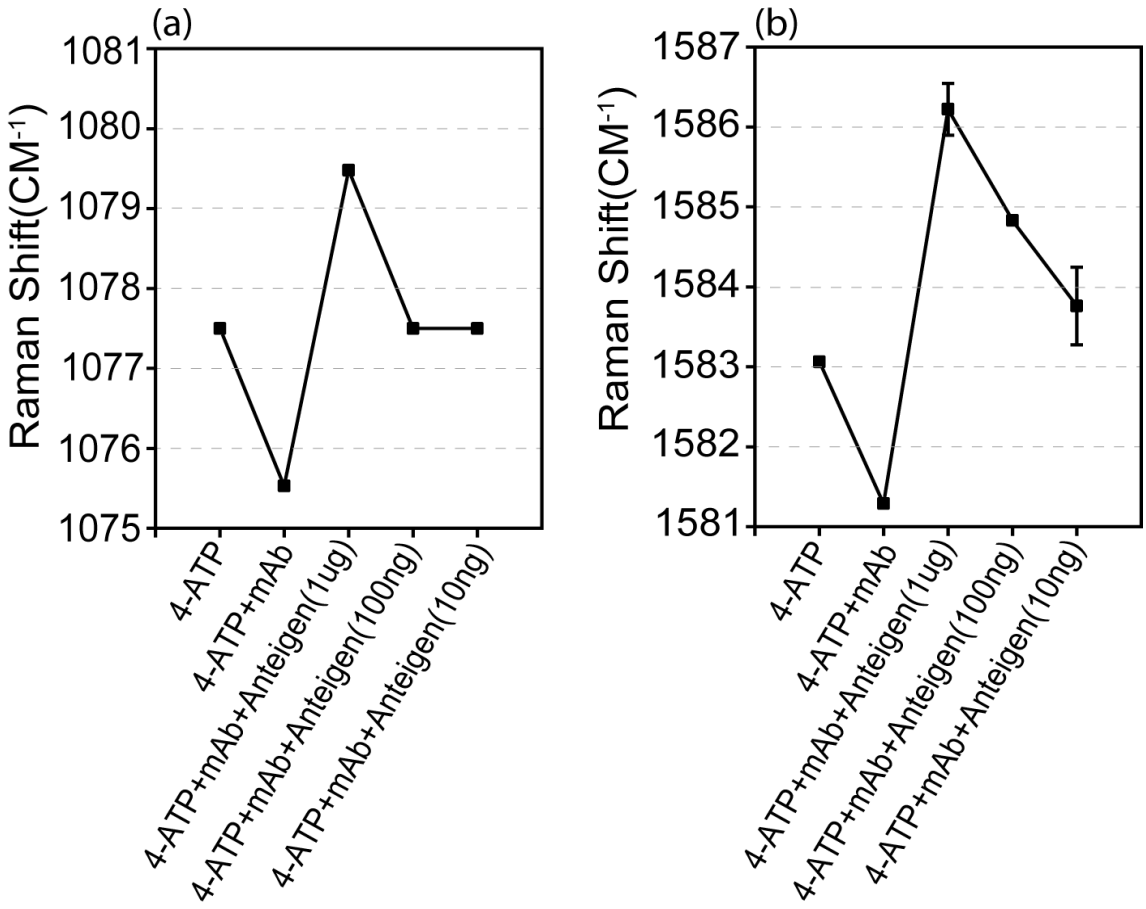

Figure 30: Response of the (a) 1077 Cm-1 and (b) 1583 Cm-1 peaks to different MUC4 protein concentrations.

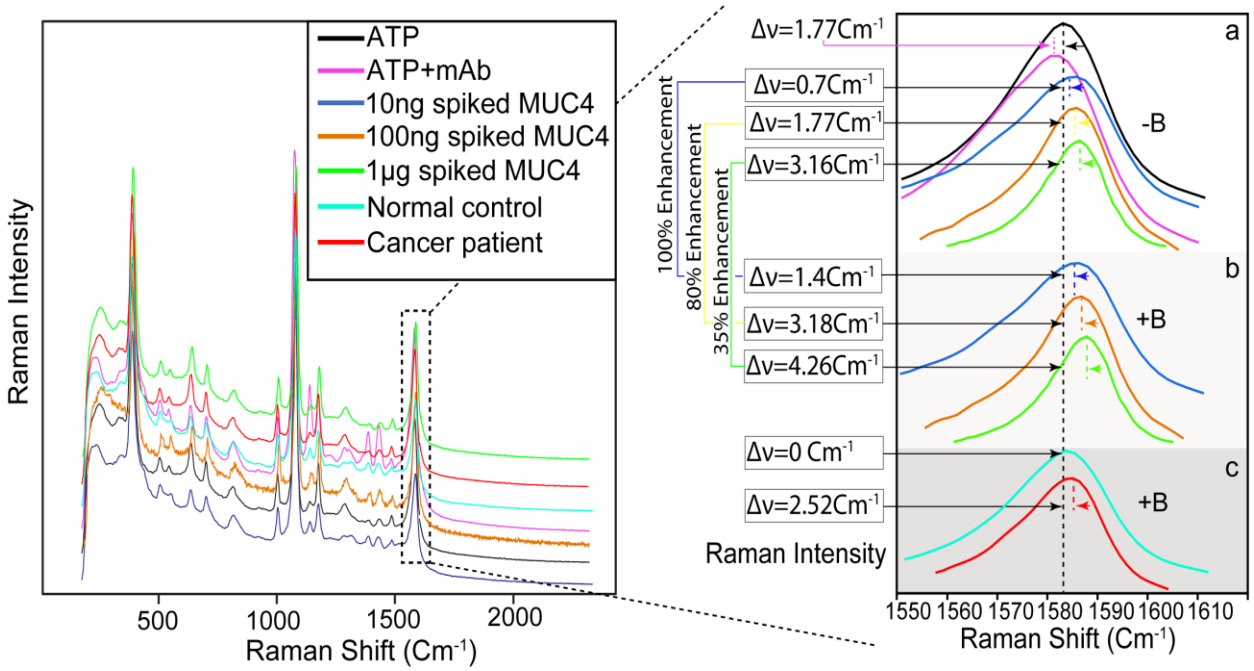

Figure 31 Detection of MUC4 spiked in normal serum and real cancer patient using magnetic enhanced Raman frequency shift assay. MUC4 recombinant proteins were spiked at different concentration in the serum. A real normal and cancer patient sample also were tested, and the shifts are shown.

decreased as a function of analyte concentration. To ensure that the Raman peak shifts of the 4ATP reporters was specifically due to antigen binding, the functionalized capture substrate was exposed to BSA without antigen as a control sample, and no frequency shifts have been observed. The peak position of the reporter on the substrate shifted $1.7 \pm 0.0\ cm^{-1}$ to the left side when it binds to antibody whereas the peak up-shifts $0.7 \pm 0.0\ cm^{-1}$, $1.77 \pm 0.31\ cm^{-1}$, $3.67 \pm 0.45\ cm^{-1}$ when it respectively binds to 1000,100,10 ng ml^{-1} spiked MUC4 in serum and averaged over five random measurements.

This approach only requires Raman active surfaces but not nanoparticles. In addition, it does not rely on the absolute intensity in the SERS spectrum and thus has the potential to achieve a very high reproducibility. This method permits direct binding of Raman Reporter to the metal substrate without use of the secondary antibody which results in higher enhancement comparing

to the conventional ERLs SERS-based immunoassay which requires two antibodies for each antigen.

5.4.2 Effect of magnetic field on antigen detection

As shown in Fig. 31 when the magnet was located underneath the substrates, a significant enhancement of frequency shift was observed, especially for the lowest concentration (10 ng ml^{-1}, i.e., 10 pM), where 100% increase was achieved. As can be seen in Fig. 31, 100%, 80% and 35% enhancement were observed for 10, 100, and 1000 ng/mL respectively. These trends observed in the SERS spectra indicated that the magnetic beads which were bound to MUC4 protein, made the antigen becoming closer to the linker/reporter monolayer under magnetic field. A relaxation of the linker molecule was examined by removing the magnetic force. These promising results demonstrate that magnetic beads can further increase the sensitivity and dynamic range of the assay.

The true and ultimate test for any immunoassay is the sensing capability for real serum sample. For sensing of one biomarker in the presence of the others and showing clinical applications of this approach, the concentration of MUC4 also is quantified in cancer patient sample. MUC4 has been identified as potential biomarkers which aberrantly expressed in several cancers including pancreatic[144], breast[145], ovarian[116] and lung cancer[146]. The serum of patients with pancreatic cancer, and normal individuals were collected under an IRB approved protocol and were identified from the UMass Memorial Medical Center Chemotherapy Infusion Center and Gastroenterology Clinics. Patients were identified from the review of the weekly schedules, and consecutive patients were enrolled to avoid bias. As shown in Fig. 31c, significantly higher levels of MUC4 was detected in PC patient's sample compared with normal control sample. Slight frequency shift (~1 cm^{-1}) also was observed for diluted (x2) PC patient's sample. These results

encourage using magnetic enhanced Raman frequency shift immunoassay as a potential application for early-stage cancer detection in clinical settings.

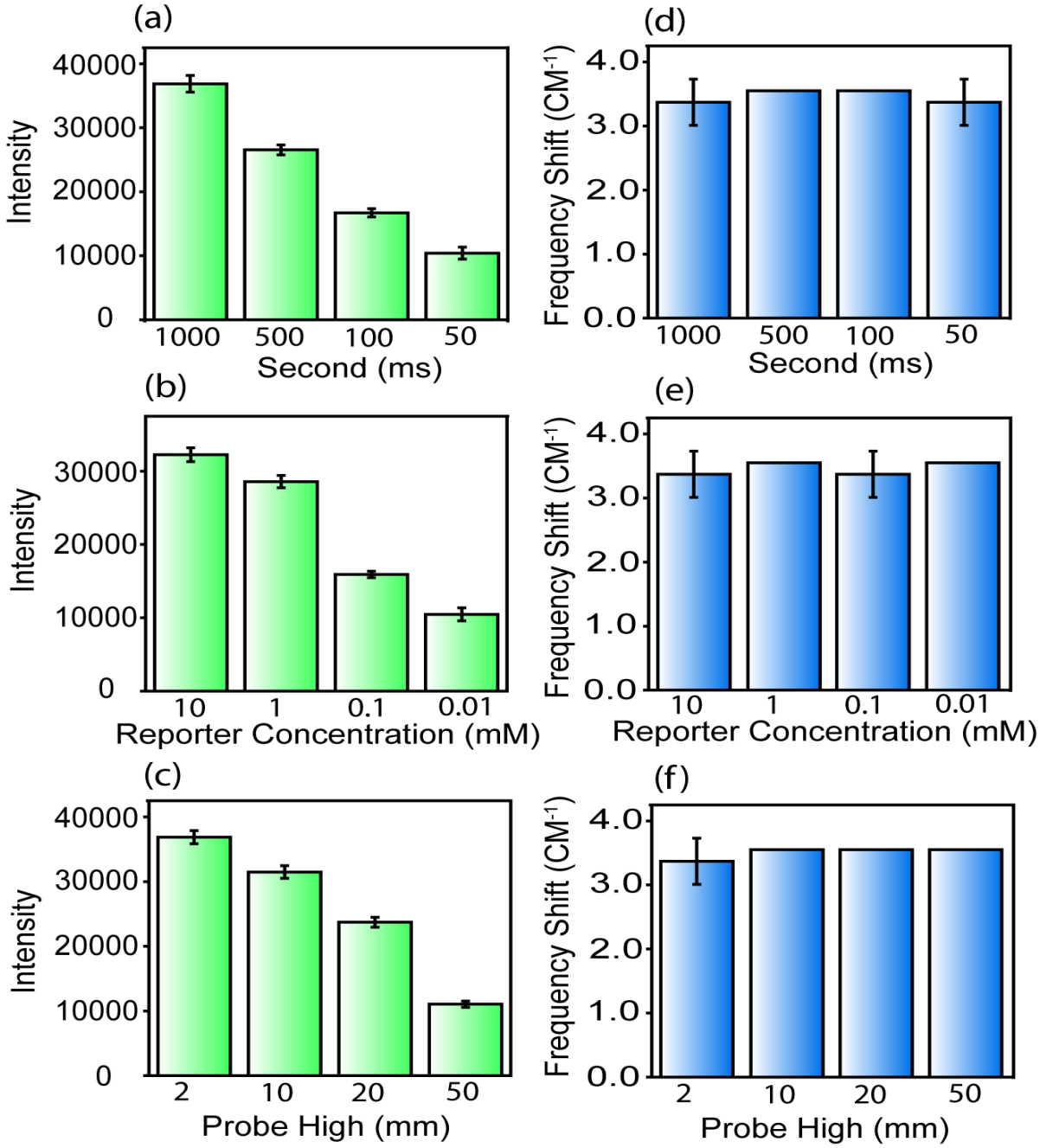

Figure 32 The effect of experimental parameters (integration time, Raman Reporter Concentration and probe high) is evaluated in (a,b,c) , intensity-based quantification and (d,e,f) Frequency shift-based quantification

5.4.3 Effect of experimental parameters on the assay

As stated earlier, intensity-based quantification can be affected by experimental parameters including the amount of Raman reporters, integration time, laser power and laser focus. Reproducibility improvement of our suggested magnetic enhanced Raman frequency shift was investigated and compared with conventional intensity-based quantification. As shown in Fig. 32, by changing the integration time, Raman reporter concentration and probe high (laser power), the intensity-based quantification undergo significant variation respectively, while the frequency-shift based approach remained almost constant.

Also, as shown in Fig. 33, very slight shift variation can be observed from five random measurements on the substrate, while there are relatively more scattered data points for intensity measurements.

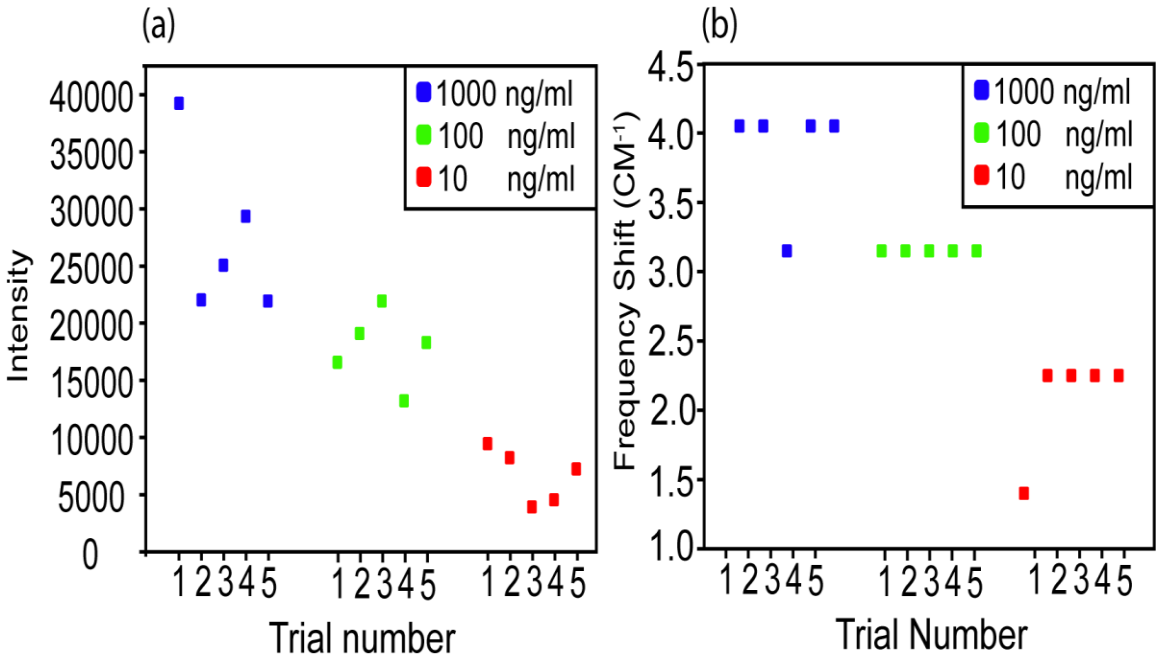

Figure 33 Scatter data points for different concentrations of spiked MUC4 in normal serum. Readouts were collected for each concentration from five random locations on the substrate.

5.4.4 Multiplex Detection of cancer biomarkers

Fig. 29 shows the experiment's steps that form the mixed binding, in which peaks belong to 4-ATP and 6-MP. Detections of binding events in each type of sensor (anti-CA19-9/4-ATP and anti-HE4/6-MP) are illustrated in Fig. 34, whereby peak shifts at 1080 cm^{-1} in the composite the bindings in the anti-CA19-9/4-ATP sensor, while those at 1290 cm^{-1}, in the anti-HE4/6-MP sensor. In the two-step functionalization, first, the initial submonolayer of 4-ATP was self-organized and attached to the gold-coated nanopillar, leading to the anti-CA19-9 self-assembled into domains

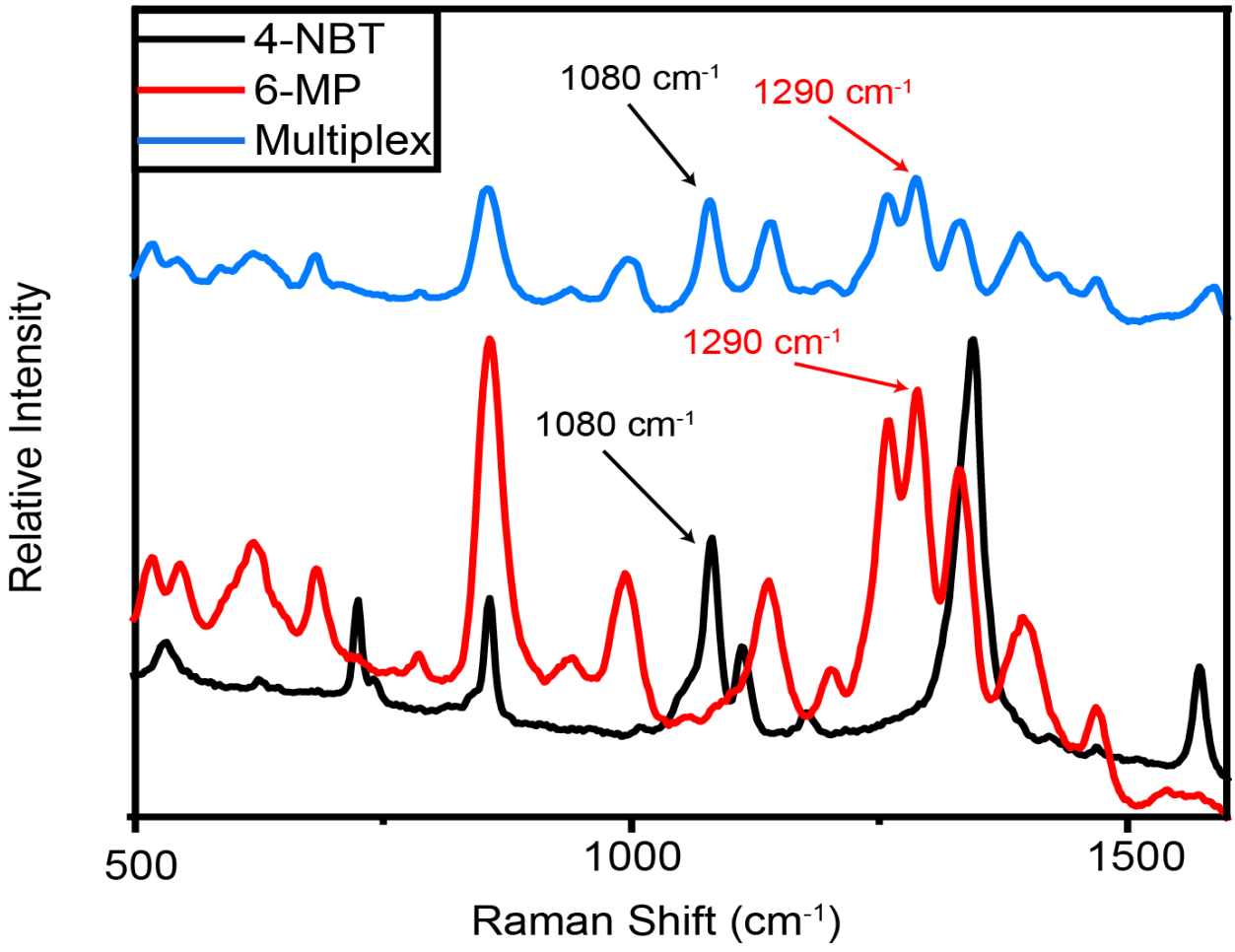

Figure 34. Typical SERS spectrum derived from multiplex detection of anti-CA19-9/4-ATP and anti-HE4/6-MP.

upon conjugating to this 4-ATP layer. Subsequent functionalization with the anti-HE4/6-MP

complex then fills up the remaining unoccupied sites on the Au surface. This two-step procedure creates submicrometer regions of anti-CA19-9/4-ATP and anti-HE4/6-MP, between which binding events do not interfere, hence the selectivity.

When the substrate was exposed to 100 and 10 ng/mL spiked antigen, the peak shifted to higher wavenumbers by 1.98 cm^{-1} and 1.18 cm^{-1} for CA-19-9, and by 1.24 cm^{-1} and 0.414 cm^{-1} for HE4 respectively, which indicates a linear relationship over this range. As can be seen in Fig. 35, in each case, only the sensor, specific to the used antigen produces the largest response, while responses in the other are suppressed, indicating some level of selectivity.

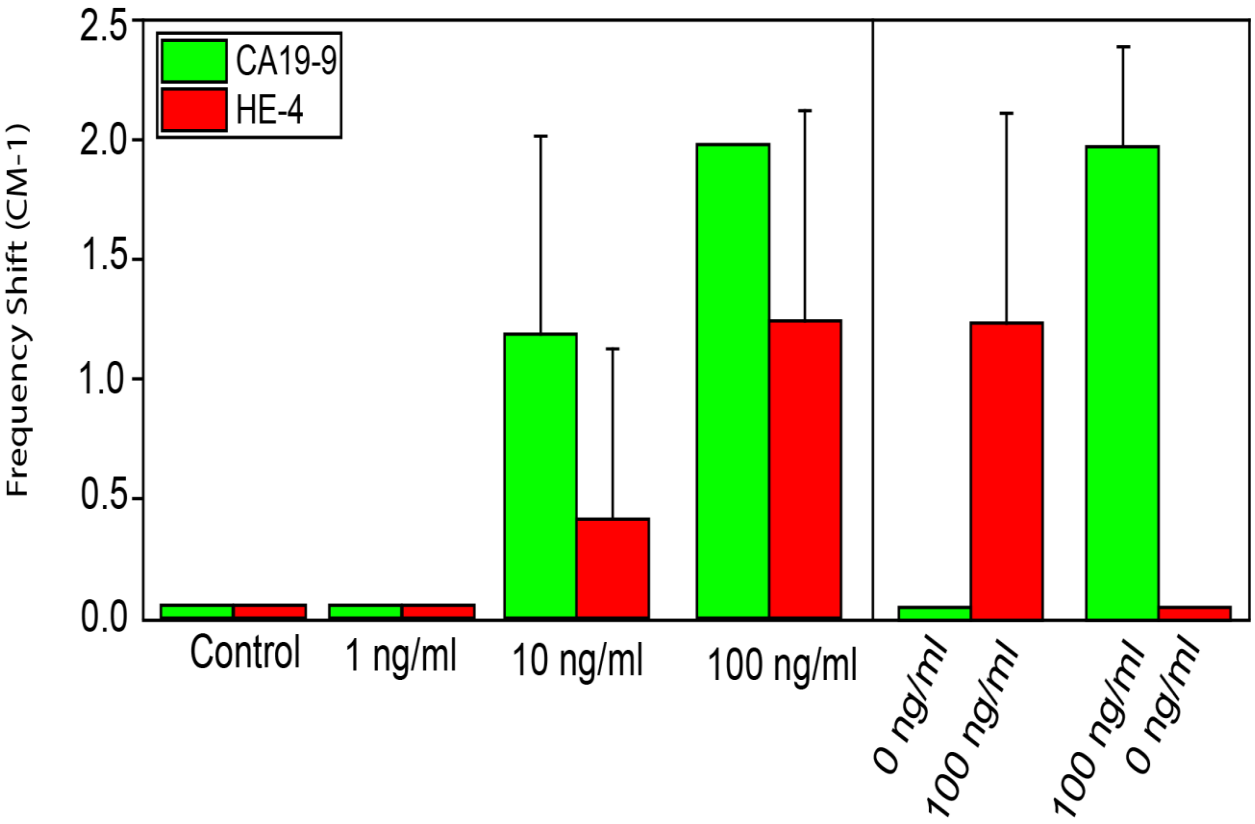

Figure 35. Responses of the 1080 and 1290 cm^{-1} peak to different antigen (CA19-9 and HE4) concentrations

5.4.5 Detection of cancer biomarkers in various type of cancers

Five most critical biomarkers (CA-125, CA19-9, CEA, OPN, Prolactin) were quantified in twenty-five serum samples of common cancer types (lung, ovarian, pancreatic, colorectal, Control) using proposed approach. as shown in Fig.36, and appendix figure 2, significantly higher levels of these critical biomarkers were detected in cancer patients compared with normal controls.

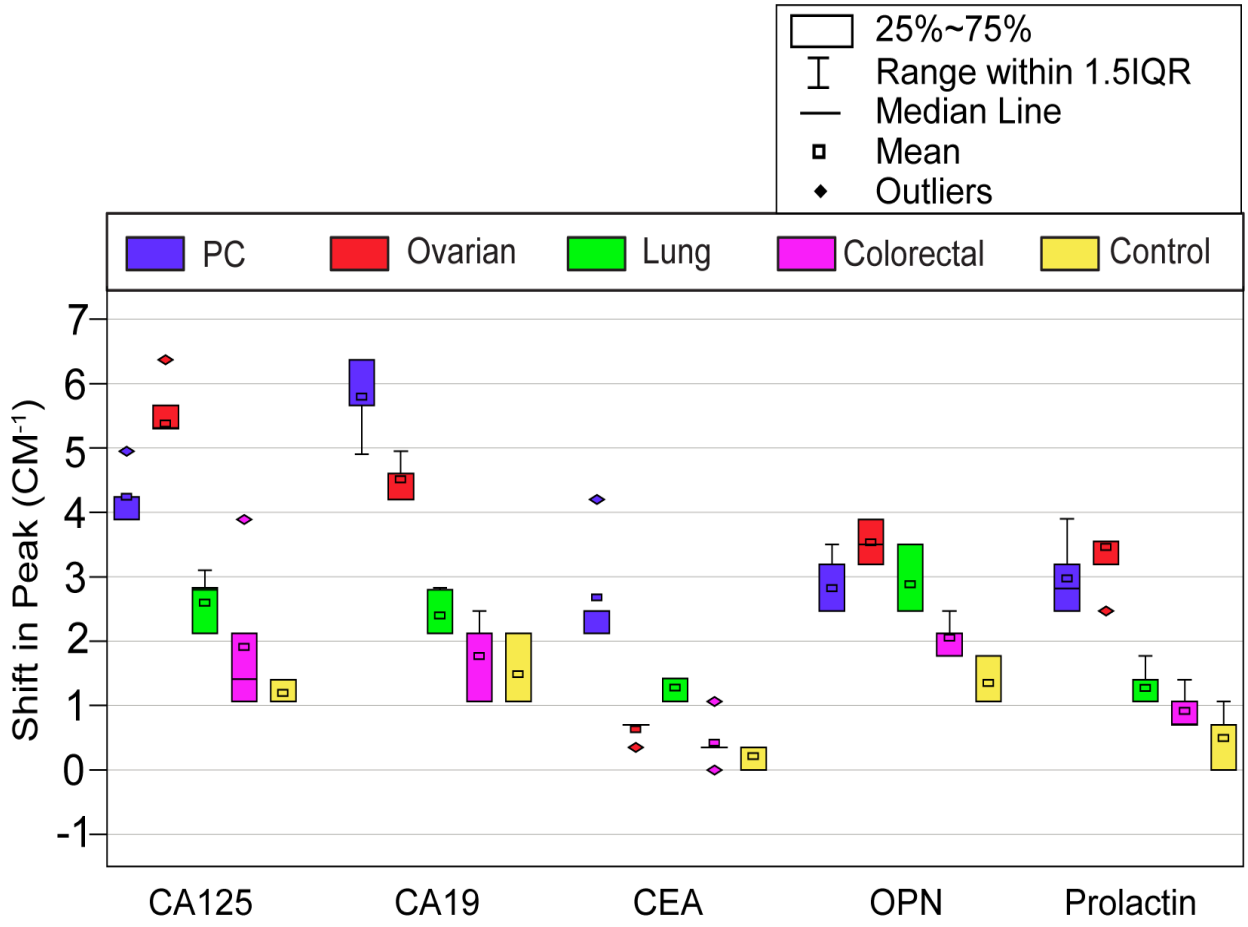

Figure 36: Detection of CA-125, CA19-9, CEA, OPN, Prolactin levels in serum of lung, ovarian, pancreatic, colorectal, Control samples using magnetic enhanced Raman frequency shift assay.

5.4.6 Differentiating pancreatic cancer from ovarian cancer

The ultimate test for any immunoassay that determined its clinical application is its capability of sensing one biomarker in the presence of others. Serums for cancer patients and healthy individuals were collected Under an IRB approved protocol and were identified from the UMass Memorial Medical Center, Chemotherapy Infusion Center, and Gastroenterology Clinics. Patients were identified by reviewing weekly schedules, and consecutive patients were enrolled to avoid bias. The expression level of five cancer biomarkers (CA-125, CA19-9, CEA, OPN, Prolactin) has been measured in serums of ovarian cancer, pancreatic cancer, and control samples (total of 15 sera samples) using magnetic enhanced Raman frequency shift immunoassay. These measurements indicate that serums from cancer patients produced a larger change in SERS frequency shift compared to that of sera from healthy individuals (Fig. 37). The P values were

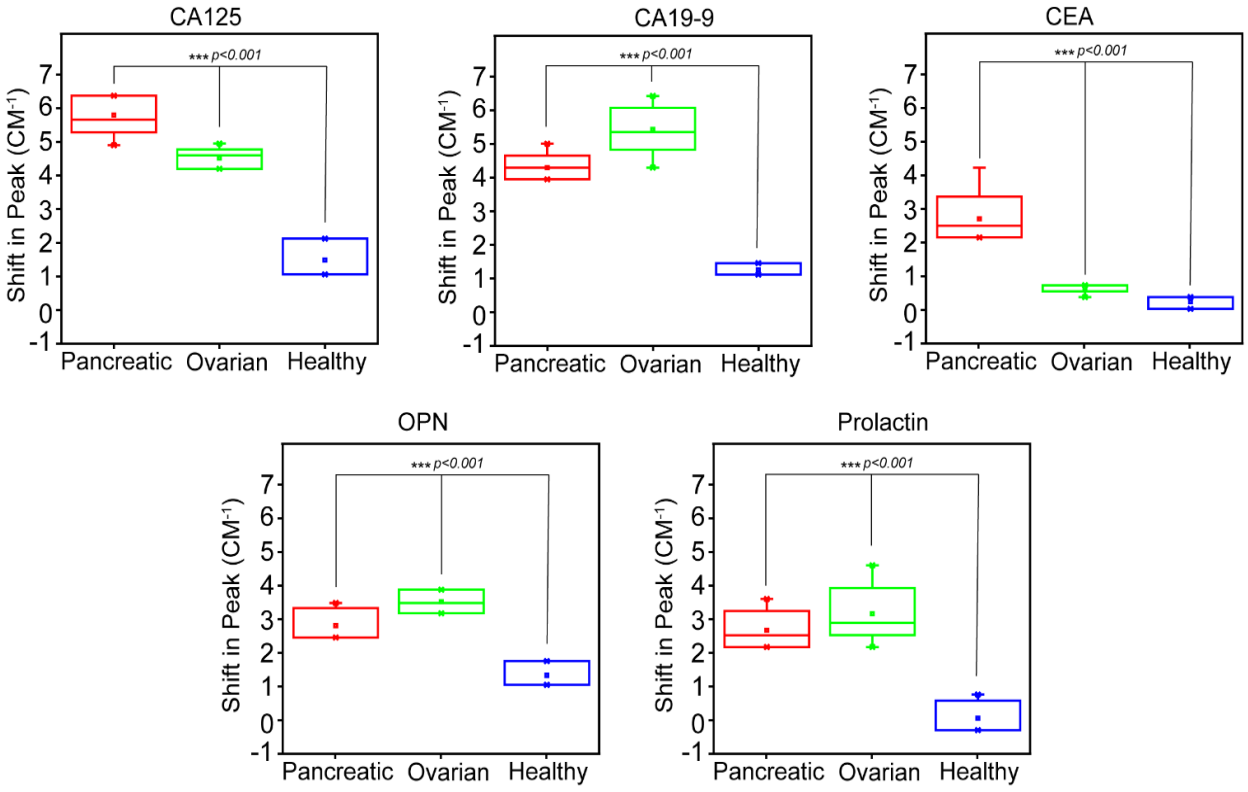

Figure 37. Detection of CA-125, CA19-9, CEA, OPN, and Prolactin levels in serum of ovarian, pancreatic and control samples using magnetic enhanced Raman frequency shift assay. P values were calculated using one-way ANOVA test. ***, P < 0.001.

calculated using a one-way ANOVA test, indicating that population means of pancreatic, ovarian, and healthy individuals are significantly different for all of the tested biomarkers. Our findings demonstrate the great promise of using magnetic enhanced Raman frequency shift immunoassay as a low-cost and high-throughput approach as the emerging liquid biopsy diagnostics method.

5.4.6.1 Data Analysis

5.4.6.1.1 Classification Algorithms

The outcome of each measurement for each biomarker in any sample is the frequency shift of the peak value in the Raman spectrum. The dataset includes five subjects in each class of pancreatic cancer, ovarian cancer, and healthy individuals. Three different biomarkers are measured for each patient, totaling 45 data points. The classification tree is employed to predict

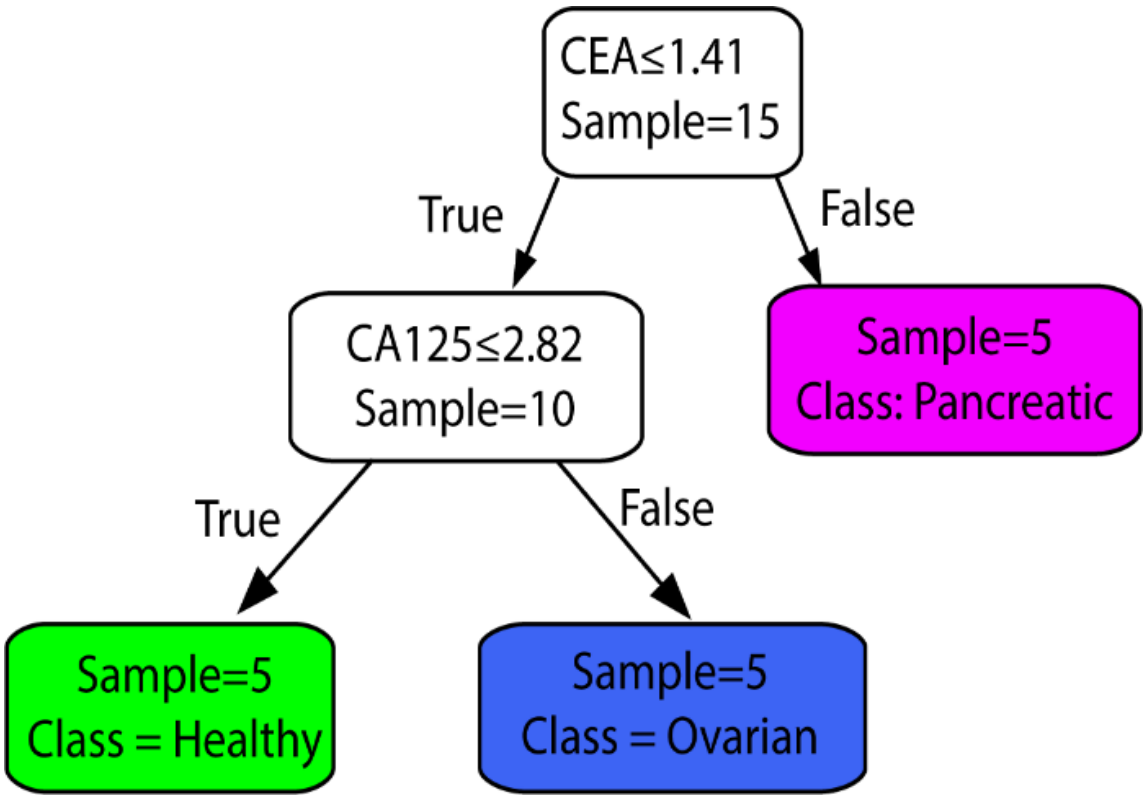

Figure 38 Classification tree trained with the whole dataset of shift frequency-value with whole dataset of peak-value Raman shifts with depth = 2

the condition of patients. Details of this approach can be found in the previous work[133]. Since the size of the dataset is limited, five-fold cross-validation is utilized to estimate the generalization error, in which the dataset is randomly partitioned into five equal subsets. In each run, four subsets are used to train the model, and the other held-out subset is used to test the performance of the trained model. The outcome of these five tests for sensitivity and specificity of the model are averaged and reported as model performance. In order to avoid over-fitting, the maximum depth of the decision tree is set to two.

5.4.6.1.2 Performance Evaluation

To evaluate the performance of each model, the sensitivity, specificity, and accuracy are computed similarly to our previous work[133]. Sensitivity is calculated as (defined as) the proportion of patients that are classified with the correct type of cancer. Specificity is calculated as (defined as) the proportion of healthy individuals that are classified as healthy. Accuracy points out to the proportion of patients that are correctly classified[147]. Using 5-fold cross-validation, the performance of the proposed method is computed as follows.

Sensitivity = 0.93, Specificity = 0.97, Accuracy = 0.96

Finally, we used the whole dataset to train the classification tree shown in Fig. 38. This plot shows that the most critical biomarker in diagnosis for Pancreatic cancer is CEA, and for ovarian cancer it is CA125. Note that the whole dataset is used to train this model. Therefore, the same data cannot be utilized to evaluate the performance of the model. It could be used, however, to predict the condition of future patients.

5.6 Conclusions

We have developed magnetic enhanced Raman frequency shift immunoassay for detection of protein biomarker. This study demonstrated the detection of the various concentration of MUC4 spiked in the human serum sample and using SERS frequency shift quantification. From the observed SERS spectra, the effect of magnetic force on the MUC4 binding magnetic beads and gold coated nanopillar substrates indicates the enhancing capability of the suggested approach for the sensitivity of the assay. To emphasize on clinical application of this method in early-stage cancer detection, the expression level of MUC4 as an essential cancer biomarker was successfully quantified and compared with normal control sample. Also, our testing results demonstrate how magnetic frequency shift immunoassay can overcome the reproducibility limitations of conventional intensity-based quantification by reducing the effect of experimental parameters (Raman reporter concentration, integration time, laser power) on the final result. We have also demonstrated multiplexed detection measurements of two cancer biomarkers HE4 and CA19-9 within one single laser spot. We employed the decision tree classification to evaluate the importance of different cancer biomarkers and estimate the specificity and accuracy of the prediction. The result from data analysis demonstrated the high predicting capability of our proposed technique for precise classification of ovarian cancer, pancreatic cancer, and healthy individuals.

5.7. Acknowledgments

This work was supported in part by the Acorn Innovation Award from the Massachusetts Technology Transfer Center.

CHAPTER 6

PUBLICATIONS

1) Banaei N, Moshfegh J, Mohseni-Kabir A, Houghton JM, Sun Y, Kim B. Machine learning algorithms enhance the specificity of cancer biomarker detection using SERS-based immunoassays in microfluidic chips. RSC Adv 2019;9(4):1859-1868.

2) Banaei N, Foley A, Houghton JM, Sun Y, Kim B. Multiplex detection of pancreatic cancer biomarkers using a SERS-based immunoassay. Nanotechnology 2017.

Papers in Preparation:

3) Banaei N, Moshfegh J, Sun Y, Kim B."Magnetic Enhanced Raman Frequency Shift Immunoassay". (**Submitted**)

4) Banaei N, Kim B SERS-Based Immunoassay Detection of Tumor-Derived Extracellular Vesicles to Differentiate Pancreatic Cancers from Chronic Pancreatitis". (**Ready to submit**)

CHAPTER 7

AWARDS

1) UMass Innovation Challenge Final Competition awardee ($15K). Awarded for the design and development of an accurate, low-cost, point-of-care platform for early diagnosis of cancers and plans to bring and fit this platform into the market.

2) The outstanding paper award highlighted by the IOPScience journal which showcases some of the best research of 2017.

3) Certificate of Achievement accompanied by $5K fellowship for accomplishing the Entrepreneurship Accelerator Program an intensive program designed to accelerate the most promising new technologies in MA

4) Received the second award for the UMass One Minute Pitch Competition which is designed for the best novel venture idea and potential to develop it into a marketable product.

APPENDIX

EXPRESSION LEVEL OF CANCER BIOMARKERS IN SERUM OF CANCER PATIENTS AND NORMAL INDIVIDULAS USING SERS-BASED IMMUNOASSAY

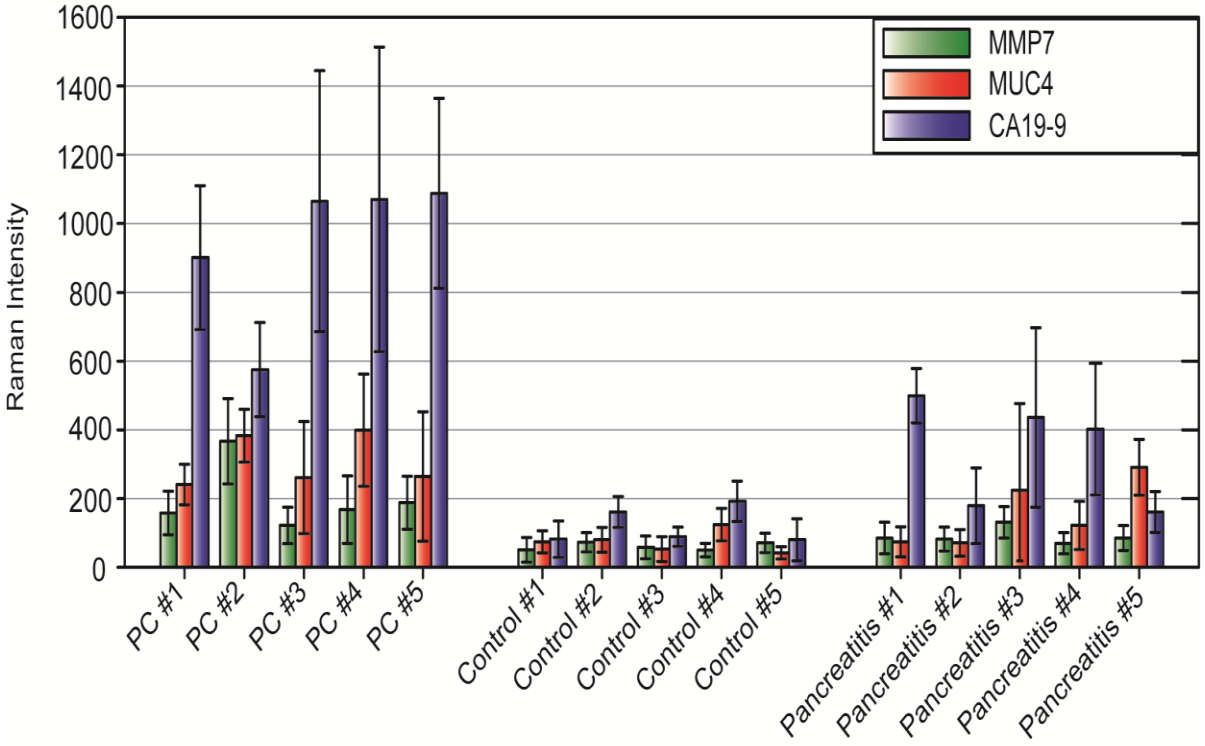

Appendix figure 1: *SERS detection of MMP7, MUC4 and CA19-9 in serum of normal, PC and pancreatitis samples (total of 15 sera samples) using the micropatterning SERS-based immunoassay. The antigen concentration was quantified using (vs(No2)) of 4-NBT intensity at the 1336 cm−1 position averaged over five readouts on each address. For reproducibility, three addresses were measured for each concentration. Error bars show the standard deviation.*

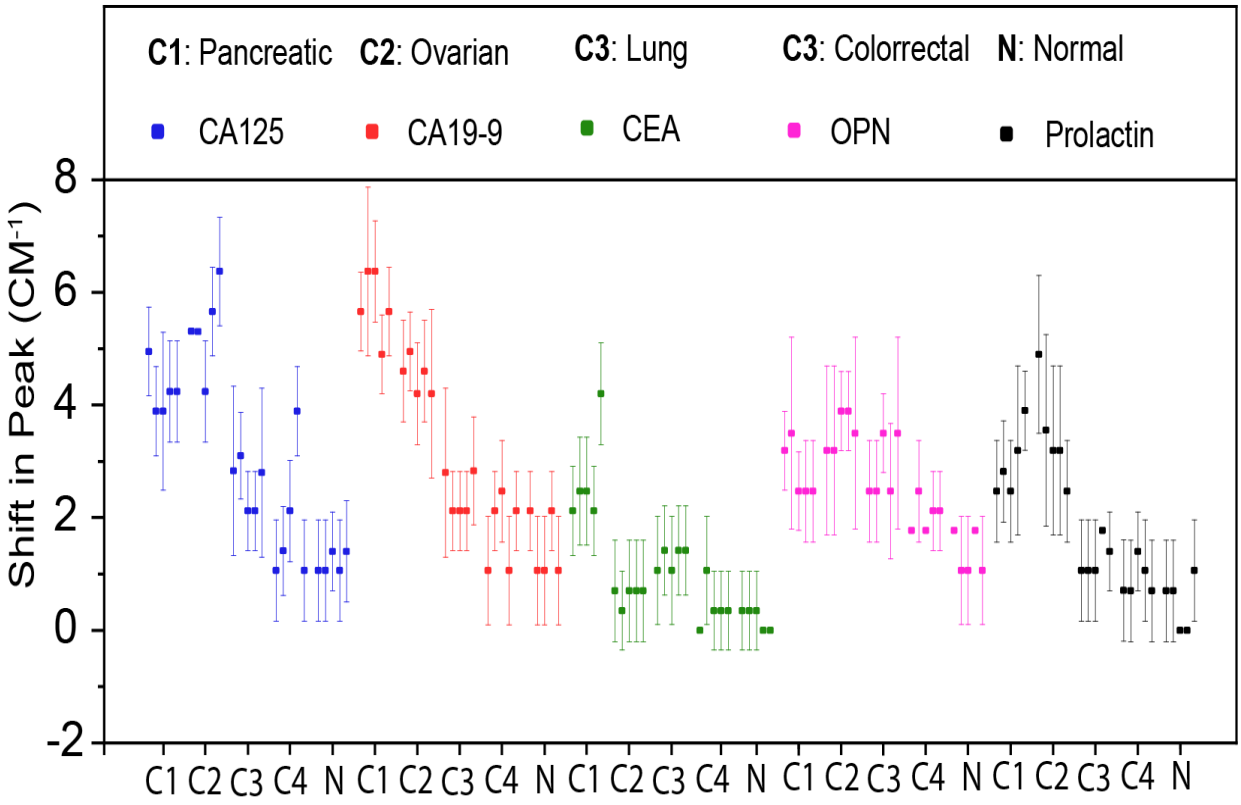

Appendix figure 2: *Detection of CA-125, CA19-9, CEA, OPN, Prolactin levels in serum of lung, ovarian, pancreatic, colorectal, Control samples using magnetic enhanced Raman frequency shift assay.*

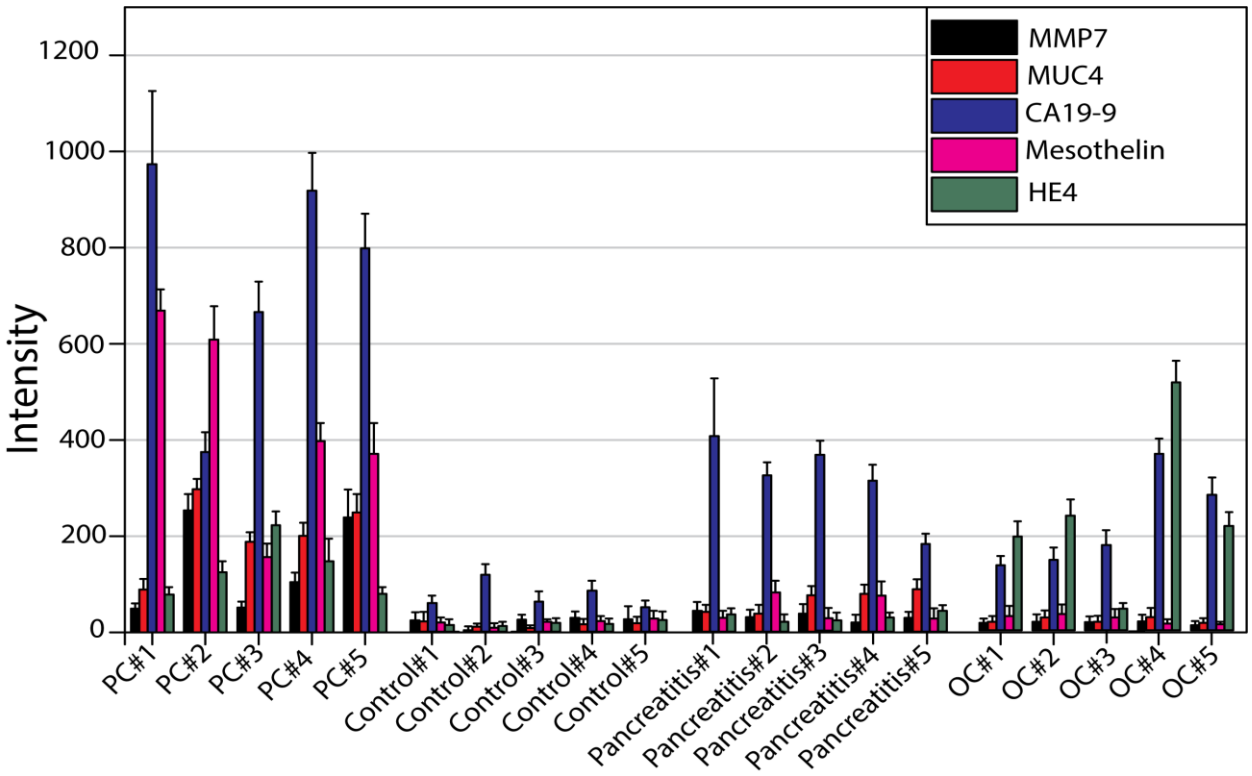

Appendix figure 3: *SERS detection of CA19-9, HE4, Mesothelin, MMP7 and MUC4in serum of normal, PC, ovarian cancer and pancreatitis samples (total of 20 sera samples). The antigen concentration was quantified using ($v_S(NO_2)$) of 4-NBT intensity at the 1336 cm^{-1} position averaged over five readouts on each address. For reproducibility, three addresses were measured for each concentration. Error bars show the standard deviation*

REFERENCES

1. Kneipp K, Kneipp H, Itzkan I, Dasari RR, Feld MS. Surface-enhanced raman scattering and biophysics. *Journal of Physics: Condensed Matter*. 2002;14(18):R597.

2. Procházka M. *Surface-enhanced raman spectroscopy: Bioanalytical, biomolecular and medical applications.* Springer; 2015.

3. Fleischmann M, Hendra PJ, McQuillan AJ. Raman spectra of pyridine adsorbed at a silver electrode. *Chemical Physics Letters*. 1974;26(2):163-166.

4. Jeanmaire DL, Van Duyne RP. Surface raman spectroelectrochemistry: Part I. heterocyclic, aromatic, and aliphatic amines adsorbed on the anodized silver electrode. *Journal of electroanalytical chemistry and interfacial electrochemistry*. 1977;84(1):1-20.

5. Park H. Chip-scale bioassays based on surface-enhanced raman scattering: Fundamentals and applications. . 2005.

6. Jemal A, Siegel R, Xu J, Ward E. Cancer statistics, 2010. *CA: a cancer journal for clinicians*. 2010;60(5):277-300.

7. Xie W, Schlücker S. Medical applications of surface-enhanced raman scattering. *Physical Chemistry Chemical Physics*. 2013;15(15):5329-5344.

8. McLarnon A. Pancreatic cancer: A novel method of imaging pancreatic cancer cells and precursors in mice could lead to early diagnosis. *Nature Reviews Gastroenterology and Hepatology*. 2012;9(8):427.

9. Duffy MJ, Sturgeon C, Lamerz R, et al. Tumor markers in pancreatic cancer: A european group on tumor markers (EGTM) status report. *Ann Oncol*. 2010;21(3):441-447.

10. Scaife CL, Shea JE, Dai Q, Firpo MA, Prestwich GD, Mulvihill SJ. Synthetic extracellular matrix enhances tumor growth and metastasis in an orthotopic mouse model of pancreatic adenocarcinoma. *Journal of Gastrointestinal Surgery*. 2008;12(6):1074-1080.

11. Chang ST, Zahn JM, Horecka J, et al. Identification of a biomarker panel using a multiplex proximity ligation assay improves accuracy of pancreatic cancer diagnosis. *Journal of translational medicine*. 2009;7(1):105.

12. Humphris JL, Chang DK, Johns AL, et al. The prognostic and predictive value of serum CA19.9 in pancreatic cancer. *Ann Oncol*. 2012;23(7):1713-1722.

13. Carrara S, Cangi MG, Arcidiacono PG, et al. Mucin expression pattern in pancreatic diseases: Findings from EUS-guided fine-needle aspiration biopsies. *Am J Gastroenterol*. 2011;106(7):1359-1363.

14. Horn A, Chakraborty S, Dey P, et al. Immunocytochemistry for MUC4 and MUC16 is a useful adjunct in the diagnosis of pancreatic adenocarcinoma on fine-needle aspiration cytology. *Arch Pathol Lab Med*. 2013;137(4):546-551.

15. Kuhlmann KF, van Till JW, Boermeester MA, et al. Evaluation of matrix metalloproteinase 7 in plasma and pancreatic juice as a biomarker for pancreatic cancer. *Cancer Epidemiol Biomarkers Prev*. 2007;16(5):886-891.

16. Wilson CL, Heppner KJ, Labosky PA, Hogan BL, Matrisian LM. Intestinal tumorigenesis is suppressed in mice lacking the metalloproteinase matrilysin. *Proc Natl Acad Sci U S A*. 1997;94(4):1402-1407.

17. Yamamoto H, Itoh F, Iku S, et al. Expression of matrix metalloproteinases and tissue inhibitors of metalloproteinases in human pancreatic adenocarcinomas: Clinicopathologic and prognostic significance of matrilysin expression. *Journal of Clinical Oncology*. 2001;19(4):1118-1127.

18. Faulds K, Smith WE, Graham D, Lacey RJ. Assessment of silver and gold substrates for the detection of amphetamine sulfate by surface enhanced raman scattering (SERS). *Analyst*. 2002;127(2):282-286.

19. Królikowska A, Kudelski A, Michota A, Bukowska J. SERS studies on the structure of thioglycolic acid monolayers on silver and gold. *Surf Sci*. 2003;532:227-232.

20. Leona M. Microanalysis of organic pigments and glazes in polychrome works of art by surface-enhanced resonance raman scattering. *Proc Natl Acad Sci U S A*. 2009;106(35):14757-14762.

21. Zhao LL, Jensen L, Schatz GC. Surface-enhanced raman scattering of pyrazine at the junction between two Ag20 nanoclusters. *Nano Letters*. 2006;6(6):1229-1234.

22. Ni J, Lipert RJ, Dawson GB, Porter MD. Immunoassay readout method using extrinsic raman labels adsorbed on immunogold colloids. *Anal Chem*. 1999;71(21):4903-4908.

23. Lopez A, Lovato F, Oh SH, et al. SERS immunoassay based on the capture and concentration of antigen-assembled gold nanoparticles. *Talanta*. 2016;146:388-393.

24. Wang Y, Yan B, Chen L. SERS tags: Novel optical nanoprobes for bioanalysis. *Chem Rev*. 2012;113(3):1391-1428.

25. Krasnoslobodtsev AV, Torres MP, Kaur S, et al. Nano-immunoassay with improved performance for detection of cancer biomarkers. *Nanomedicine: Nanotechnology, Biology and Medicine*. 2015;11(1):167-173.

26. Porter MD, Lipert RJ, Siperko LM, Wang G, Narayanan R. SERS as a bioassay platform: Fundamentals, design, and applications. *Chem Soc Rev*. 2008;37(5):1001-1011.

27. Wang G, Park H, Lipert RJ, Porter MD. Mixed monolayers on gold nanoparticle labels for multiplexed surface-enhanced raman scattering based immunoassays. *Anal Chem*. 2009;81(23):9643-9650.

28. Oldenburg SJ, Jackson JB, Westcott SL, Halas NJ. Infrared extinction properties of gold nanoshells. *Appl Phys Lett*. 1999;75(19):2897-2899.

29. Felidj N, Aubard J, Levi G, et al. Optimized surface-enhanced raman scattering on gold nanoparticle arrays. *Appl Phys Lett*. 2003;82(18):3095-3097.

30. Driskell JD, Lipert RJ, Porter MD. Labeled gold nanoparticles immobilized at smooth metallic substrates: Systematic investigation of surface plasmon resonance and surface-enhanced raman scattering. *The Journal of Physical Chemistry B*. 2006;110(35):17444-17451.

31. Maurel J, Nadal C, Garcia-Albeniz X, et al. Serum matrix metalloproteinase 7 levels identifies poor prognosis advanced colorectal cancer patients. *International journal of cancer*. 2007;121(5):1066-1071.

32. Maker AV, Katabi N, Gonen M, et al. Pancreatic cyst fluid and serum mucin levels predict dysplasia in intraductal papillary mucinous neoplasms of the pancreas. *Annals of surgical oncology*. 2011;18(1):199-206.

33. Granger JH, Granger MC, Firpo MA, Mulvihill SJ, Porter MD. Toward development of a surface-enhanced raman scattering (SERS)-based cancer diagnostic immunoassay panel. *Analyst*. 2013;138(2):410-416.

34. Wang G, Lipert RJ, Jain M, et al. Detection of the potential pancreatic cancer marker MUC4 in serum using surface-enhanced raman scattering. *Anal Chem*. 2011;83(7):2554-2561.

35. Zou Q, Zhu C, Yang Y, et al. An improved approach to detection of amplitude of low-frequency fluctuation (ALFF) for resting-state fMRI: Fractional ALFF. *J Neurosci Methods*. 2008;172(1):137-141.

36. Abraham SC, Wilentz RE, Yeo CJ, et al. Pancreaticoduodenectomy (whipple resections) in patients without malignancy: Are they allchronic pancreatitis'? *Am J Surg Pathol*. 2003;27(1):110-120.

37. World Health Organization. Latest global cancer data: Cancer burden rises to 18.1 million new cases and 9.6 million cancer deaths in 2018. *International Agency for Research on Cancer.Geneva: World Health Organization*. 2018.

38. Lennon AM, Wolfgang CL, Canto MI, et al. The early detection of pancreatic cancer: What will it take to diagnose and treat curable pancreatic neoplasia? *Cancer Res*. 2014;74(13):3381-3389.

39. Gorgannezhad L, Umer M, Islam MN, Nguyen N, Shiddiky MJ. Circulating tumor DNA and liquid biopsy: Opportunities, challenges, and recent advances in detection technologies. *Lab on a Chip*. 2018;18(8):1174-1196.

40. Dasari S, Wudayagiri R, Valluru L. Cervical cancer: Biomarkers for diagnosis and treatment. *Clinica chimica acta*. 2015;445:7-11.

41. Baine M, Ochi N, Wallace MB, et al. Ngal in pancreatic juice helps to discriminate chronic pancreatitis and pancreatic cancer patients from healthy controls. *Gastroenterology*. 2011;140(5):S-35.

42. Bloomston M, Frankel WL, Petrocca F, et al. MicroRNA expression patterns to differentiate pancreatic adenocarcinoma from normal pancreas and chronic pancreatitis. *JAMA*. 2007;297(17):1901-1908.

43. Talar-Wojnarowska R, Gąsiorowska A, Olakowski M, et al. Utility of serum IgG, IgG4 and carbonic anhydrase II antibodies in distinguishing autoimmune pancreatitis from pancreatic cancer and chronic pancreatitis. *Advances in medical sciences*. 2014;59(2):288-292.

44. Slesak B, Harlozinska-Szmyrka A, Knast W, Sedlaczek P, van Dalen A, Einarsson R. Tissue polypeptide specific antigen (TPS), a marker for differentiation between pancreatic carcinoma and chronic pancreatitis: A comparative study with CA 19-9. *Cancer*. 2000;89(1):83-88.

45. Menges M, Lerch MM, Zeitz M. The double duct sign in patients with malignant and benign pancreatic lesions. *Gastrointest Endosc*. 2000;52(1):74-77.

46. Johnson PT, Outwater EK. Pancreatic carcinoma versus chronic pancreatitis: Dynamic MR imaging. *Radiology*. 1999;212(1):213-218.

47. Rosty C, Goggins MS. Early detection of pancreatic carcinoma. *Hematol Oncol Clin North Am*. 2002;16(1):37-52.

48. Duffy MJ, Sturgeon C, Lamerz R, et al. Tumor markers in pancreatic cancer: A european group on tumor markers (EGTM) status report. *Annals of oncology*. 2010;21(3):441-447.

49. Abraham SC, Wilentz RE, Yeo CJ, et al. Pancreaticoduodenectomy (whipple resections) in patients without malignancy: Are they allchronic pancreatitis'? *Am J Surg Pathol*. 2003;27(1):110-120.

50. Kuhlmann KF, Van Till JO, Boermeester MA, et al. Evaluation of matrix metalloproteinase 7 in plasma and pancreatic juice as a biomarker for pancreatic cancer. *Cancer Epidemiology and Prevention Biomarkers*. 2007;16(5):886-891.

51. Zhang L, Jin H, Guo X, et al. Distinguishing pancreatic cancer from chronic pancreatitis and healthy individuals by 1H nuclear magnetic resonance-based metabonomic profiles. *Clin Biochem*. 2012;45(13-14):1064-1069.

52. Maas SL, Breakefield XO, Weaver AM. Extracellular vesicles: Unique intercellular delivery vehicles. *Trends Cell Biol*. 2017;27(3):172-188.

53. Van Niel G, d'Angelo G, Raposo G. Shedding light on the cell biology of extracellular vesicles. *Nature reviews Molecular cell biology*. 2018;19(4):213.

54. Willms E, Cabañas C, Mäger I, Wood MJ, Vader P. Extracellular vesicle heterogeneity: Subpopulations, isolation techniques, and diverse functions in cancer progression. *Frontiers in immunology*. 2018;9:738.

55. Yáñez-Mó M, Siljander PR, Andreu Z, et al. Biological properties of extracellular vesicles and their physiological functions. *Journal of extracellular vesicles*. 2015;4(1):27066.

56. Cicero AL, Stahl PD, Raposo G. Extracellular vesicles shuffling intercellular messages: For good or for bad. *Curr Opin Cell Biol*. 2015;35:69-77.

57. Brinton LT, Sloane HS, Kester M, Kelly KA. Formation and role of exosomes in cancer. *Cellular and molecular life sciences*. 2015;72(4):659-671.

58. György B, Szabó TG, Pásztói M, et al. Membrane vesicles, current state-of-the-art: Emerging role of extracellular vesicles. *Cellular and molecular life sciences*. 2011;68(16):2667-2688.

59. Raposo G, Stoorvogel W. Extracellular vesicles: Exosomes, microvesicles, and friends. *J Cell Biol*. 2013;200(4):373-383.

60. Anderson HC, Mulhall D, Garimella R. Role of extracellular membrane vesicles in the pathogenesis of various diseases, including cancer, renal diseases, atherosclerosis, and arthritis. *Laboratory investigation*. 2010;90(11):1549-1557.

61. van der Pol E, Boing AN, Harrison P, Sturk A, Nieuwland R. Classification, functions, and clinical relevance of extracellular vesicles. *Pharmacol Rev*. 2012;64(3):676-705.

62. Muralidharan-Chari V, Clancy JW, Sedgwick A, D'Souza-Schorey C. Microvesicles: Mediators of extracellular communication during cancer progression. *J Cell Sci*. 2010;123(Pt 10):1603-1611.

63. Boukouris S, Mathivanan S. Exosomes in bodily fluids are a highly stable resource of disease biomarkers. *PROTEOMICSâ€“Clinical Applications*. 2015;9(3-4):358-367.

64. Van der Pol E, Böing AN, Harrison P, Sturk A, Nieuwland R. Classification, functions, and clinical relevance of extracellular vesicles. *Pharmacol Rev*. 2012;64(3):676-705.

65. O'Driscoll L. Expanding on exosomes and ectosomes in cancer. *N Engl J Med*. 2015;372(24):2359-2362.

66. Khan S, Jutzy JM, Valenzuela MMA, et al. Plasma-derived exosomal survivin, a plausible biomarker for early detection of prostate cancer. *PloS one*. 2012;7(10):e46737.

67. Melo SA, Luecke LB, Kahlert C, et al. Glypican-1 identifies cancer exosomes and detects early pancreatic cancer. *Nature*. 2015;523(7559):177-182.

68. Liang K, Liu F, Fan J, et al. Nanoplasmonic quantification of tumour-derived extracellular vesicles in plasma microsamples for diagnosis and treatment monitoring. *Nature biomedical engineering*. 2017;1(4):1-11.

69. Shih C, Chong K, Hsu S, et al. Development of a magnetic bead-based method for the collection of circulating extracellular vesicles. *New biotechnology*. 2016;33(1):116-122.

70. Gholizadeh S, Draz MS, Zarghooni M, et al. Microfluidic approaches for isolation, detection, and characterization of extracellular vesicles: Current status and future directions. *Biosensors and Bioelectronics*. 2017;91:588-605.

71. Rojalin T, Phong B, Koster HJ, Carney RP. Nanoplasmonic approaches for sensitive detection and molecular characterization of extracellular vesicles. *Frontiers in chemistry*. 2019;7:279.

72. Thakur A, Qiu G, Siu-Pang NG, et al. Direct detection of two different tumor-derived extracellular vesicles by SAM-AuNIs LSPR biosensor. *Biosensors and Bioelectronics*. 2017;94:400-407.

73. Yang Y, Zhai C, Zeng Q, Khan AL, Yu H. Multifunctional detection of extracellular vesicles with surface plasmon resonance microscopy. *Anal Chem*. 2020;92(7):4884-4890.

74. Schlücker S. Surface-Enhanced raman spectroscopy: Concepts and chemical applications. *Angewandte Chemie International Edition*. 2014;53(19):4756-4795.

75. Li J, Skeete Z, Shan S, et al. Surface enhanced raman scattering detection of cancer biomarkers with bifunctional nanocomposite probes. *Anal Chem*. 2015;87(21):10698-10702.

76. Devi RV, Doble M, Verma RS. Nanomaterials for early detection of cancer biomarker with special emphasis on gold nanoparticles in immunoassays/sensors. *Biosensors and Bioelectronics*. 2015;68:688-698.

77. Zhang X, Young MA, Lyandres O, Van Duyne RP. Rapid detection of an anthrax biomarker by surface-enhanced raman spectroscopy. *J Am Chem Soc*. 2005;127(12):4484-4489.

78. Yan F, Vo-Dinh T. Surface-enhanced raman scattering detection of chemical and biological agents using a portable raman integrated tunable sensor. *Sensors Actuators B: Chem*. 2007;121(1):61-66.

79. Yang L, Gao MX, Zhan L, Gong M, Zhen SJ, Huang CZ. An enzyme-induced au@ ag core–shell nanoStructure used for an ultrasensitive surface-enhanced raman scattering immunoassay of cancer biomarkers. *Nanoscale*. 2017;9(7):2640-2645.

80. Usta DD, Salimi K, Pinar A, Coban I, Tekinay T, Tuncel A. A boronate affinity-assisted SERS tag equipped with a sandwich system for detection of glycated hemoglobin in the hemolysate of human erythrocytes. *ACS Applied Materials & Interfaces*. 2016;8(19):11934-11944.

81. Liang K, Liu F, Fan J, et al. Nanoplasmonic quantification of tumour-derived extracellular vesicles in plasma microsamples for diagnosis and treatment monitoring. *Nature biomedical engineering*. 2017;1(4):1-11.

82. Banaei N, Foley A, Houghton JM, Sun Y, Kim B. Multiplex detection of pancreatic cancer biomarkers using a SERS-based immunoassay. *Nanotechnology*. 2017;28(45):455101.

83. Archin NM, Liberty AL, Kashuba AD, et al. Administration of vorinostat disrupts HIV-1 latency in patients on antiretroviral therapy. *Nature*. 2012;487(7408):482-485.

84. Kowal J, Arras G, Colombo M, et al. Proteomic comparison defines novel markers to characterize heterogeneous populations of extracellular vesicle subtypes. *Proceedings of the National Academy of Sciences*. 2016;113(8):E968-E977.

85. MAREK. PROCHAZKA. *SURFACE-ENHANCED RAMAN SPECTROSCOPY: Bioanalytical, biomolecular and medical applications.* SPRINGER; 2017.

86. He M, Crow J, Roth M, Zeng Y, Godwin AK. Integrated immunoisolation and protein analysis of circulating exosomes using microfluidic technology. *Lab on a Chip*. 2014;14(19):3773-3780.

87. Théry C, Zitvogel L, Amigorena S. Exosomes: Composition, biogenesis and function. *Nature reviews immunology*. 2002;2(8):569-579.

88. Miyazaki T, Kato H, Fukuchi M, Nakajima M, Kuwano H. EphA2 overexpression correlates with poor prognosis in esophageal squamous cell carcinoma. *International journal of cancer*. 2003;103(5):657-663.

89. Duxbury MS, Ito H, Zinner MJ, Ashley SW, Whang EE. EphA2: A determinant of malignant cellular behavior and a potential therapeutic target in pancreatic adenocarcinoma. *Oncogene*. 2004;23(7):1448-1456.

90. Logsdon CD, Simeone DM, Binkley C, et al. Molecular profiling of pancreatic adenocarcinoma and chronic pancreatitis identifies multiple genes differentially regulated in pancreatic cancer. *Cancer Res*. 2003;63(10):2649-2657.

91. Pei H, Li L, Fridley BL, et al. FKBP51 affects cancer cell response to chemotherapy by negatively regulating akt. *Cancer cell*. 2009;16(3):259-266.

92. Zou Q, Zhu C, Yang Y, et al. An improved approach to detection of amplitude of low-frequency fluctuation (ALFF) for resting-state fMRI: Fractional ALFF. *J Neurosci Methods*. 2008;172(1):137-141.

93. Chari ST, Kelly K, Hollingsworth MA, et al. Early detection of sporadic pancreatic cancer: Summative review. *Pancreas*. 2015;44(5):693-712.

94. Bozic I, Reiter JG, Allen B, et al. Evolutionary dynamics of cancer in response to targeted combination therapy. *elife*. 2013;2:e00747.

95. Kim VM, Ahuja N. Early detection of pancreatic cancer. *Chin J Cancer Res*. 2015;27(4):321-331.

96. Cohen JD, Li L, Wang Y, et al. Detection and localization of surgically resectable cancers with a multi-analyte blood test. *Science*. 2018:eaar3247.

97. Cohen JD, Javed AA, Thoburn C, et al. Combined circulating tumor DNA and protein biomarker-based liquid biopsy for the earlier detection of pancreatic cancers. *Proc Natl Acad Sci U S A*. 2017;114(38):10202-10207.

98. Mäbert K, Cojoc M, Peitzsch C, Kurth I, Souchelnytskyi S, Dubrovska A. Cancer biomarker discovery: Current status and future perspectives. *Int J Radiat Biol*. 2014;90(8):659-677.

99. Legrand F, Berrebi D, Houhou N, et al. Early diagnosis of adenovirus infection and treatment with cidofovir after bone marrow transplantation in children. *Bone Marrow Transplant*. 2001;27(6):621.

100. Patz Jr EF, Campa MJ, Gottlin EB, Kusmartseva I, Guan XR, Herndon JE. Panel of serum biomarkers for the diagnosis of lung cancer. *Journal of Clinical Oncology*. 2007;25(35):5578-5583.

101. Misek DE, Kim EH. Protein biomarkers for the early detection of breast cancer. *Int J Proteomics*. 2011;2011:343582.

102. Mor G, Visintin I, Lai Y, et al. Serum protein markers for early detection of ovarian cancer. *Proc Natl Acad Sci U S A*. 2005;102(21):7677-7682.

103. Engelen MJ, de Bruijn HW, Hollema H, et al. Serum CA 125, carcinoembryonic antigen, and CA 19-9 as tumor markers in borderline ovarian tumors. *Gynecol Oncol*. 2000;78(1):16-20.

104. Duffy MJ, Sturgeon C, Lamerz R, et al. Tumor markers in pancreatic cancer: A european group on tumor markers (EGTM) status report. *Annals of oncology*. 2009;21(3):441-447.

105. Moore RG, McMeekin DS, Brown AK, et al. A novel multiple marker bioassay utilizing HE4 and CA125 for the prediction of ovarian cancer in patients with a pelvic mass. *Gynecol Oncol*. 2009;112(1):40-46.

106. Simmons AR, Baggerly K, Bast RC,Jr. The emerging role of HE4 in the evaluation of epithelial ovarian and endometrial carcinomas. *Oncology (Williston Park)*. 2013;27(6):548-556.

107. O'Neal RL, Nam KT, LaFleur BJ, et al. Human epididymis protein 4 is up-regulated in gastric and pancreatic adenocarcinomas. *Hum Pathol*. 2013;44(5):734-742.

108. Huang T, Jiang S, Qin L, et al. Expression and diagnostic value of HE4 in pancreatic adenocarcinoma. *International journal of molecular sciences*. 2015;16(2):2956-2970.

109. McKINNON B, Mueller MD, Nirgianakis K, Bersinger NA. Comparison of ovarian cancer markers in endometriosis favours HE4 over CA125. *Molecular medicine reports*. 2015;12(4):5179-5184.

110. Lamy P, Plassot C, Pujol J. Serum HE4: An independent prognostic factor in non-small cell lung cancer. *PloS one*. 2015;10(6):e0128836.

111. Tang QF, Zhou ZW, Ji HB, Pan WH, Sun MZ. Value of serum marker HE4 in pulmonary carcinoma diagnosis. *Int J Clin Exp Med*. 2015;8(10):19014-19021.

112. Kuhlmann KF, van Till JW, Boermeester MA, et al. Evaluation of matrix metalloproteinase 7 in plasma and pancreatic juice as a biomarker for pancreatic cancer. *Cancer Epidemiol Biomarkers Prev*. 2007;16(5):886-891.

113. Argani P, Iacobuzio-Donahue C, Ryu B, et al. Mesothelin is overexpressed in the vast majority of ductal adenocarcinomas of the pancreas: Identification of a new pancreatic cancer marker by serial analysis of gene expression (SAGE). *Clin Cancer Res*. 2001;7(12):3862-3868.

114. Hassan R, Laszik ZG, Lerner M, Raffeld M, Postier R, Brackett D. Mesothelin is overexpressed in pancreaticobiliary adenocarcinomas but not in normal pancreas and chronic pancreatitis. *Am J Clin Pathol*. 2005;124(6):838-845.

115. Havrilesky LJ, Whitehead CM, Rubatt JM, et al. Evaluation of biomarker panels for early stage ovarian cancer detection and monitoring for disease recurrence. *Gynecol Oncol*. 2008;110(3):374-382.

116. Chauhan SC, Singh AP, Ruiz F, et al. Aberrant expression of MUC4 in ovarian carcinoma: Diagnostic significance alone and in combination with MUC1 and MUC16 (CA125). *Modern Pathology*. 2006;19(10):1386.

117. Hassan R, Remaley AT, Sampson ML, et al. Detection and quantitation of serum mesothelin, a tumor marker for patients with mesothelioma and ovarian cancer. *Clin Cancer Res*. 2006;12(2):447-453.

118. Beeharry MK, Liu WT, Yan M, Zhu ZG. New blood markers detection technology: A leap in the diagnosis of gastric cancer. *World J Gastroenterol*. 2016;22(3):1202-1212.

119. Huang SK, Hoon DS. Liquid biopsy utility for the surveillance of cutaneous malignant melanoma patients. *Molecular oncology*. 2016;10(3):450-463.

120. Dinish US, Balasundaram G, Chang YT, Olivo M. Sensitive multiplex detection of serological liver cancer biomarkers using SERS-active photonic crystal fiber probe. *Journal of biophotonics*. 2014;7(11-12):956-965.

121. Zavaleta CL, Smith BR, Walton I, et al. Multiplexed imaging of surface enhanced raman scattering nanotags in living mice using noninvasive raman spectroscopy. *Proc Natl Acad Sci U S A*. 2009;106(32):13511-13516.

122. Guarrotxena N, Liu B, Fabris L, Bazan GC. Antitags: Nanostructured tools for developing SERS-Based ELISA analogs. *Adv Mater*. 2010;22(44):4954-4958.

123. Feng S, Chen R, Lin J, et al. Nasopharyngeal cancer detection based on blood plasma surface-enhanced raman spectroscopy and multivariate analysis. *Biosensors and Bioelectronics*. 2010;25(11):2414-2419.

124. Lin D, Feng S, Pan J, et al. Colorectal cancer detection by gold nanoparticle based surface-enhanced raman spectroscopy of blood serum and statistical analysis. *Optics express*. 2011;19(14):13565-13577.

125. Lee M, Lee K, Kim KH, Oh KW, Choo J. SERS-based immunoassay using a gold array-embedded gradient microfluidic chip. *Lab on a Chip*. 2012;12(19):3720-3727.

126. Gao R, Ko J, Cha K, et al. Fast and sensitive detection of an anthrax biomarker using SERS-based solenoid microfluidic sensor. *Biosensors and Bioelectronics*. 2015;72:230-236.

127. Breiman L. *Classification and regression trees.* Routledge; 2017.

128. Kim KS, Choi HH, Moon CS, Mun CW. Comparison of k-nearest neighbor, quadratic discriminant and linear discriminant analysis in classification of electromyogram signals based on the wrist-motion directions. *Current applied physics*. 2011;11(3):740-745.

129. Tayeb S, Pirouz M, Sun J, et al. Toward predicting medical conditions using k-nearest neighbors. . 2017:3897-3903.

130. Prasath VB, Alfeilat HAA, Lasassmeh O, Hassanat A. Distance and similarity measures effect on the performance of K-nearest neighbor classifier-A review. *arXiv preprint arXiv:1708.04321*. 2017.

131. Hand DJ. Principles of data mining. *Drug safety*. 2007;30(7):621-622.

132. Pedregosa F, Varoquaux G, Gramfort A, et al. Scikit-learn: Machine learning in python. *Journal of machine learning research*. 2011;12(Oct):2825-2830.

133. Banaei N, Moshfegh J, Mohseni-Kabir A, Houghton JM, Sun Y, Kim B. Machine learning algorithms enhance the specificity of cancer biomarker detection using SERS-based immunoassays in microfluidic chips. *RSC Adv*. 2019;9(4):1859-1868.

134. Banaei N, Foley A, Houghton JM, Sun Y, Kim B. Multiplex detection of pancreatic cancer biomarkers using a SERS-based immunoassay. *Nanotechnology*. 2017.

135. Granger JH, Granger MC, Firpo MA, Mulvihill SJ, Porter MD. Toward development of a surface-enhanced raman scattering (SERS)-based cancer diagnostic immunoassay panel. *Analyst*. 2013;138(2):410-416.

136. Wang Z, Zong S, Wu L, Zhu D, Cui Y. SERS-activated platforms for immunoassay: Probes, encoding methods, and applications. *Chem Rev*. 2017;117(12):7910-7963.

137. Zong C, Xu M, Xu L, et al. Surface-enhanced raman spectroscopy for bioanalysis: Reliability and challenges. *Chem Rev*. 2018;118(10):4946-4980.

138. Kho KW, Dinish US, Kumar A, Olivo M. Frequency shifts in SERS for biosensing. *ACS nano*. 2012;6(6):4892-4902.

139. Owens P, Phillipson N, Perumal J, O'Connor GM, Olivo M. Sensing of p53 and EGFR biomarkers using high efficiency SERS substrates. *Biosensors*. 2015;5(4):664-677.

140. Tang B, Wang J, Hutchison JA, et al. Ultrasensitive, multiplex raman frequency shift immunoassay of liver cancer biomarkers in physiological media. *ACS nano*. 2016;10(1):871-879.

141. Dieringer JA, McFarland AD, Shah NC, et al. Introductory lecture surface enhanced raman spectroscopy: New materials, concepts, characterization tools, and applications. *Faraday Discuss*. 2006;132:9-26.

142. Kukushkin VI, Van'kov AB, Kukushkin IV. Long-range manifestation of surface-enhanced raman scattering. *JETP letters*. 2013;98(2):64-69.

143. Schmidt MS, Hübner J, Boisen A. Large area fabrication of leaning silicon nanopillars for surface enhanced raman spectroscopy. *Adv Mater*. 2012;24(10):OP11-OP18.

144. Saitou M, Goto M, Horinouchi M, et al. MUC4 expression is a novel prognostic factor in patients with invasive ductal carcinoma of the pancreas. *J Clin Pathol*. 2005;58(8):845-852.

145. Rakha EA, Boyce RW, El-Rehim DA, et al. Expression of mucins (MUC1, MUC2, MUC3, MUC4, MUC5AC and MUC6) and their prognostic significance in human breast cancer. *Modern Pathology*. 2005;18(10):1295.

146. Llinares K, Escande F, Aubert S, et al. Diagnostic value of MUC4 immunostaining in distinguishing epithelial mesothelioma and lung adenocarcinoma. *Modern pathology*. 2004;17(2):150.

147. Hand DJ. **Principles of data mining**. . 2007;30(7).